UNIVERSITÀ DEGLI STUDI DI TRIESTE

SDBM
PhD Program in Molecular Biomedicine
XXIII cycle

Detection of Angiogenic Growth Factor by Microcantilever Biosensors

PhD Thesis

Riccardo Castagna

2009 – 2010

UNIVERSITÀ DEGLI STUDI DI TRIESTE

XXIII CICLO DEL
DOTTORATO DI RICERCA IN

BIOMEDICINA MOLECOLARE

Detection of Angiogenic Growth Factor by Microcantilever Biosensors

Settore scientifico disciplinare: BIO/11 BIOLOGIA MOLECOLARE

DOTTORANDO

RICCARDO CASTAGNA

RESPONSABILE DOTTORATO DI RICERCA

PROF. Giannino Del Sal (Università degli Studi di Trieste)

FIRMA: _____

RELATORE

PROF. Paolo Gasparini (Università degli Studi di Trieste)

FIRMA: _____

TUTORE

DR. Carlo Ricciardi (Politecnico di Torino

FIRMA: _____

ANNO ACCADEMICO 2009/2010

Sommario

Abstract

The opportunity to operate with very small quantities of material and to skip fluorescent labeling are in general the striking advantages of micro and nano-cantilever (MC) based biosensors. Their working principle is simple: the MC is functionalized with a proper probe which can selectively bind to the target molecule. The functionalized MC is subsequently placed into an environment containing the target. The interactions between the binding sites of probe and target change the mechanical response of the MC system. Readout of this variation is at the base of the transduction mechanism. Probe/target interactions sort two main effects on the MC system: mass change and bending, the last being due to the surface stress generated by the changes in Gibbs free energy upon chemical species interaction.

In this project the way of detection is to exploit the oscillation properties of the MC, and it is usually called dynamic mode or microbalance mode. The resonant frequency of a cantilever is dependent, in first approximation, on its stiffness, mass and geometry. Changes of the cantilever mass or spring constant due to molecule absorption will induce a frequency shift. Therefore, in this mode detection is performed by tracking the shift of the resonant oscillation frequency of the MC during (or after) selective absorption of target molecules.

Thus, we optimized an antibody-antigen biodesign to detect Angiopoietin-1, a key molecule in angiogenesis and a putative cancer marker. We focused on the repeatability and reproducibility of our cantilever-based system, combining results coming from both the first and second mode of vibration. In such a way, our microcantilever-based system was successfully used to detect Angiopoietin-1 masses of the order of few hundreds of picograms with less than 0.5% of relative uncertainty. Negative controls (PBS without proteins) and specificity tests (PBS with a “false” antigen) demonstrated the effectiveness of our method: the evaluation of related frequency shifts from non-specific interactions were found to be no less than one order of magnitude lower than typical variations due to specific protein binding. Finally we showed that evaluating the protein surface density (number of molecules per cm^2), it is possible to reveal interesting features concerning the conformational state of the targeted protein.

After that, since a robust biosensor should work properly with real matrices, we developed a protocol for the depletion of albumin and immunoglobulin components of murine plasma and successfully tested the microcantilever detection of enriched clarified plasma with Ang-1.

Besides, we focused on the integration of microcantilever detection in a microfluidic platform. In fact, microfluidic integration appears as a highly performing technological solution to exploit real

time monitoring of biomolecular interactions, while limiting sample handling and promoting portability and automation of routine diagnostic tests (Point-Of-Care devices).

Therefore, we focused on the realization and optimization of a microcantilever-based Lab-on-Chip, showing that microplates rather than microbeams exhibit largest mass sensitivity in liquid, while pirex rather than polymers represents the best choice for microfluidic channels. Maximum Q factor achieved was 140, as our knowledge the highest value reported in literature for cantilever biosensors resonating in liquid environment without electronic feedback. Then, we proved the successfully detection of Angiopoietin-1, showing that the related frequency shifts coming from non-specific interactions (negative controls) are roughly one order of magnitude lower than typical variations due to specific protein binding. Furthermore, we monitored the formation of antibody–antigen complex on MC surface in real-time.

In the end, thanks to its optimal specificity and fine precision, our microcantilever-based system can be successfully applied as a quantitative tool for systems biology studies such as the comprehension of protein multimerization state and its role into angiogenic machinery and cancer progression.

Chapter 1

Cantilever Biosensors

1.1. Biosensors

Sensors capable of measuring biological substances have been the subject of extensive research during the last decade. The importance to many applications of being able to monitor a specific biological substance has increased interest in biosensors [1].

A biosensor consists of three parts: a detector, which recognizes the signal (electrical, positional, piezoelectric, etc.); a transducer (optical, thermal, piezoelectric, etc.), which converts the signal into a more useful output; and a readout system (computer, digital interface, data logger, etc).

Thus a biosensors is a sensor that conjugate the sensitivity of detectors with the specificity of bio-molecules recognition, used to modify the surfaces of detectors with a selective layer capable of detecting specific molecules and bio-molecules, i.e. for targeted detection [2]. Depending on the bio-molecules adopted to functionalize the sensor, there are several target analyte that can be detect and quantify by biosensors (Figure 1.1).

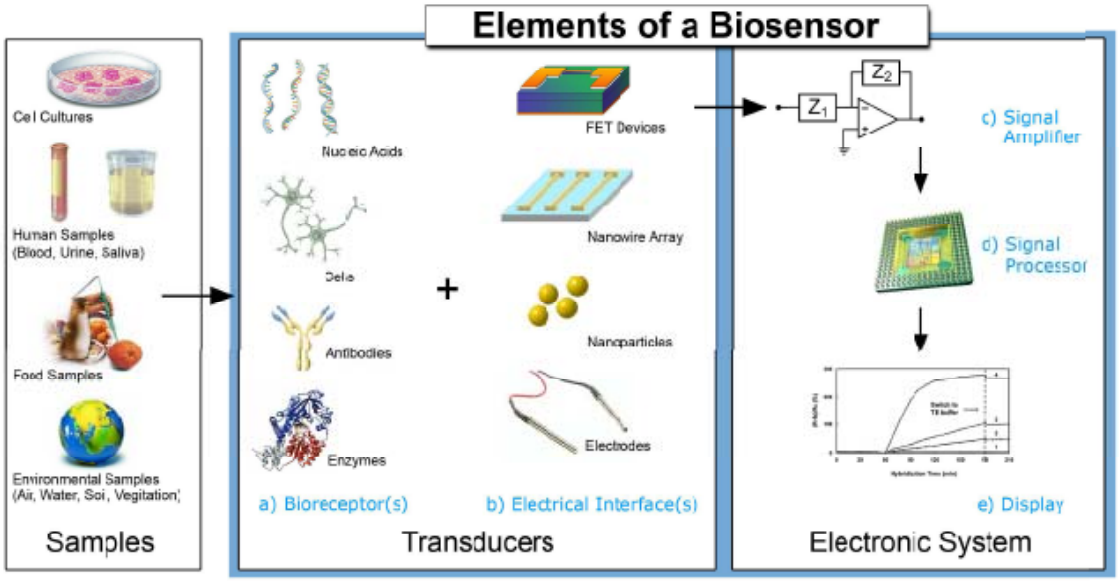

Figure 1.1 - Illustration of the elements composing a biosensors: bio-receptors and interfaces act as detectors and transducers, leading to the signal that determine the measurement.

Most recently developed biosensor techniques account ImmunoAssay Multi-Photon Detection (IA-MPD) [3-4], fiber-optics [5], piezoelectric biosensors based on Quartz Crystal Microbalance (QCM) [6], Surface Plasmon Resonance (SPR) [7] and immuno-PCR [8-9], require complex amplification schemes. IA-MPD are extremely sensitive, but involve multi-step protocols and require skilled laboratory personnel. Most fiber optic biosensors require pre-enrichment or amplification of the sample, because the target species is typically present in concentrations below the limit of detection. QCM is a disk-like device that uses a crystal at a particular resonance frequency in the thickness shear-mode QCM analysis is not very sensitive (10-8 g/Hz) and, therefore, is of limited use when the target is present at low concentrations and/or with a high level of contaminants. SPR usually requires some sample preparation and is limited by low sensitivity (ng/mL) and poor specificity in complex matrices with a high degree of background noise. PCR methods require amplification, have a high cost, and require skilled personnel.

In this scenario, cantilever-based biosensors provide an alternative method for detecting biological targets. Commercial cantilevers constructed of silicon, silicon nitride, or silicon dioxide are available in a variety of shapes, dimensions, and force sensitivities [10]. Recent developments, consisting in improvement of the design, have decreased the length of silicon-based cantilevers to the micrometer or nanometre scale to increase overall mass sensitivity [11-14]. The smaller

cantilevers result in liquid behaviour dominated by a low Reynolds number (Re<1) and, therefore, are critically damped. Changes in medium visco-elasticity or total mass can shift the cantilever's resonance frequency. A more viscous medium or added mass damps the cantilever's oscillation and lowers the resonance frequency, while attenuating the peak sharpness, or quality factor (Q), to about 1 [15]. Therefore, a majority of measurements made with nano- and micrometre scale cantilevers are made in air or vacuum. Silicon-based cantilevers rely on traditional transduction modes, such as thermal stresses and the addition of mechanical energy, to convert the recognition event into micromechanical motion. These transduction modes generate vibrational motion that is damped in liquid. Mechanical energy can be provided by piezoelectric material, that changes its dimensions when stressed electrically by a voltage and generates an electric charge when stressed by a force, i.e. piezoelectric actuators convert electrical energy to mechanical energy, and piezoelectric sensors convert mechanical energy into electrical energy. The switch from QCM, which operates in the shear resonance mode, to cantilever geometry, which operates in the bending resonance mode, produces a more sensitive device without the associated loss of sensitivity.

Table 1 summarise currently used measurement techniques for biologics in complex media and their mass-change sensitivities. Although the technology exists to detect the presence of low concentrations of biologics, a method is needed that can detect fg/mL to pg/mL concentrations in a complex liquid without complicated sample preparation or use of labelled reagents.

Detection Limits of Various Protein and Cellular Detection Platforms

Target	Platform	Measurement Technique	Range / Sensitivity
Protein	Optical	Au nanoparticles	~ 5 ng/mL
	Optical	Au nanoshells	0.88 ng/mL
	Optical	Surface plasmon resonance (SPR)	~1 pM (0.2 ng/mL)
	Optical	Immunoassay multi-photon detection (IA-MPD)	fg/mL
	Optical	ELISA	pM range
	Optical	Super-ELISA	50 fg/mL
	Optical	DNA-encoded antibody libraries (DEAL)	10 fM
	Mechanical / Optical	Microcantilever	0.2 ng/mL

Cell	Optical	Miniaturized SPR	8.7 x 106 CFU/mL
	Optical	Waveguide Biosensor	10 cells
	Optical	SPR Sandwich Assay	103 CFU's
	Optical	Fiber Optic Biosensors	5.2 x 102 CFU/mL
	Optical	Immunomagnetic Beads	10-3 – 10 4 CFU/mL
	Piezoresistive	Quartz Crystal Microbalance	1.7 x 105
		Polymerase Chain Reaction (PCR)	1.3 x 104 CFU/mL
	Piezoelectric	Microcantilever	140 pg/Hz
	Piezoelectric	Nanoelectromechanical systems	1 fg/Hz

Table 1.1 – Measurement techniques for proteins and cells in complex media and their mass-change sensitivities

1.2. Cantilever Biosensors

The opportunity to operate with very small quantities of material and to skip fluorescent labelling are in general the striking advantages of micro and nano-cantilever based biosensors. Their working principle is simple: the MC is functionalized with a proper probe which can selectively bind to the target molecule. The functionalized MC is subsequently placed into an environment containing the target. The interactions between the binding sites of probe and target change the mechanical response of the MC system. Readout of this variation is at the base of the transduction mechanism. Probe/target interactions sort two main effects on the MC system: mass change and bending, the last being due to the surface stress generated by the changes in Gibbs free energy upon chemical species interaction [16-17]. The principal modes of operation of MC biosensors derive from the monitored effect and are therefore mainly two [18]. In this project the way of detection is to exploit the oscillation properties of the MC, and it is usually called dynamic mode or microbalance mode. The resonant frequency of a cantilever is dependent, in first approximation, on its stiffness, mass and geometry. Changes of the cantilever mass or spring constant due to molecule absorption will induce a frequency shift. Therefore, in this mode detection is performed by tracking the shift of the resonant oscillation frequency of the MC during (or after) selective absorption of

target molecules [11, 19-24]. There are several advantages with this approach. The sensitivity of dynamic mode is potentially higher than for static mode, as witnessed in the last two years by successful experiments that culminated in pushing the state-of-the-art down to single virus detection i.e. to a mass of few femtograms [25-26]. Calculations predict an improvement of sensibility that touches the single molecule level (zeptograms). Finally, this method allows both in-situ and ex-situ measurements (with respect to the target environment). By developing the model that governs the MC oscillation it is potentially possible to get more than simple on-off sensing information. Actually, molecular layers immobilized onto the MC surface change the total mass of the system as well as its spring constant. Thus by more sophisticated analysis of the MC oscillation one might gain insight into the physical chemistry of the system, including layer density and molecular interactions. As it emerges from the state-of-the-art, MC based molecular recognition presents a number of challenges that the scientific community has just started to face. Those are the requirements for the development of mass detector biosensor based on MC systems that would permit to shift from qualitative data to quantitative measurements of key molecules involved in physiological processes.

1.3. Detection mechanisms of microcantilever sensors

After the invention of AFM it was discovered that the thin silicon beams used for scanning surfaces can act as excellent probes also without tips [27]. Analogous to contact and non-contact modes in AFM, cantilever-based sensors involve measurements of deflections, resonance frequencies and, in some cases, damping characteristics. However, as shown in the following scheme (Figure 1.2), chemical, physical and biological sensing is based on transductions mechanisms which differ from the one used in SPM instruments [28].

Depending on the measured parameter (cantilever deflection or resonance frequency) the operation mode in principle can be referred to as either static or dynamic. Each of these modes, in turn, can be associated with different transduction scenarios. Static cantilever deflections can be caused by either external forces exerted on the cantilever (as in AFM) or intrinsic stresses generated on the cantilever surface or within the cantilever. While cantilever microfabrication technology is capable of producing nearly stress-free suspended beams, additional intrinsic stresses may subsequently originate from thermal expansion, interfacial processes and physicochemical changes.

On the other hand, cantilever sensors operating in dynamic mode are essentially mechanical oscillators, whose resonance characteristics depend upon the attached mass as well as viscoelastic

properties of the medium. [29]. For instance, adsorption of analyte molecules on a resonating cantilever results in lowering of its resonance frequency due to the increased suspended mass of the microbeam [30]. Depending on nature of the input stimuli, microcantilever sensors can be referred to as physical, chemical or biological sensors. The variety of transduction modes stems from the fact that a stimulus of each type may affect the mechanical state of the transducer directly or may undergo one or several transformations before the measured mechanical parameter of the transducer is affected.

In the followings the main properties of the two operating modes (static and dynamic) are separately analyzed, and the possible applications and what kind of information it is possible to extract from each modality are described.

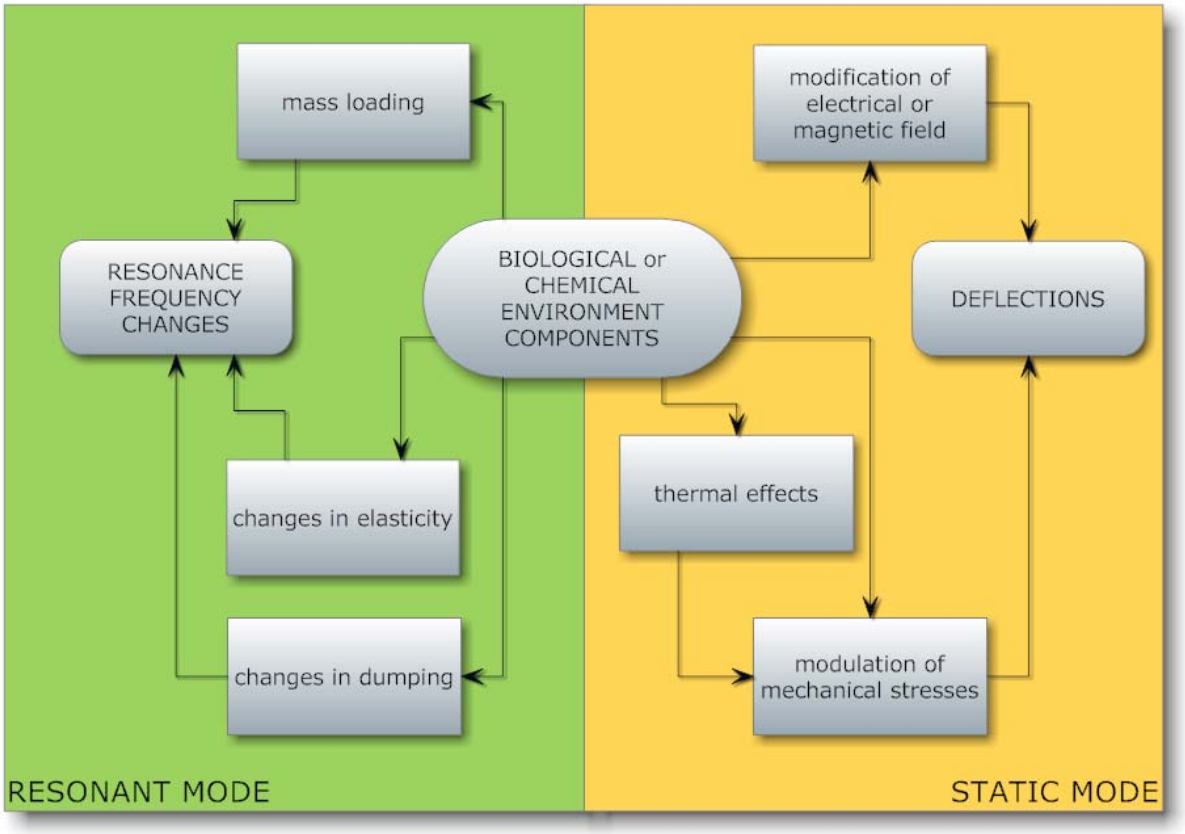

Figure 1.2 - Scheme of the transduction mechanisms for cantilever sensors. The operation mechanisms can be divided on static and dynamic (resonant) mode.

1.3.1 Static mode

The first operating mode of cantilever as a sensor is the so-called static mode. In this mode a beam deflection is revealed and associated with the beam interaction with external (physical, mechanical, chemical, biological) stimuli (see Figure 1.3). In the absence of external gravitational, magnetic and electrostatic forces, cantilever deformation is unambiguously related to a gradient of mechanical stress generated in the device. Depending on a particular origin of this stress, analytical models suitable for quantitative analysis of microcantilever responses may or may not be available.

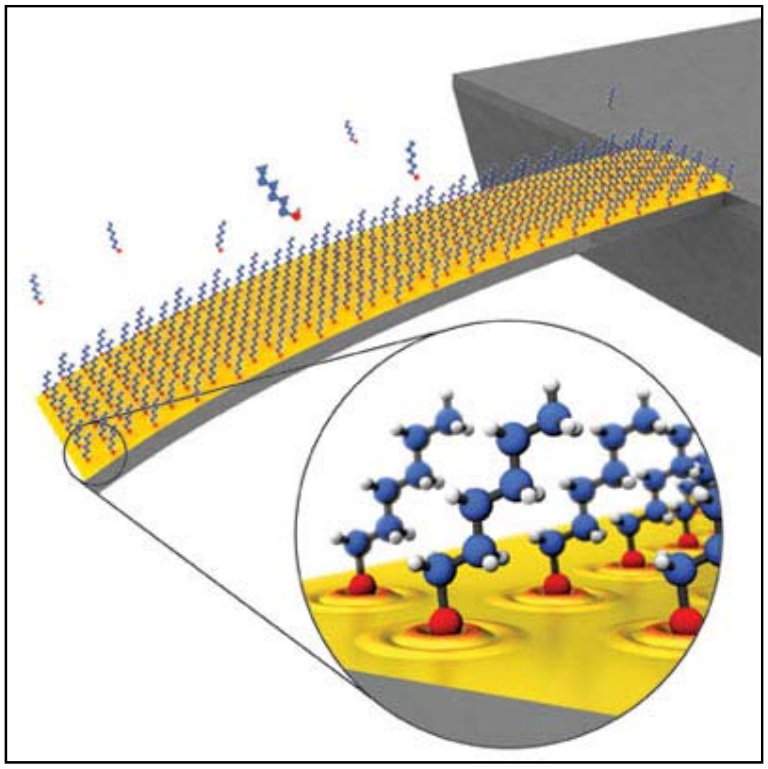

Figure 1.3 - Scheme of a cantilever sensor based on the static mode detection. A DNA hybridization experiment in shown in the drawing: the sensor output is the cantilever deflection [31]

A first simple example of this operation mode is temperature measurement using the bimetallic effect: a cantilever made by two layers of different materials is sensible to temperature variations, because the different thermal expansions of the two layers cause a thermally induced stress and a consequent static deflection of the beam. An analytical evaluation of the problem is reported by Weaver [32], who gave an expression for the radius of curvature of a bi-material cantilever as a function of materials and temperature variation. While the objective of Weaver's original work was

only the evaluation of temperature effects on a thin suspended structure, it has to note that similar phenomena can give a lot of information in the field of chemical detection. In fact, a strain-induced deformation is an important response mechanism on cantilever based chemical sensors, in which a chemically selective layer undergoes expansion upon interaction with its chemical medium [33], and in general for the monitoring of every exothermal surface reaction. Molecular adsorption processes and interfacial chemical reactions may also affect mechanical stresses in thin plates more directly and independently of thermal effects. It has been known since the 1960's that molecular and atomic adsorbates on atomically pure faces of single crystals tend to induce significant surface stress changes. Long before the first microfabricated cantilevers were created, changes in surface stresses in simple systems have been studied by measuring minute deformations of relatively thin (up to 1 mm) plates (the beam-bending technique) [34]. The mathematical model to relate the surface stress and the related variation of the surface free energy is provided by the Shuttleworth equation

$$\sigma = \gamma + \left(\frac{\partial \gamma}{\partial \varepsilon} \right) \qquad (1.1)$$

σ is the surface stress (N/m), γ is the surface free energy (J/m2) and dε is the surface strain, defined as the relative change in surface area (dε=dA/A). For a simple demonstration of Eq.(1.1), see for example ref. [35]. Fundamental understandings of adsorption and absorption-induced mechanical phenomena had limited implications for chemical sensors until mass produced AFM microcantilevers became widely available. As compared with their macroscopic redecessors, microcantilevers coupled with the optical lever readout greatly simplify and improve sensitivity on real-time measurements of surface stress changes. Cantilevers intended for use as chemical sensors are typically modified so that one of the sides is relatively inert while the other exhibits high affinity to the targeted analyte. In order to understand how different modifying coatings provide responses of cantilever sensors in the static bending mode, it is useful to consider three distinctive physical models (stresses related to pure surface effects, to bulk effects or a combination of the two). The first model is most adequate when interactions between the cantilever and its surrounding environment are predominantly surface phenomena. Adsorption of analyte species on transducer surfaces may involve physisorption (weak bonding, with binding energies smaller than 0.1 eV) or chemisorption (stronger bonding, binding energies greater than 0.3 eV). Physisorption is associated with van der Waals interactions between the adsorbate and the adsorbent substrate. As the analyte species approach the surface, they can polarize the surface creating induced dipoles which cause the weak bonding. Much higher binding energies are characteristic of chemical bonding between the

analyte and the surface in the case of chemisorption. In general, changes in surface stresses can be largely attributed to changes in Gibbs free energy associated with adsorption processes. An example of this situation is showed in Figure 1.4, where chemisorption of straight-chain thiol molecules on a gold coated cantilever is schematically depicted. Since spontaneous adsorption processes are driven by an excess of the interfacial free energy, they are typically accompanied by the reduction of the interfacial stress. In other words, surfaces usually tend to expand as a result of adsorptive processes. This type of surface stress change is defined as compressive, referring to a possibility of return of the surface into the original compressed state. The opposite stress change (with a contraction of the surface) is defined as tensile. The larger the initial surface free energy of the substrate, the greater the possible change in surface stress results from spontaneous adsorption processes. Compressive surface stresses have been experimentally observed on the gold side of gold coated cantilevers exposed to vapor-phase alkanethiols [36]. The mathematical model usually adopted to relate the surface stress formation and the consequent cantilever bending is based on the Stoney's formula

$$\frac{1}{R} = \frac{6(1-\nu)}{Et^2}\Delta\sigma \qquad (1.2)$$

Here R is the radius of curvature of the bent structure (supposed as a constant for all the beam), ν and E are the Poisson's ratio and the Young's modulus of the beam material, t is the cantilever thickness and finally $\Delta\sigma$ is the differential surface stress (the stress difference between the two main cantilever surfaces).

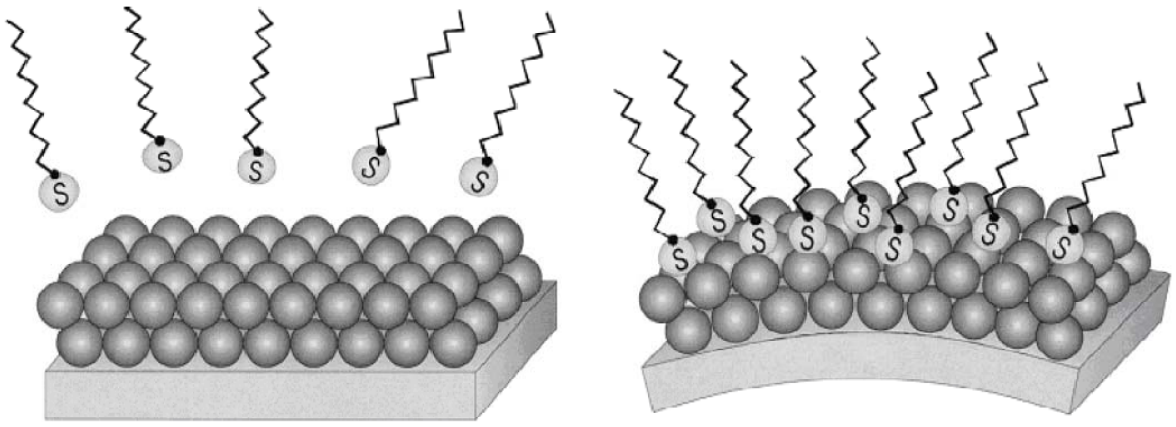

Figure 1.4 - Interaction between a gold-coated surface and straight-chain thiol molecules. The spontaneous chemisorption process produces a reduction of the interfacial stress (compressive stress), reflected on a cantilever bending.

It is possible to relate the radius of curvature with the displacement Δz of the cantilever free end, as:

$$\Delta z = \frac{1}{2}\frac{l^2}{R} = \frac{3l^2(1-\nu)}{Et^2}\Delta\sigma \qquad (1.3)$$

Eq.(1.2) can be obtained directly from the definition of surface stress and its relation with the surface strain [79]. Many assumptions have to be imposed to draw out Eq.(1.2). First of all, the cantilever bending has to be very small, so the coordinates are maintained during the bending process. Furthermore this relation is valid only for an oblong structure (e.g. $l>>w>>t$, where l, w and t are length, width and thickness of the beam respectively). This formula is appropriated to study surface adsorption, so it is valid only if the thickness of the surface region is of the order of several atomic layer and therefore negligible in comparison with t. The bending is assumed to be only along the z direction (normal to the main surfaces of the plate). Finally, the holder does not exert any force on the cantilever. This formula can also be derived from the minimization of the work performed during the bending process [37].

It is worth noting that the limitations of the Stoney's formula listed above are not so restrictive (a cantilever is by definition an oblong structure and the cantilever deflection is always revealed and measured at the free end of the beam, which is the most distant point from the clamp). So, a general conclusion is that this formula can be considered valid and reliable for the comparison with the experimental data. Therefore, up to now the use of cantilever bending method combined with the Stoney's formula is considered the only reliable experimental method to measure (relative) surface stresses. Anyhow with this method it is only possible to obtain a relative stress evaluation, not an absolute value for the stress on one side of the beam. Some experimental methods to measure absolute surface stress are proposed in literature [38], but none of them can be considered as a reliable and sure method to obtain such physical quantity. Being the Stoney's formula approximate, many works have been done trying to improve the model. For example, Sader [39] presents a series of generalizations of the Stoney's formula, to avoid the imposition of many restrictive conditions in the theory. A series of analytic equation are presented, in different asymptotic case as a function of the ratio l/w. The second model of analyte-induced stresses is applicable for a cantilever modified with a much thicker than a monolayer analyte-permeable coating. Taking into account interactions of the analyte molecules with the bulk of the responsive phase, a predominant mechanism of cantilever deflection can be described as deformation due to analyte-induced swelling of the

coating. Such swelling processes can be quantified using approaches developed in colloidal and polymer science. Depending on whether it is more appropriate to describe the responsive phase as solid or gel-like, these altered forces can be put into accordance with, respectively, stress or pressure changes inside the coating. An in-plane component of this change multiplied by the coating thickness yields an apparent surface stress change that can be used in Stoney's model - Eq.(1.2)- in order to estimate deflections of a cantilever coated with thin, soft, responsive films. It is important to note that the magnitude of apparent surface stress scales up in proportion with the thickness of the responsive phase.

The third model is most relevant to nanostructured interfaces and coatings: analyteinduced deflections of cantilevers with structured phases combine mechanisms of bulk, surface, and inter-surface interactions. A combination of these mechanisms facilitates efficient conversion of the energy of receptor-analyte interactions into mechanical energy of cantilever bending. Recent studies demonstrate that up to two orders of magnitude increases in cantilever responses can be obtained when receptor molecules are immobilized on nanostructured instead of smooth gold surfaces [40]. With the increasing amount of energy released during the interaction there are not any analytical model (such as the Stoney's model) to interpret the experimental data in the general case. It is to underline that, even in the first model (in which a theoretical formula has been presented), static measurements give a qualitative point of view of the surface interactions. From these kinds of measurements it is possible to study specific interactions between target molecules and functionalized surfaces, but there is no way to quantify how many molecules have been detected. Thus, biological and chemical sensors based on static mode operation can supply only "on/off" measurements, but they do not allow a real (absolute) quantification of the substances which are interacting with the surface. The surface stress induced by single atom adsorption on microcantilevers surface has been studied either experimentally and by means of finite element analysis [41]. However, when dealing with, as it is often the case for biosensors, there is a number of other possible surface stress sources, than simple ion adsorption onto a crystal surface, such as: electrostatic interactions among neighboring biomolecules, conformational changes of the adsorbed molecules, Hydration forces, changes in surface hydrophobicity. Those interactions may all induce stresses on the cantilever surface, which may contrast with each other. In Wu et al [42], it has been observed that DNA hybridization upon a microcantilever surface, which has previously been functionalized with single strand DNA, may cause either a reduction or an increase in the compressive surface stress, and thus in the cantilever deflection, depending on the ionic strength of the buffer solution in which the hybridization takes place. This behaviour has been interpreted as the interplay between two opposite driving forces: a reduction of the DNA configurational entropy

after the hybridization, which tends to lower the surfaces stress, and the increasing electrostatic repulsion among DNA fragments, which tends to increase the surface stress. On the other hands, a measurement based on static deflection is quite independent from the external conditions (if some parameters, like temperature for example, are controlled in a strong accurate way; also the measuring of differential variation within an array of cantilevers with a different surface functionalization is a common way to take into account and differentially eliminate the effects of environmental variations on beam deflection). Thus static operation mode is a good candidate to perform measurements both in gas and in liquid environment, and real-time measurements in liquid are very interesting for a wide range of applications.

1.3.2 Dynamic mode

The dynamic operation mode (see Figure 1.5) will be the core of the experimental part of this dissertation, therefore in this section the main features and physical detection principles are resumed.

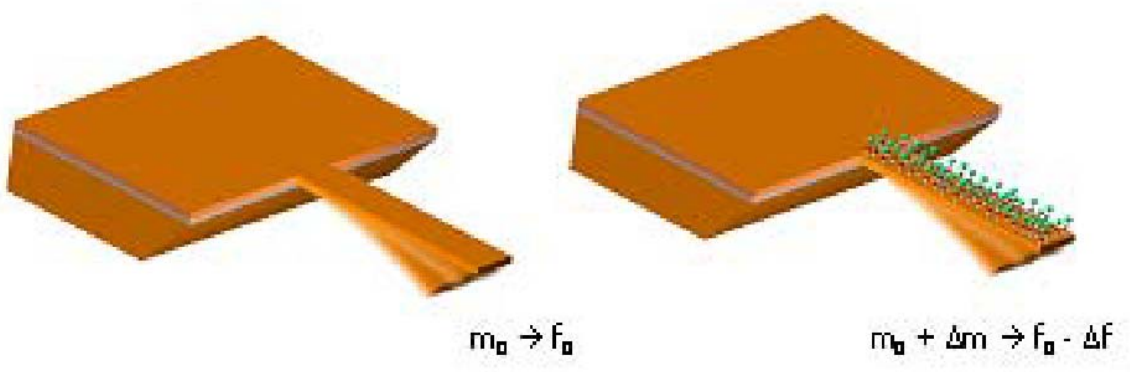

Figure 1.5 – Operation scheme of a cantilever sensor based on dynamic operation mode. Mass variation of the oscillator is relate to changes in resonance characteristics of the structure

Cantilever transducers vibrating in gases or in vacuum can be treated as weakly damped mechanical oscillators. A good approximation for the motion of the free end of the beam is to consider the displacement as directly proportional to the force extended to the cantilever tip (linear regime described by the Hooke's law). In such harmonic approximation, the resonance condition can be evaluated as:

$$f_n = \frac{1}{2\pi}\sqrt{\frac{k}{m*}} \qquad (1.4)$$

The vibration characteristics depend on the mass of the oscillator, so a mass variation Δm is reflected on a consequent variation of the resonance frequency Δf. Considering a spring constant k which is independent from the mass variation, the two parameters can be related with a simple formula:

$$\frac{\Delta m}{m} = -2\frac{\Delta f}{f_n} \qquad (1.5)$$

Using Eq.(1.5) it is possible to quantify the amount of mass adsorbed during a chemical/biological interaction procedure. In this respect, dynamic operation mode is a powerful tool for quantitative measurements, which can be very useful in a lot of applications, especially in biological studies.
Eq.(1.5) is founded on important assumption, i.e. the spring constant of the beam remains the same before and after mass change. In other words, surface stress related to external molecules adsorptions is assumed to not affect the cantilever rigidity. It is well established from the static analysis and from theoretical works that formation of a surface adsorbed layer is accompanied by a change in surface stress. If the surface stress influences the spring constant k, Eq.(1.5) cannot be written and a gravimetric evaluation of surface adsorbates with this simple model becomes non-applicable. It is an open question to understand if this "static" surface stress influences the dynamic properties of the beam. Also this topic will be faced in the next Chapter of this work.
The cantilever vibration is also influenced by the surrounding medium in which the vibration occurs. For example, the drag force related to the surrounding gas has an influence on cantilever vibration characteristics. Obviously, the more dense is the medium in which the vibration occurs, the more difficult is the movement of the vibrating plate. In other terms quality factor of the oscillator will be lower for vibrations in a more dense fluid. This simple fact suggests the idea that a sensor based on oscillating cantilevers find a more difficult application for measurements on a liquid environment. However, in the last years both the increasing interest in biosensors to carry out the measurement in real-time and consequently in liquid and the exigency to extend the SPM techniques to liquid environments has motivated several work about the enhancement of quality factor [43]. A method for the digital control of the oscillation in liquid has been reported [44] and it

has been shown that the quality factor can be increased by two order of magnitude for vibration in liquid with an electronic control.

1.4. Application of Cantilever Sensors

Microcantilevers have been demonstrated to be excellent physical (temperature, pressure, viscosity), chemical, and biological sensors. Their small size and ability to target specific molecules make microcantilevers particularly. The mechanism of detection in cantilever resonance systems is the shift in resonance frequency resulting from the addition of a bound mass. By altering the surface to allow selective binding, a microcantilever can be designed to detect a targeted species with extreme sensitivity. To date, cantilevers have been successfully used to detect viable cells, virus particles, pathogens, proteins, toxins, DNA molecules, and other chemicals at various concentrations in and out of liquid systems [8, 10, 18, 41, 45]. Sensitivity with respect to limit of detection and selectivity in complex matrices have been the major limitations.

1.4.1. Proteins

Cantilever sensors have been developed to measure concentrations of various proteins in vacuum, air and liquid environment.

Wee et al. [46] utilized a thin-film piezoresistive silicon microcantilever for detection of label-free disease marker proteins. The sensors were cleaned, immobilized with a self-assembled monolayer capable of recognizing the ammonium ions of protein, and unreactive sites were blocked with bovine serum albumin. After immobilization, C-reactive protein (CRP) and prostate specific antigen (PSA) were injected at three different concentrations: 10 ng/mL, 100 ng/mL, and 1 μg/mL. The change in sensor resistance was measured as a function of voltage across a Wheatstone bridge, gradually increased over time for the three PSA solutions. Fluorescently tagged PSA showed increasing intensity in Ag-Ab binding proportional to increasing concentration. Similar results were obtained for various concentrations of CRP; however, the response of the cantilever to CRP was not as sensitive as the response to PSA.

A nanomechanical PZT cantilever, 100 μm wide, 300 μm long, and 2.08 μm thick, was used to detect myoglobin without the use of labelled reagents [47]. Streptavidin (10 μg/mL) in PBS was immobilized on the sensor surface, and surface was then passivated with bovine serum albumin (BSA). Biotinylated monoclonal antibody to myoglobin (10 μg/mL) was incubated with the streptavidin immobilized cantilever surface. The sensor was then exposed to 1 μg/mL, 100 ng/mL, 10 ng/mL, and 1 ng/mL solutions of fluorescently tagged myoglobin antigen and changes in

resonance frequency were monitored. The fluorescence image showed an increase in confocal intensity as a function of antigen concentration, while the resonance negative shift increased with increasing antibody concentration. The results indicated that the biosensor could detect proteins on the order of 1 x 10^{-8} g/mL.

Shekhawat et al. [48] embedded a metal-oxide semiconductor field-effect transistor (MOSFET) into the base of a silicon nitride cantilever to record decreases in drain current. This modification allowed for detection of deflections as small as 5 nm. The cantilever was cleaned, functionalized with a linker molecule, and streptavidin (10 μg/mL) was immobilized overnight. The nonspecific binding sites were blocked with BSA. The functionalized cantilevers were then exposed to biotin in PBS at concentrations of 100 fg/mL, 100 pg/mL, and 100 ng/mL. The resulting decrease in drain current, due to microcantilever bending as a result of biotin binding, was inversely proportional to the biotin concentration. Similar results were obtained when a cantilever functionalized with rabbit IgG was exposed to goat antibody to rabbit IgG.

Lee et al. [22] utilized a monolithic PZT thin film microcantilever for the label-free detection of a fluorescently-labelled, C-reactive protein (CRP). The sensors were cleaned, gold coated, and immobilized with a self-assembled monolayer capable of recognizing the ammonium ions of protein. The resonance frequency shift was monitored after CRP was introduced to the antibody immobilized sensor surface. The results indicated that resonance frequency decreased due to CRP binding. The frequency change increased with higher antigen loading, and the limit of detection was estimated to be in the nanomolar range.

An array of eight silicon microcantilevers were functionalized with single-chain Fv (scFv) antibody fragments as receptor molecules for detecting cysteine residues [49]. The sensors were cleaned and coated with titanium and gold in a vacuum chamber then exposed to the scFV fragments (100 μg/mL) for 30 – 60 minutes at room temperature. Protein solutions were injected at a flow rate of 40 μL/min and the binding event was monitored for one hour. Deflection of the cantilever detected the antigen in the 1 nM range, approximately three orders of magnitude more sensitive than the 1 μM detection limit previously reported for the cardiac marker, myoglobin, using a similar cantilever- based instrument and a full-chain antibody [50]. Changes in deflection of a biotinylated, v-shaped silicone nitride cantilever were used for monitoring the binding of streptavidin [51]. The sensor was gold coated, then incubated for 2 hours in a 1 mM solution of biotin thiol in ethanol. A 10 nM streptavidin solution in PBS was injected into the flow cell, and the response of the sensor was recorded. The bending of the sensor as a result of the binding event depended on the biotin-modified surface. When streptavidin was introduced, biotin-HPDP cantilevers bent downward, biotin-SS-NHS cantilevers bent upward, and biotin-PEG cantilevers did not bend. The authors

hypothesized that the charge difference between the biotin-PEG and biotin-SS-NHS surfaces, as well as the well packed monolayers on the bioten–PEG surface, caused the different nanomechanical responses. The limit of streptavidin detection on the biotin-HPDP sensor was between 1 and 10 nM.

Campbell et al. [21] used a self-excited PZT-silica glass cantilever to monitor the binding and unbinding of model proteins in PBS. The cantilever was 3 mm long, 1 mm wide, and ~ 300 μm thick. The sensor was cleaned and aminated to add free amine terminals for reaction with the carboxylic groups in the target antibodies. Solutions of anti-Group A *Streptococcus pyrogenes* (GAS), rabbit IgG, and anti-*E. coli* O157:H7 were prepared at concentrations of 1 and 0.1 mg/mL. The resonance frequency of the functionalized cantilever was monitored while the sensor was immersed in protein solutions for one hour. Resonance frequency changes of ~550 and 1800 Hz were obtained for anti-EC concentrations of 0.1 and 1.0 mg/mL, respectively. Similarly, 1.0 mg/mL of anti-GAS gave a higher resonance frequency shift than the 0.1 mg/mL solution. When the sensor was exposed to rabbit IgG at a concentration of 0.1 mg/mL, the resonance frequency decreased by approximately 300 Hz. After binding rabbit IgG, the cantilever was exposed to 0.1 mg/mL biotin-conjugated anti-rabbit IgG, and the resonance frequency decreased ~ 280 Hz. Exposure of the sensor surface to 0.1 mg/mL captavidin caused the steady state resonance value to decrease an additional 500 Hz. The binding events were confirmed by releasing the captavidin and anti-rabbit IgG with a low pH buffer. Campbell et al. also used a piezoelectric-excited millimetre-sized cantilever to detect *Staphylococcus* enterotoxin B (SEB) in buffer [52]. The cantilever was cleaned and aminated, and antibody specific to SEB was immobilized to the surface. The prepared sensor was inserted into a liquid flow cell, and the resonance frequency was stabilized in PBS at a flow rate of 1 mL/min. Antigen solutions containing 50 pg/mL, 200 pg/mL, 1 ng/mL, and 50 ng/mL SEB were recirculated past the sensor in a stepwise fashion until the resonance frequency reached new steady states. The binding event was confirmed by releasing the antigen with a low pH solution. The detection limit of the PEMC sensor to SEB was between 12.5 and 50 pg/mL. Dauksaite et al.[46] used a piezoresistive array platform with electrical readout for protein detection using glutathione-S-transferase (GST) and GST antibodies. The sensors were used to detect the static surface stress that arises when the protein interacts with the immobilized molecules on the device surface. The sensor was functionalized with GST antibodies, and GST diluted in PBS was introduced in increasing concentrations (0.1, 1, and 10 μg/mL). No significant signal was received for 0.1 μg/mL GST; however, both 1 and 10 μg/mL solutions gave a measurable response.

Other studies used Wheatstone bridge circuits in conjunction with microcantilevers to detect IgG (0.225 μM) and egg albumin (4.4 μM). A mass sensitivity ~ 200 fg/Hz was reported for a partial

immersion detection method[49]. A biosensor composed of a microcantilever and a piezoelectric PZT film was used to detect human insulin-antihuman insulin binding. The device was 100 μm in length, 30 μm in width, and 5 μm in thickness, with a PZT film 2.5 μm thick and 50 μm long. A 217 Hz frequency shift was noted using a self-oscillating circuit when the human insulin was attached to the antibody immobilized on the sensor surface. The experimentally determined mass of insulin binding protein was 0.595 x 10^{-15} g, compared to the calculated mass of 0.458 x 10^{-15} g. Microfabricated cantilever sensors have also been also used for detecting other protein biomaterials, such as Taq polymerase[51] and BSA [53]. The experiments were conducted under batch aqueous conditions and used different detection systems than those described above.

1.4.2. Pathogens

Cantilever sensors have been developed to detect a variety of pathogens.

Capobianco et al. [54] used (PMN-PT)/Sn piezoelectric microcantilever sensors to detect pathogens in phosphate buffered saline (PBS). The sensors were constructed from 22 μm thick, free-standing PMN-PT films, with a 15-30 nm chromium/nickel bonding layer, a 4-μm tin layer, a 150 nm platinum layer, and a 10 nm titanium bonding layer. The sensor was 725 μm long and 750 μm wide. The sensor was electrically insulated, then antibody to *E. coli* O157:H7 was immobilized to the surface. Detection experiments were carried out in a flow cell at 0.5 mL/min. Resonance frequency shifts of 1,650, 1,300, 600, and 200 Hz were obtained for *E. coli* suspensions of 10_6, 10_4, 10_3, and 10_2 cells/mL, respectively, in pure PBS, with a 75 Hz standard deviation. Mass-change sensitivity was estimated to be of 3 pg/Hz. A bulk micromachined, low-stress silicon nitride cantilever was used to detect *E. coli* cell-antibody binding events[15]. The sensors varied in length (15-400 μm) and width (5-50 μm), with a constant thickness of 320 μm. The devices were actuated utilizing thermal mechanical noise and the change was monitored via optical deflection. Affinity-purified goat anti-*E. coli* O157:H7 was coated on the sensor surface by a 5 minute immersion in a 1 mg/mL solution. The cantilevers were then rinsed with deionized water and dried in nitrogen. The immobilized sensors were immersed for 15 minutes into solutions of *E. coli* O157:H7 ranging from 10_5 to 10_9 cfu/mL, rinsed, and dried. Resonance frequency spectra were taken before and after antibody and cell exposure. The experiments showed a shift of 4.6 kHz due to the immobilization of a single cell calculated as 665 fg, which is consistent with other reported values. The mass-change sensitivity of the device was estimated to be 1.1 and 7.1 Hz/fg, respectively, for cantilevers 25 and 15 μm long.

Ilic et al. [55] also used an array of bulk micromachined resonance cantilevers for detecting bound *E. coli* O157:H7. Signal transduction of the devices was accomplished by measuring the out-of-plane vibrational resonance mode using an optical deflection system. The two cantilevers had

dimensions of 100 to 500 μm in length, and 320 to 600 nm in thickness. The cantilevers were antibody immobilized, then immersed in *E. coli* solutions ranging from 10_6 to 10_9 cells/mL at room temperature for 15 minutes, rinsed, and dried. Resonance frequency spectra were taken before and after cell exposure. In the range where the total cell mass is much smaller than the mass of the oscillator, the frequency shift was linearly related to cell mass. No resonance frequency shift occurred in a positive control (non-antibody immobilized sensor in cell solution). The sensitivity of the two cantilevers was estimated to be 5.12 and 6.81 Hz/pg for the small and large sensors, respectively.

A surface-stress based, v-shaped silicon microcantilever was developed for the *in situ* detection of *E. coli* O157:H7. The deflection due to increased mass was detected optically. Following covalent immobilization of the antibody, the sensor was inserted into a flow cell at 20°C. After the sensor was exposed to 5 x 10^6 cfu/mL *E. coli,* the microcantilever immediately bent down, due to capture of the *E. coli*. When the cell solution was replaced by buffer, the cantilever remained bent due to the added mass, which ruled out physical adsorption. The reference sensor showed little or no deflection when exposed to the *E. coli* sample. The sensor's limit of detection was estimated to be 1 x 10^{-6} cfu/mL. When the data were fit to a Langmuir model, the reaction rate was calculated as 2.3 x $10^{-4\ s-1}$.

Campbell et al. [20] used a composite, self-excited lead zirconate titanate (PZT)- glass cantilever to detect the pathogen, *E. coli* O157:H7, in buffered salt solutions. Two cantilevers, 5 and 3 mm in length, 1.8 and 2.0 mm in width, and ~340 μm in total thickness were used. The device was fabricated using a PZT sheet bonded to a 50 μm-thick stainless steel layer and a 160 μm glass cover slip. The stainless steel film served as the bottom electrode while a top electrode was attached directly to the thin PZT film. The cantilever was actuated using a excitation voltage of 100 mV generated by an impedance analyzer. The glass surface was aminated, and a monoclonal antibody to *E. coli* O157:H7 was covalently linked. The antibody immobilized sensor was submerged in various concentrations of the pathogen. A non-pathogenic strain of *E. coli* (JM101) was used to determine sensor selectivity. The frequency responses of the cantilever to *E. coli* O157:H7 at concentrations of 7 x 10^2, 7 x 10^4, 7 x 10^6, and 7 x 10^7 were approximately 600, 400, 280, and 180 Hz, respectively. Lower concentrations of *E. coli* O157:H7 resulted in a longer time for the system to reach steady state. Visual confirmation was provided by scanning electron micrography, and secondary confirmation was provided by low pH release of the bound cells. When the total cell count held constant, a mix of pathogenic and non-pathogenic strains resulted in a lower resonance frequency shift than a purely pathogenic sample. In the absence of the pathogenic strain, the resonance frequency shift was ~ 0 Hz.

A surface-micromachined cantilever beam-based resonator was used by Gupta et al. [56] to detect the mass of the bacterium, *Listeria innocua*. A novel technique was developed to fabricate thin low-stress, single-crystal cantilever beams. Thermal and ambient noise were used to actuate the cantilever beams, and the resulting vibration spectra were measured in air. Bacterial suspensions in concentrations ranging from 5 x 10^6 to 5 x 10^8 cells/mL were introduced to the antibody immobilized sensor surface. Bovine serum albumin was used as a blocking agent to prevent nonspecific binding, and Tween-20 in PBS was used to remove loosely bound bacteria. The resonance frequency was measured after immobilization using antibody plus BSA, and after exposure to the bacterial samples. Attachment of the bacterial cells caused a shift of ~ 500 Hz. The effective number of bacterial cells captured was ~ 62 (based on dry cell estimates of effective mass determinations of 85 fg).

Campbell and Mutharasan used PEMC sensors to detect *Bacillus anthracis* (BA) in batch [57] and flow[58] systems. The sensors were fabricated with a PZT sheet 1.5 mm long, 1 mm wide, and 127 μm thick, and a glass cover clip 3.5 to 4.0 mm long, 1 mm wide, and 160 μm thick. The sensors were immobilized with antibody specific to *B. anthracis* spores, and the sensor was exposed to concentrations ranging from 300 to 3 x 10^6 spores/mL. During the batch experiments, the antibody immobilized sensor was placed on an XYZ positioner and inserted 1 mm into a 1 mL sample of spore solution. The resonance frequency was monitored until a new steady state value was reached. The resonant frequency decreased at a rate proportional to the spore concentration. Exposure to 0, 3 x 10^2, 3 x 10^3, 3 x 10^4, and 3 x 10^6 spores/mL resulted in steady state frequency changes of 5 ± 5 Hz (n=3), 92 ± 7 Hz (n=3), 500 ± 10 Hz (n=3), 1030 ± 10 Hz (n=2), and 2696 ± 6 Hz (n=2), respectively.

The batch method was also used to evaluate selectivity of the antibody-functionalized sensor by exposing the sensors to mixed spore suspensions containing *B. anthracis* and *Bacillus thuringienisis* (BT) in various volume:volume ratios. Resonance frequency decreases of 2345, 1980, 1310, 704, and 0 were obtained for BA:BT ratios of 1:0, 1:125, 1:250, 1:500, and 0:1, respectively. Detection capability of the sensor was also tested in a flow apparatus with 300 spores/mL sample of BA at a flow rate of 1 mL/min. The flow cell held 300 μL and showed small frequency fluctuations at flow rates of 1 to 17 mL/min. The total resonance frequency change was 162 ± 10 Hz (n=2), compared to 90 ± 5 Hz under batch detection. To examine the selectivity of the PEMC sensor, Campbell et al.[59] developed a method for detecting BA spores in the presence of large amounts of BT and *Bacillus cereus* (BC). The sensors were fabricated with a PZT sheet 4.0 mm long, 1 mm wide, and 127 μm thick, and a glass cover slip 1.5 mm long, 1 mm wide, and 160 μm thick. The glass surface was immobilized with rabbit polyclonal antibody to BA. All experiments were carried out at 25°C and a

flow rate of 1 mL/min. The concentration of BA spores was kept constant at 333 spores/mL. The BA:BT+BC concentration ratio of 0:1, 1:0, 1:1, 1:10, 1:100, and 1:1000 resulted in resonance frequency changes of 14 ± 31 (n=11), 2,742 ± 38 (n=3), 3,053 ± 19 (n=2), 2,777 ± 26 (n=2), 2,953 ± 24 (n=2), and 3,105 ± 27 (n=2) Hz, respectively in 0, 27, 45, 63, 154, and 219 minutes. Confirmation of detection was obtained by releasing the spores with a low pH solution. An exponential decrease in attachment rate was observed with increasing BT+BC concentration, and the authors concluded that the observed binding rate constant could be derived from the Langmuir kinetic model Davila et al. [58]used microcantilevers to detect BA spores in air and liquid. The cantilevers were fabricated using silicon-on-insulator (SOI) wafers and standard surface micromachining techniques. The cantilevers had nominal lengths of 100, 75, 50, 40, and 20 μm, and uniform width and thickness of 9 μm and 200 nm, respectively. For air measurement, 20 μL of BA spores (1 x 10^9 spores) were introduced onto the cantilever surface for 4 hours, the chip was dried, and the resonance frequency was measured. For measurements in water, the surface was antibody-immobilized, rinsed, blocked using BSA, and rinsed with Tween to remove loosely bound antibody. The resonance frequency was then determined in air and water. Following another rinse, 20 μL of BA spores (1 x 10^9 spores) were introduced onto the cantilever surface for 16 hours. The chip was dried, and the resonance frequency was again measured in air and water. Using a linear fit of frequency shift versus number of bound spores, the mass-change sensitivity of the 20 μm long cantilever was calculated to be 9.23 Hz/fg and 0.1 Hz/fg, in air and water, respectively.

1.4.3. Virus

In addition ot proteins and bacteria, cantilever sensors have been used to detect viruses.

Gunter et al.61 used piezoresistive microcantilever-based sensors to detect a vaccinia virus in aerosol and solution forms. In these sensors, the piezoresistive microcantilever was embedded in the sensing material, as opposed to the sensing layer being bound to the sensor surface. When the virus was adsorbed, the volume of the sensing material changed and the volumetric change was measured as resistance changes in the microcantilever. The sensing material in this case was a composite of vaccinia polyclonal antibody with the host polymer poly(ethylene oxide) or PEO. In these experiments, 150 mL of water with 2.0 mg/mL virus was aerosolized and combined with nitrogen in a 50/50 mix. The sensor measured a total change in resistance of ~ 20 – 23 ohms. In another experiment, antibody was attached to a glass substrate and used as a pure biological sensing layer for the virus in solution. In this case, the glass slide was cleaned, aminated, and functionalized with the vaccinia antibody. The functionalized surface was exposed to 10 μL of virus in a 0.2 mL water

drop, resulting in a 4.2 ohm rise in resistance. A similar experiment with a different virus particle produced no resistance change confirmin the specificity of the antibody.

In another study, vaccinia virus particles were detected using silicon cantilever beams, about 3 – 5 μm long, 1.4 – 1.5 μm wide, and 0.3 nm thick [11]. The resonance spectra were determined by measuring the thermal spectra of the cantilevers and fitting them to the amplitude response of a simple harmonic oscillator. The sensor was cleaned, dried, and immobilized with 15 μL of biotinylated BSA (1.5 mg/mL) followed by 15 μL of streptavidin (5 mg/mL) and 15 μL of biotinylated antibody to vaccinia virus (5 mg/mL). The antigen mixture (~10_{11} pfu/mL) was allowed to interact with the protein-coated cantilever for 30 minutes. The sensor was rinsed in ethanol and then dried. The loading of the virus as a point mass caused a resonance frequency shift in line with approximate analytical predictions. Moreover, they extended the work with microresonators by detecting a vaccinia virus using an array of silicon cantilever beams with nanoscale thickness. The cantilevers were approximately 5 μm long, 1.5 μm wide, and 30 nm thick. The cantilever was exposed to purified vaccinia virus particles (~10_9 pfu/mL) in distilled water for 30 minutes. The sensor was then rinsed with ethanol and dried, and the resonance frequency was measured in air, using a microscope scanning laser Doppler vibrometer. The number of bound virus particles was determined using SEM. There was a linear relationship between the resonance frequency shift and the effective number of virus particles. With an average measured dry mass of 9.5 fg/vaccinia particle, the mass-change sensitivity was calculated to be 6.3 Hz/ag. Arrays of chemically functionalized, surface micromachined polycrystalline silicon cantilevers were used by Ilic et al.[14] to detect the binding events of a model insect baculovirus (*Autographa californica* nuclear polyhedrosis virus). The fabricated cantilever was 6 μm long, 0.5 μm wide, and 150 nm thick, with a 1 μm x 1 μm paddle. The resonance frequency of the device was measured in a vacuum chamber at a pressure of 4 x 10^{-6} torr. The antibody was immobilized, and the sensors were then immersed in a buffer solution with baculovirus concentrations between 10_5 and 10^7 pfu/mL for one hour. The devices were rinsed, dried, and placed back in the vacuum chamber for resonance frequency determination. The sensors were able to detect frequency changes due to exposure to 10^5 pfu/mL baculovirus. Assuming the average weight of a single baculovirus is 1.5 fg, the results indicate that detection of a single virus particle is possible.

Johnson et al.[63] silicon cantilevers actuated by thermal noise and a PZT piezoelectric ceramic to detect and characterize virus particles. The deflection of the devices was measured optically. The two cantilevers were 21 x 9 x 0.2 μm and 6 x 4 x 0.2 μm (length x width x thickness), respectively. The cleaned sensors were exposed to 20 μL of purified vaccinia virus particles at a concentration of ~10^9 pfu/mL for 30 minutes at room temperature, then rinsed in ethanol and dried prior to recording

the resonance frequencies. Atomic force microscopy was used to image the bound virus particle. The calculated mass of the virus particle derived from resonance frequency shift was within the expected range for the two cantilevers. The PZT-excited cantilever had an order of magnitude higher sensitivity than the thermal noise actuated device.

1.4.4. DNA

Because DNA is a biomolecule of specific interest in a number of fields, including forensic medicine, a number of studies have developed cantilever-based sensors to detect it. McKendry et al. [59]used a microarray of cantilevers to detect multiple unlabeled biomolecules simultaneously at nanomolar concentrations. Microfabricated arrays of eight silicon cantilevers were cleaned with piranha and 10 % HF in water. The arrays were coated with a 2-nm titanium adhesion layer followed by 20 nm of gold. The sensor was functionalized with a thiolated probe sequence using microcapillaries. Individual cantilevers were inserted into a 40 μM solution of 12-mer thiolated probe DNA in triethyl ammonium acetate buffer for 20 minutes, then rinsed, and dried. All measurements were taken in air at 22°C. A linear position-sensitive detector was used for beam-deflection readout. Different concentrations of target DNA were injected at various flow rates, and the hybridized oligonucleotides were denatured chemically by purging the cell with dehybridization agents. Injection of a 500 nM solution of 12-mer target strand into the liquid cell caused bending and an average differential deflection signal of 9.8 nm, equivalent to a compressive surface stress of 2.7 x 10^{-3} N/m. Sequence specificity was challenged using a mixture of 250 nM complimentary and 20 μM non-complementary DNA. The results indicated that the sensors could detect unlabeled DNA targets in 80-fold excess of non-matching background DNA.

Hansen et al.[60] detected DNA mismatches without the need for labelling, using a microcantilever-based optical deflection assay. Chromium and gold were sequentially deposited on the upper surface of the silicon cantilevers. Probe DNA moleules, 20 and 25 nucleotides in length, were synthesized with C-6 5'-thiol modification for immobilization to the sensor surface. Four thiolated probes were used: three 20-mers in flow-through conditions and one 25-mer in static conditions. The flow-through probe experiments were carried out with a 10-mer complementary strand, and three different mismatched 10-mer strands - a proximal terminal mismatch, one internal mismatch, or two internal mismatches. For the static experiment, two 10-mer mismatch sequences were used, with one internal mismatch or two internal mismatches. The functionalized cantilevers were immersed in flow cell sand stabilized in phosphate buffer. For both static and flow experiments, 20 μg/mL targets were used, and the temperature was held at 25°C. The flow-through experiments used a rate of 2 mL/hr. Hybridization of fully complementary10-mer targets resulted in a net

upward deflection of the cantilever. Compariosn of hybridization with 10-mer versus 9-mer strands showed that the deflection was due to hybridization. Terminally mismatched 9-mer strands resulted in the formation of nine-base pair dsDNA up to the point of mismatch. Hybridization of 10-mer large oligonucleotides with one or two internal mismatches to 20- and 25-mer probes resulted in a net downward deflection, indicative of higher repulsive forces. The magnitude of the deflection was proportional to the number of mismatches. Hansen et al. [61] continued his work by measuring oligonucleotde hybridization using gold-coated thiol-functionalized cantilevers. Two sets of experiments were conducted: on set varied the length of the complementary strand; the second set varied the sequence to create a mismatch. The experiments were carried out in a flow-through system, with flow rates of 1 – 2 mL/min. When the probe functionalized cantilever was exposed to complimentary strands of varying length, the magnitude of the positive deflection increased in proportion to the length. When different sequences were compared, the sensors could apparently discern a single base mismatch. Complementary strands containing the same number of units as the probe DNA gave the largest deflection. Similar work conducted by Fritz et al.[66] using a cantilever array to monitor the hybridization of complementary oligonucleotides could detect a single base pair mismatch between complementary 12-mer strands during hybridization.

Calleja et al.[62] developed cantilever arrays fabricated of SU-8 and coated with gold to detect the adsorption of ssDNA. SU-8 is an epoxy-based photoresist with high chemical resistance. The cantilevers varied in length (100 to 200 μm), width (20 to 50 μm), and thickness (1.3 to 2 μm). Cantilever deflection measurements were carried out in air, using optical beam deflection. DNA probes were 12 nucleotides long with a thiol molecule on the 5' end. 6-Mercapto-1-hexanol (MCH) was used as a spacer molecule after probe immobilization. After cleaning, 20 mL of a 2 μM solution of probe solution was introduced to the sensor surface creating the expected downward deflection due to compressive stress. One mM MCH was then introduced, and further downward deflection was noted. The deflection of the polymeric probes was six times higher than that of a commercially available silicon nitride cantilever. Su et al.[69] used a V-shaped silicon nitride microcantilever with gold nanoparticle-modified probes to detect DNA hybridization. The cantilevers were 150 μm long, 90 μm wide, and 0.6 μm. The hybridization was measured by the attachment of Au nanoparticles on the surface and subsequent chemical amplification of the signal. Gold-coated, probe-immobilized (1 mM) sensors were dipped into the target DNA solution (0.05 to 10 nM) for hybridization. Each ssDNA sequence was 15 nucleotides long. The gold nanoparticle-labeled DNA strands (2 nM) were then hybridized on the other end of the target. The gold nanoparticles acted as a nucleating agent for the formation of silver, resulting in a frequency shift due to added effective mass. The resonance frequency shifts were monitored in air, using an atomic

force microscope. The results showed a linear relationship between the frequency shift and the concentration of target ssDNA over the range of 0.05 – 10 nM. A single nucleotide mismatch did not show a significant frequency shift. Detection of the target strands was further confirmed using secondary ion mass spectrometry (SIMS).

Marie et al.[63] used a gold-coated piezoresistive cantilever array, 150 μm long, 40 μm wide, and 1.3 μm thick, to determine the adsorption kinetics and mechanical properties of a thiol-modified DNA strand. The sensor was actuated by 2V and the detection mechanism monitored the induced surface stress. A DNA sequence 25 nucleotides long was brought into contact with the sensor in a flow configuration (25 μL/min). The adsorption rate increased as the ssDNA concentration increased from 1 to 4 .2 to 25 μM. When the data were fit to the Langmuir isotherm, the observed rate constant increased linearly with increasing DNA concentration.

1.4.5. Small Molecules

Cantilever sensors have been quite extensively used for detecting the adsorption of various chemical species onto a prepared substrate. Much of this work was derived from the formation of self-assembled monolayers (SAM) on sensing surfaces [64] Campbell et al.[65] used a gold-coated PEMC sensor to measure the formation of self-assembled monolayers with different terminal head groups. Formation of the SAM was monitored by recording changes in resonance frequency. The PEMC sensor was constructed of two layers: a PZT layer 5 mm long, 2 mm wide, and 127 μm thick, and a stainless steel layer 10.5 mm long, 2 mm wide, and 50 μm thick. The stainless steel foil was covered with chromium, followed by 10-nm of gold. The surface was cleaned with piranha solution and rinsed three times with deionized water. One mL stock solutions of 1-decanethiol, 11-mercapto-1-undecanol, and 11-mercaptoundeconoic acid were prepared in ethanol to a final concentration of 1 mM. The gold coated sensor was immersed 1.5 mm into 1 mL of the target solutions for one hour. Upon immersion, the resonance frequency showed an exponential decrease, ultimately reaching a constant value. The total frequency change was 885 ± 21 (n=2), 590 ± 14 (n=2), and 383 ± 10 (n=2) Hz for 11- mercaptoundeconoic acid, 11-mercapto-1-undecanol, and 1-decanethiol, respectively.

Campbell and Mutharasan [66] evaluated the formation of an alkanethiol monolayer on a gold-coated millimetre-sized, rectangular-shaped lead zirconate titanate (PZT) cantilever. The cantilever had dimensions of 3.5 x 2 x 0.05 mm, and was actuated using an alternating current generated from an impedance analyzer. After cleaning and gold-coating, the sensor was dipped in solutions of *n*-alkanethiol at various concentrations. The total resonance frequency changes in response 1 nM, 10 nM, 100 nM, 1 μM, 4 mM, 8 mM, and 10 mM thiol were 116 ±2 (n=2), 225 (n=1), 270 ± 10 (n=2),

440 ± 10 (n=2), 900 ± 10 (n=2), 900 ± 10 (n=2), and 900 ± 10 (n=2) Hz, respectively. In agreement with previous work[75, 76], the results indicated that the rate of monolayer formation is concentration dependent, and that the exponential change during adsorption follow s the reversible first-order Langmuir model. Similar work, conducted by Berger et al. [67], used a v-shaped micromechanical silicon nitride cantilever to evaluate the surface stress changes and kinetics during the self-assembly of alkanethiols on gold. The gold sensor surface was exposed to alkanethiol vapors with alkyl chains ranging from 4 to 14 in carbon length. A strong response in sensor deflection with a distinct saturation point was observed. The surface stress was proportional to the number of molecules adsorbed, and the stress curves generated during adsorption fit the Langmuir adsorption isotherm model. The saturated surface stress generated by the monolayers also increased linearly with total chain length, indicating that the compressive surface stress change was directly proportional to alkyl chain length.

Yan et al.[68] utilized V-shaped silicon microcantilevers 180 μm long, 25 μm wide, and 1 μm thick to detect the oxidation of glucose by glucose oxidase. The microcantilever was gold-coated and inserted into a flow-through glass cell for continuous measurement with an optical beam. A 25 – 30 nm layer of polyethyleneimine/glucose oxidase was immobilized on the sensor surface, and various concentrations of glucose flowed past the surface at a rate of 72 ml/Hr. The deflection of the cantilever increased as the glucose concentration increased in the 1 – 10 mM range. Further experiments showed that deflection amplitudes at equilibrium were directly proportional to glucose concentrations between 1 and 50 mM [69]. A microfabricated silicon cantilever array was used to observe the transduction of physical and chemical processes into nanomechanical motion[81]. The array consisted of eight linearly-arranged cantilever-type sensors (500 μm long, 100 μm wide, 1 μm thick), housed in an aluminum sample chamber with analyte inlet and outlet, and windows for monitoring beam deflection. Each sensor was coated with 30 nm of gold, and polymers (5 mg/mL) were spray-coated onto one side of the cantilever to form a homogeneous layer of ~ 5 μm thick. A homologous series of primary alcohols, from methanol to heptanol, were flowed past the sensor surface. The results gave distinct clusters in principal component space, allowing unambiguous identification of the alcohol. Similar experiments were performed for various alcohol mixtures and solvents, and were successful in identification and selectivity. However, successful detection in a mixture was only possible when the individual components were previously characterized.

Ilic et al. [12] used a nanoscale, micromachined polycrystalline silicone and silicone nitride oscillator to detect the presence of thiolate self-assembled monolayers (SAM). The device was 4 μm long, 500 nm wide, and 160 nm thick, and terminated in a 1 x 1 μm gold-coated paddle. Resonance frequency values were recorded in a vacuum chamber at a pressure of 3 x 10^{-6} torr. An rf

spectrum analyzer was used to mechanically excite the NEMS structures and measure the signal for the optical detector. Following baseline measurement, the sensors were submerged in a solution of dinitrophenyl poly(ethylene glycol) undecanthiol for 3 hours. The devices were then rinsed with methylene chloride, acetone, and isopyropyl alcohol, and dried with nitrogen, and resonance frequency was again recorded in a vacuum chamber. Based on the frequency shifts, the smallest resolvable mass was estimated to be 0.39 ag.

1.4.6. Viable Cells

There is a rapidly growing need in point-of-care (POC) medicine, food processing, biopharmaceutical processing, and other areas to monitor viable cell growth. The presence of actively growing bacterial cells, for example, can indicate infection that might result in hospitalization and possibly death. The ability to discern live from inactive organisms can be used to determine the safety of food products. Traditional methods of determining live cells rely on plate counting techniques, which are time consuming and costly. Cantilever-based sensors could provide a more rapid means of identifying contaminant growth, which would be greatly beneficial.

Detzel et al. [70] reported on a piezoelectric-excited, millimeter sized glass cantilever for detecting the real-time growth of *E. coli* JM101. A 127 μm thick PZT sheet was bound to a 160 μm glass cover slip. Each had dimensions of 1 x 5 mm, total surface sensing area was 1 mm^2. The cantilever was cleaned with Piranha solution (7:3 volume ratio of concentrated H_2SO_4 and 30% H_2O_2), followed by deionized water and ethanol. After cleaning, 2 μL of Luria broth agar was spread into a 200 μm film on the sensing surface. The agar was inoculated with 0.5 μL of exponentially growing *E. coli* culture and maintained at 29°C. During the 6 hour growth phase, the cantilever measured a total frequency change of 5.08 ± 0.01 kHz. A model showed a close correlation between resonance frequency and the exponential growth rate (μ) of the bacterial cultures. The results were obtained approximately 10 times more rapidly than similar experiments with QCM.

A eight silicon-cantilever array was used by Gfeller et al. [23] to rapidly detect actively growing *E. coli* cells. The cantilevers were 500 μm long, 100 μm wide, and 7 μm thick. Following cleaning and amination, each sensor was coated with agarose to provide a suitable growth substrate. The experiments were carried out at 37°C and 93% relative humidity. A subset of the eight cantilevers was inoculated with an *E. coli* suspension; the other sensors were controls. Post inoculation, the sensors were immersed for 10 minutes in pure LB broth without *E. coli* cells. The resonance frequency change was monitored optically every 30 minutes by a Position-Sensitive Detector (PSD). No resonance frequency change was observed with the reference cantilevers. The inoculated cantilevers showed a resonance frequency shift rate of ~ 200 Hz/hr during the exponential growth

phase, which was easily detected in ~1 hour. The mass-change sensitivity of the device was estimated to be 140 pg/Hz. The exponential decrease in frequency was assumed to be due to growing cells; however, this was not confirmed correlation with growth kinetics or growth rate.

Nugaeva et al.[71] demonstrated a new cantilever-based biosensor for detecting vital spores of the fungus, *Aspergillus niger*. The cantilever device was a silicon microfabricated array operated in dynamic sensing mode. The eight cantilevers in the array, each 500 μm long, 100 μm wide, 4 μm thick, were cleaned with Piranha and deionized water, then coated with anti-*A. niger* polyclonal antibody. The immobilized sensor indicated an initial resonance frequency shift, due to binding on the sensor surface, 1-hr after exposure to the spore. The sensor was then placed in a humidity chamber to promote favorable spore growth conditions, and a second shift was noted four hours later. Scanning electron microscopy confirmed active spore germination during the second resonance frequency shift. Assuming an average *A. niger* weight of 47 pg, the calculated mass-change sensitivity ranged 3 to 53 pg/Hz for the first three modes.

More recently, silicon arrays of microcantilever were used to directly bind and quantify living cells of Salmonella enteritidis . The cantilever arrays operated in dynamic sensing mode, and the detection occurred in liquid and vacuum conditions.

The resonance of the fifth mode of vibration in liquid environment of a cantilever after antibody immobilization (Ab) and after flowing an aliquot of 20 μL of Salmonella suspension (10^5 cfu/mL) at a flow rate of 0.5 μl/min resulted in visible frequency shift of 660 Hz the due to the immobilization of entire bacteria thanks to antibody binding with their membrane proteins. Monitoring first six flexural modes of vibration it could be possible to detect the presence of Salmonella *enteritidis* in concentration of 10^5 cfu/mL in just 40 min (i.e., the time needed to flow the entire aliquot), without any enrichment and/or sample preparation. Such a concentration is comparable with previously reported literature data, where Salmonella cells have been successfully detected in the range 10^8-10^3 cfu/mL with cantilevers partially immersed in a macroscopic fluid cell under static flow conditions [23, 90]

In the latter method, the MC array is dipped in the solution for the bacteria incubation (typically for 1-2 h), washed, dried, and placed in a vacuum chamber. Thanks to the minimizing of the viscous effects of the environment, the cantilever vibrating in vacuum reveals the highest resonant frequencies and the greatest Q-factors, resulting in a significant enhancement of mass sensitivity. In this way, they characterized different cantilever arrays exposed to varying bacteria dilutions and were able to successfully detect the presence of S. enteritidis in concentration as low as 10^3 cfu/mL.

1.4.7. Detection in Real Matrices

As discussed, the ability to detect trace molecules in complex solutions has numerous applications in many industries. To date, however, cantilever-based technology has not provided simple methods for detecting biomolecules in solutions more complex than salt-buffer. Currently available techniques require some sample preparation, and are limited by low sensitivity (pg/mL to ng/mL) and poor specificity in complex matrices with a high degree of background noise. The lack of sensitivity and selectivity is particularly problematic for body fluids, such as blood, plasma, and urine, where many materials are present. Wu et al.[103] utilized v-shaped silicon nitride cantilevers of various dimensions to detect prostate-specific antigen (PSA) in bovine serum albumin (BSA), human serum albumin (HAS), and human plasminogen (HP). Following cleaning, a 25 nm thick gold film was deposited on the cantilever, and rabbit anti-human PSA was immobilized on the surface. Free PSA solutions were prepared at concentrations ranging from 0.1 to 60,000 ng/mL. The sensor was inserted in a flow cell and brought into contact with the PSA solutions under static conditions. Cantilever deflection was measured as a function of time for different concentrations of PSA in BSA, HAS, and HP. The lowest PSA concentration detected using a 200 µm long, 40 µm wide, and 0.5 µm thick cantilever was 6 ng/mL. PSA was detectable at 0.2 ng/mL when the dimensions of the cantilever were changed to 600 µm long, 40 µm wide, and 0.65 µm thick.

Campbell and Mutharasan[104] used piezoelectric-excited, millimetre-sized cantilever (PEMC) sensors to detect *E. coli* O157:H7 in ground beef samples. The goal was to compare PEMC sensor cycle time and sensitivity to conventional plating techniques. A modified sensor design with only PZT and glass layers was used. The sensing surface was derivitized with an amine-terminal silane, and affinity-purified polyclonal antibody to *E. coli* O157:H7 was immobilized. The sensor was inserted into a flow cell, and samples were introduced at a flow rate of 1 mL/min. Samples and controls were prepared in Stomacher bags. Pathogen samples consisted of 100 mL of broth inoculated with 25 *E. coli* O157:H7 cells, 100 mL of broth with 25 g of raw ground beef, or 100 mL of broth with 25 g of sterile ground beef inocluated with 25 cells. Controls were 100 mL of broth with 25 g of sterile ground beef. The total resonance frequency changes after 2, 4 and 6 hours of growth were 16 ± 2 Hz (n=2), 30 Hz (n=1), and 54 ± 2 Hz (n=2), respectively, for broth plus *E. coli* cells, and 21 ± 2 Hz (n=2), 37 Hz (n=1), and 70 ± 2 Hz (n=2) for cells in ground beef. The device was capable of 50-100 cells/mL in a ground beef background.

Chapter 2

Design, Fabrication and Characterization of Silicon Cantilevers

2.1. Cantilever fabrication review

Micro Electro Mechanical Systems or MEMS is a term coined around 1989 by Prof. R. Howe [72] and others to describe an emerging research field, where mechanical elements, like cantilevers or membranes, were manufactured at a scale more akin to microelectronics circuit than to lathe machining. Actually, the fabrication of MEMS is an entire field of research on its own . It is extremely diverse and still expanding. With the growing number of companies that fabricate MEMS, the technology is continually improving. With each breakthrough, MEMS technology becomes more affordable, better, and easier to fabricate in ever increasing quantities. The technology is also pushing the size envelope and continually working towards the development of

smaller devices such as NEMS [73]. The acronym MEMS is used today to define both the fabrication processes and the devices resulting from these processes.

It appears that these devices share the presence of features below 100 μm that are not machined using standard machining but using other techniques globally called microfabrication technology. Of course, this simple definition would also include microelectronics, but there is a characteristic that electronic circuits do not share with MEMS. While electronic circuits are inherently solid and compact structures, MEMS have holes, cavity, channels, cantilevers, membranes, etc, and, in some way, imitate 'mechanical' parts. That has a direct impact on their manufacturing process. Even when MEMS are based on silicon, microelectronics process needs to be adapted to cater for thicker layer deposition, deeper etching and to introduce special steps to free the mechanical structures [74]. Then, many more MEMS are not based on silicon and can be manufactured in polymer, glass, quartz or even in metals. By far, miniaturization is often the most important driver behind MEMS development. Microfabrication processes can be effectively applied to yield a single device or thousands of devices. The so-called batch processing, i.e., the fabrication of many devices in parallel, does not only lead to a tremendous cost reduction, but also enables the production of array structures or large device series with minute fabrication tolerances. The common perception is that miniaturization reduces cost, but an important collateral benefit is also in the increase of applicability. Actually, reduced mass and size allow placing the MEMS in places where a traditional system it is not able to fit.

Finally, these two effects concur to increase the total market of the miniaturized device compared to its costlier and bulkier ancestor. However, miniaturization itself cannot justify the development of new MEMS. After all if the bulky component is small enough, reliable enough, and particularly cheap then there is probably no reason to miniaturize it. Microfabrication processes cost cannot usually compete with metal sheet punching or other conventional mass production methods. Nevertheless, MEMS technology allows at the same time very high reproducibility repeatability and sensitivity. Another advantage that MEMS can bring relates with the system integration. Instead of having a series of external components (sensor, inductor...) connected by wire or soldered to a printed circuit board, the MEMS on silicon can be integrated directly with the electronics. Whether it is on the same chip or in the same package it results in increased reliability and decreased assembly cost, opening new application opportunities. As firstly reported by W. Trimmer [75], the large decrease in size during miniaturization, that in some case can reach one or two orders of magnitude, has a tremendous impact on the behaviour of micro object when compared to larger size one. For example, the decrease of volume/surface ratio has profound implications for the design of MEMS. Actually it means that at a certain level of miniaturization, the surface effect will start to be

dominant over the volume effects. For example, friction force (proportional to surface) will become larger than inertia (proportional to mass hence to volume), heat dissipation will become quicker and heat storage reduced: energy storage will become less attractive than energy coupling. It appears that some forces that are insignificant at large scale becomes predominant at smaller scale. In general, fabrication of MEMS devices is based on two distinct micromachining strategies: bulk micromachining and surface micromachining. Bulk micromachining involve removal of substantial portions (i.e., "bulk") of the substrate. Bulk micromachining is often used to create devices with three-dimensional architecture or suspended structures. Surface micromachining remain the original substrate mostly intact and use it as a base for a device formed as a result of additive (deposition) and subtractive (etching) processes [76].

The most commonly used surface micromachining process is sacrificial-layer etching [77]. In this process, a microstructure, such as a cantilever beam, is released by removing a sacrificial thin-film material, which was previously deposited underneath the microstructure Simplified schematics of the two techniques as applied to cantilevers are shown in Figure 2.1 (a) and 3.4 (b), respectively. The key difference between these techniques is the sacrificial layer which, when removed, releases the devices from the substrate. In bulk micromachining, the bulk silicon wafer is used as the sacrificial layer. In surface micromachining, there is no back side processing, and the silicon wafer is left intact. A sacrificial oxide layer is first grown on a silicon wafer, followed by deposition of the device layer.

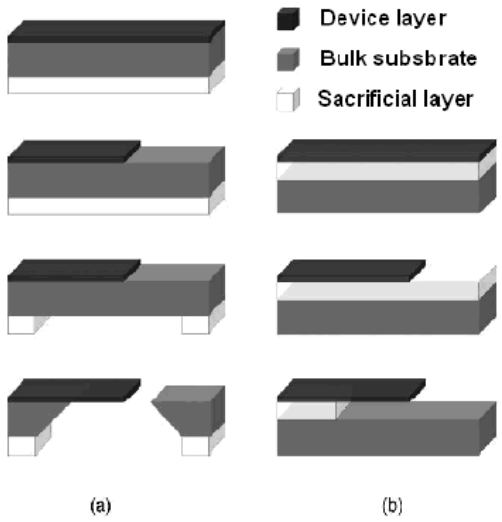

Figure 2.1 - Representative process flow for bulk micromachining (a) and surface micromachining (b).

Fabrication of a suspended microstructure, such as a cantilever transducer, consists of deposition, patterning and etching steps that define, respectively, thickness, lateral sizes, and the surrounding of the cantilever. Different kind of lithographic techniques have been employed to realize or modify microcantilever i.e. FIB [78], EBL [79] and laser lithography [80]. Generally the four basic microfabrication techniques for cantilever creation are identical with those used in IC fabrication: deposition, patterning, doping and etching. A recent review on microfabrication in biology and medicine and a review on microfabrication for biosensors can be found respectively in ref. [81].

Commercially available AFM probes made of silicon or silicon nitride have been used extensively in research on cantilever based sensors AFM cantilevers are designed and fabricated to satisfy a number of the application specific requirements, which become partly redundant in the case of cantilever transducers for sensor applications. The most notable of such redundant features are the presence of a sharp tip on the cantilever. Concerning microcantilevers for AFM application, in order to allow the tip accessibility to a sample surface the bulk techniques is more used than surface micromachining. In analogy to AFM cantilevers the most common materials used for cantilever sensors are single crystal silicon [82] polycrystalline silicon (polysilicon) [83], silicon oxide [84], silicon-nitride [85], gallium-arsenide [86], amorphous carbon [87], metal [88], and occasionally diamond [89]. In order to avoid any bulk micromachining, such as through-etch of silicon in KOH, various cantilever surface fabrication processes based on the use of a sacrificial layer were developed [90]. These processes frequently rely on silicon oxide as a material for the sacrificial layer [91]. In microcantilever fabrication, low pressure chemical vapor deposition (LPCVD) and plasma-enhanced chemical vapour deposition (PECVD) techniques are widely used to form silicon dioxide and silicon nitride structural or sacrificial layers. Although a variety of substrates and thin films can be used to fabricate microcantilever devices using bulk or surface micromachining, one of the most preferred substrates is single crystal silicon. In fact, MEMS fabrication relies heavily on approaches previously developed for microfabrication of conventional electronic devices. A largely used substrate in cantilever sensor fabrication is the silicon on insulator (SOI) substrate [92]. The use of silicon substrate material enables the co-integration of transducers and circuitry, an advantage which is explored, e.g., in CMOS-based Microsystems [93]. Besides its favourable electrical properties, single crystal silicon also has excellent mechanical properties, which enable the design of micromechanical structures. A large number of micromachining techniques have been developed to structure silicon substrates [94]. Consequently, silicon is also the most common substrate material for microfabricated chemical and biosensors. Glasses and ceramics are used extensively as substrate for hybrid microelectronics and are common in microelectronics packaging. The chemical inertness, biocompatibility, and mechanical stability make ceramics a very interesting

material for microsystems. Most microfabrication techniques for ceramic materials have been adapted from microelectronics packaging processes. Ceramics have been employed to obtain cantilever structures [95].

Over the last years, polymers have been more and more explored as inexpensive substrate materials. Special processes, such as hot embossing, injection molding, laser machining, or stereolithography, have been developed to structure polymer materials even in the micrometer range. For instance, lithographically defined polymer microcantilevers were fabricated from epoxy based photoresist (SU-8) with integrated gold layers serving as the piezoresistors or as a mirror for the optical read-out [96]. The elastic modulus of SU-8 is nearly 40 times lower than silicon making the polymeric cantilevers significantly soft and indicated to the static mode measurement. These structures can support reversible deflections up to nearly 100 μm which is rarely sustainable with silicon cantilevers. However, it is important to note that the gauge factor of the SU-8 is nearly 50 times smaller than that of silicon, causing the effective piezoresistive sensitivity on the same order as silicon based cantilevers. Genolet and co-workers have produced scanning probe microcantilevers from a photopolymer (SU-8) [97]. Their approach was to etch a mold in a piece of silicon, fill the mold with SU-8, cure the SU-8, and attach a base part for mounting in an AFM. Using nearly the same technique, Wang et al. created microcantilevers (SPM probes) using a photopolymer (polyimide) with elastomeric tips [98]. Gammelgaard presented an SU-8 micrometer sized cantilever strain sensor with an integrated piezoresistor made of a conductive composite of SU-8 polymer and carbon black particles [99]. Thaysen et al. [100] made photopolymer-based piezoresistive me- chanical sensors also employing IC techniques. Lee et al. produced microcantilever arrays from fluoropolymers by using photolithograpy to produce a pattern on the polymeric substrate and then selectively remove material using normal and oblique ion beam etching [101].

2.2. Cantilever sensor design

As described previously, the performance of the microcantilever based sensor device is proportional to the natural frequency of the cantilever beam structure and inversely proportional to the effective mass acting on the structure. Moreover, it is clear that the natural frequency of vibration is inversely proportional to the effective mass of the structure. Thus, in this study, different geometrical shapes of the cantilever beam structures were investigated to increase the performance of the device. The minimum planar dimension was fixed to 20 μm in order to facilitate the laser alignment of the readout system and to avoid laser scattering out of the cantilever structure.

Different shapes, dimensions, and mass were designed for cantilever biological mass measurements (see Figure 2.2) in air and vacuum environment in the range from few picograms to fraction of nanogram.

As described, surface micromachining requires less process step, the close proximity of the devices to the silicon wafer may present a problem in some applications. If the sacrificial layer is not thick enough stiction may occur if the suspended device layer comes in contact with the surface. This typically permanent problem makes the devices unusable. Moreover for cantilever involved in liquid bath both for functionalization and detection step the presence of the capillary force in the small gap between structure and substrate can entrap droplet and cause anomalous resonance response. Stiction was avoided by using bulk micromachining, which also opens up the possibility of addressing both sides of the cantilever.

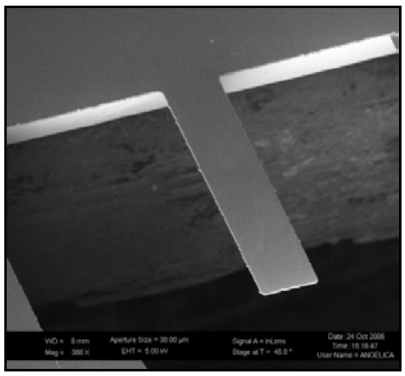

Figure 2.2 - FESEM image of a microfabricated cantilever (700x70x2,5 μm3)

Array from three to twelve microcantilevers were designed in order to dispose of multiple signal simultaneously and concerning the same analytical sample. The uniformity of the planar dimension of the cantilever due to the etching processes as well the variability in the substrate thickness in one chip turn out to be within a few percent of the average resonance frequency for cantilevers with the same nominal dimensions. As all cantilevers are structural connected through the same membrane crosstalk between responses from individual cantilevers cannot be completely excluded. In order to investigate the crosstalk phenomena finite element analysis (Comsol, Multiphysics) were carried out. Analyses in the frequency domain were performed to extract the frequency response of two microbeams with about the same dimensions (within the fabrication tolerances) with axial separation of 200μm. To “mimic” the piezo-actuation, the displacement of the bottom surface of the bulk layer has been swept in frequency, while the harmonic responses of the microbeams have been extracted in correspondence of their free end. As showed in Figure 2.3, the frequency response of each microcantilever shows no additional peak in correspondence of the resonance of the other one.

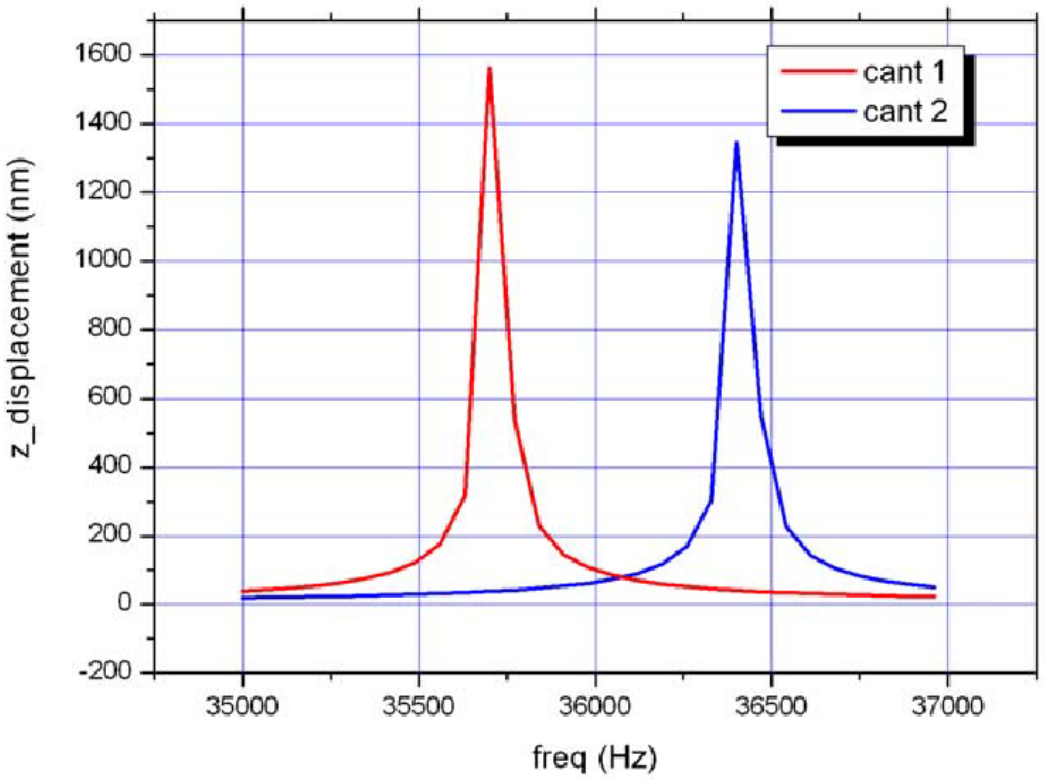

Figure 2.3 - Simulated resonance curves of two cantilevers (500 x 60 x 7 µm3 and 495 x 60 x 7 µm3, 200 µm spaced) obtained exciting in vacuum condition through harmonic constrain displacement.

2.3. Cantilevers fabrication process flows

The process flow was optimized with the aim of reducing the number of lithographic masks and process steps. To facilitate the automation and the large scale production particular critic steps was engineered (i.e use of polymeric mask protection for the device layer in the wet etching of bulk silicon in KOH solution).

Two different process flows were developed to fabricate microcantilevers in order to test the suitability of polymeric protective coatings in MEMS technology (see Figures 2.4). A quarter of SOI wafer were used for cantilever fabrication. Several chips were realized on the substrate and V-shape trenches were defined on the backside of the wafer in order to obtain initial guide for the release of the chip.

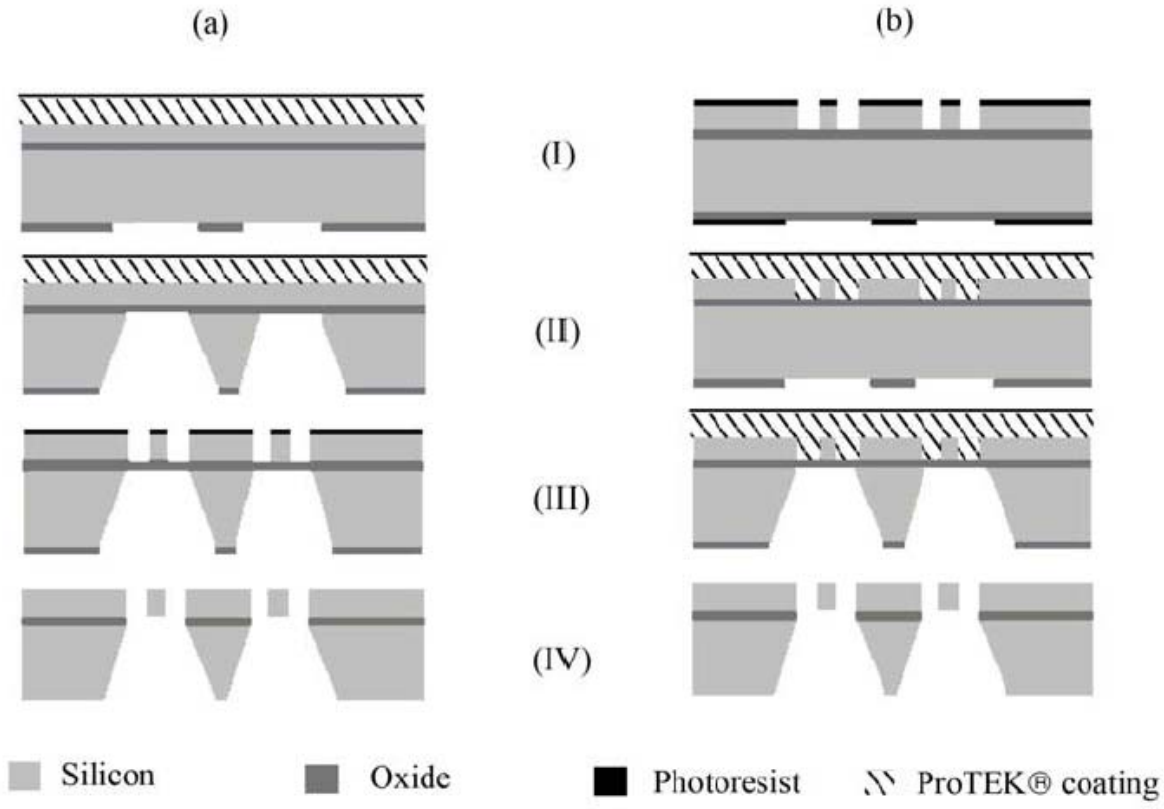

Figure 2.4 - Process flow (a): (I) SOI wafer coated with ProTEKR _ B2 material; (II) KOH etching; (III) reactive ion etching (RIE); (IV) cantilever release. Process flow (b): (I) RIE; (II) SOI wafer coated with ProTEKR _ B2 material; (III) KOH etching; (IV) cantilever release.

In the first process flow proposed in Figure 2.4 panel (a), the cantilevers are released through the following steps: photolithography on the back side, wet etching in BOE solution for the patterning of the mask layer on the back side, front side protection with a polymeric coating, wet etching in KOH solution, sample cleaning, photolithography on the front side of the membrane, RIE of silicon, removal of the buried oxide layer in BOE and cleaning by piranha solution. In the second flow proposed in Figure 2.4 panel (b), the cantilevers are patterned before the KOH etching through the following steps: photolithography on the front side and RIE of the silicon. Then the protective coating is applied directly on the pattern of the device, and KOH etching is carried out and followed by releasing and cleaning of the cantilevers.

2.4. Cantilever Resonance Frequency Characterization Set-Up

To characterize the vibration properties of microcantilevers home made system was used. The following scheme is designed on the basis of the most diffused AFM microscope models, in which the detection of the cantilever movement is made with the optical lever method. The main parts that constitute the sensing apparatus are:

• the actuation system, with the use of a piezoelectric crystal;

• the detection system, with the sensing of the light produced from a laser diode, focalized on the cantilever surface, reflected from it and revealed with a Position Sensitive Photo-detector (PSD);

• the electronic chain which collects the signal from the PSD and filters the external noise components before sending it to a pc for the data storage;

• the vacuum system which allows to control the pressure into the chamber where the cantilever is mounted, in various conditions ranging from high vacuum to ambient pressure.

A block scheme of the entire experimental set-up is represented in Figure 2.5

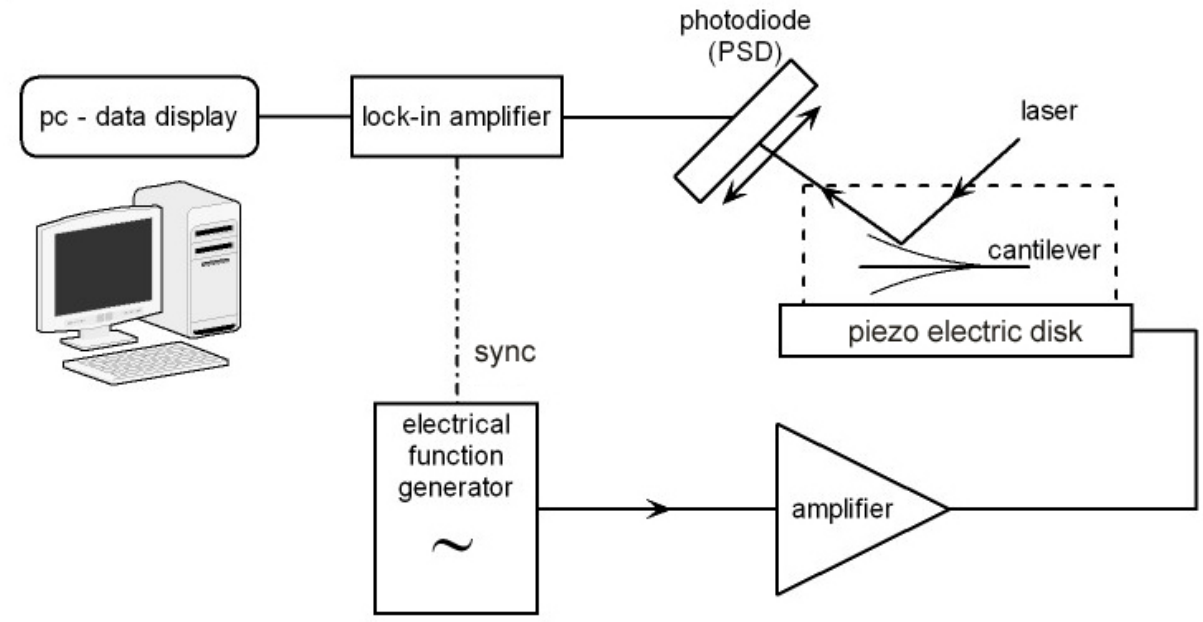

Figure 2.5 - Schematic of the circuit and components which constitutes the set-up for the cantilever characterization

To set up the system, the geometrical structure of an ellipsometer was used. The complete experimental set-up is positioned on a heavy optical bench, to avoid the effect of the main structural vibration noise.

2.4.1. Actuation System

To actuate the cantilevers piezoelectric crystals with an electronic apparatus togenerate and control the vibration were used. 300 μm thin discs of lead zirconium titanate (PZT) material (PI ceramics) with a 20-50 mm diameter were used. Discs present anickel/copper metallization on both sides. The top side that presents a uniformmetallization is distinguishable from the bottom side where the metal contacts are reported. In such a way the electric connections were positioned only on one face of the actuator,leaving the other one free from contacts. Thus one can obtain a wide plane area that can be used for the sample holding. On the bottom side the disc was connected to a peltierelement. Conductive copper trails and pad were drawn on the peltier surface and the PZT sample was connected and fixed with a rigid thin layer of conductive glue.

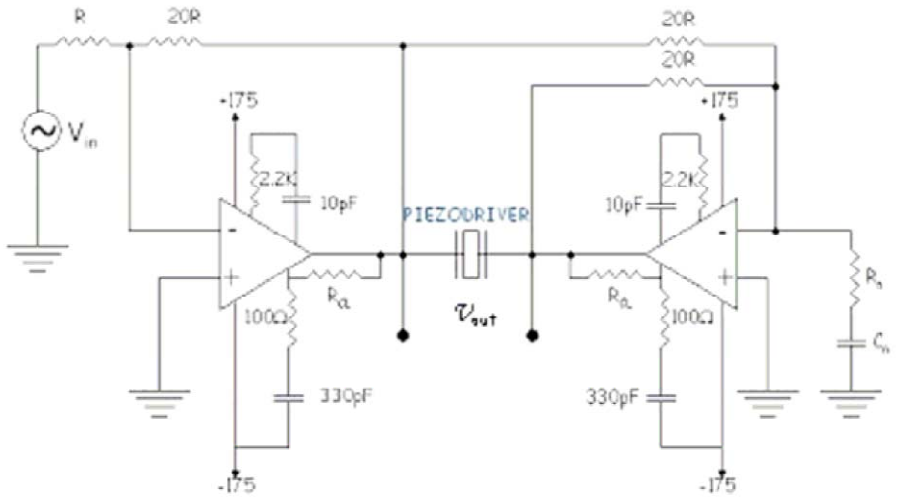

Figure 2.6 - Schematic representation of the electronic circuit for the alimentation of the piezodriver

The actuation disc could be piloted by a pre-amplifier (APEX Microtech). From the analysis of the electronic circuit it is possible to see that the outputs of the two operational amplifiers are:

$$V_{out1} = -20V_{in}, \quad V_{out2} = +20V_{in}$$

For what concern the input signal, a square wave at variable frequency is supplied by a function generator (HP 33120A). The maximum peak-to-peak amplitude of the alternate signal Vin is 10 V. The alternate signal is added to a DC component, given by two DC power supplies (HP 6110A and Systron RS320). The amplitude of the DC signals are equals and opposites in sign, up to a maximum value of ±175 V; the DC power supplies are connected to a common ground. The amplifier output is a square wave at the sam frequency of the input AC signal and with adapted enhanced amplitude. The two opposite outputs of the pre-amplifier are send to the front and back contacts of the piezodriver. By controlling the amplitude of the modulating signal (by varying the DC alimentation of the operational amplifiers) one can control the amplitude of the piezo vibration. Since the frontal dimensions of the disc are much greater than its thickness, the obtained vibration is directed mainly along the z direction and no lateral vibrations are present. The cantilever sample is simply connected to the top side of the actuator by a thin layer of glue with higher thermal conductivity (Thermal Bonding System by Electrolube Derbyshire, UK).

2.4.2. Detection System

The sensing of the cantilever vibration is performed by the optical lever technique. Briefly, the light produced by a laser source is focused on the front side of the cantilever, which reflects it towards a photo-detector. The diode collects the reflected light and transforms it on an electric signal to be sent to an electronic chain for the data collection and storage. At this purpose, a small low power laser diode (Coherent VLM2) was used. The main characteristics of the laser light source are listed in Table 3.1. No particular characteristics are requested for the light source, except for a good stability during time and a low power density to avoid an excessive heating of the sample and of the surrounding medium. Using low power laser without a strong focalization of the light spot the thermal induced noise can be neglected (especially for cantilever on the micrometer scale, while for nano-cantilever the thermal noise becomes an important aspect to be considered).

Two photographs of the system are represented in Figure 2.7. The laser source is mounted on a solid support: at this purpose, the geometrical structure of an old ellipsometer was used. An optical microscope (magnification 50x) is focused on the cantilever surface, to control the laser spot positioning near to the free end of the beam. The reflected light is collected on the other side of the structure, where there is the PSD.

Figure 2.7 - A photograph of the measurement setup.

The PSD used on the experiments (Hamamatsu S1662) is a continuum position sensor. The detector can produce a photocurrent with intensity proportional to the incidence position of the laser light. The diode is a p-i-n planar junction. The surface sensitive area of the detector is 13x13 mm^2. The p-layer converts the incident light on a photocurrent, which is collected on the two lateral electrodes. The amount of charge collected at every electrode is inversely proportional to the distance between the electrode and the hitting point of the detector light spot .

The differential result is independent from the power of the incident light and from the shape and dimension of the light spot. It is clear that such kind of photodiode can only detect a dynamic light signal, because it is the position variation of the light spot which gives the differential variation of the charge collected at the electrodes. So this kind of detection system allows only an evaluation of the vibration shape, and not a static evaluation of the position of the light (and the corresponding position of the cantilever).

2.4.3. Electronic chain for Data Collection, Filtering and Storage

The PSD detector collects the signal related to the movement of the cantilever, but also every other moving light (such as the ambient environment surrounding light produced from the neon) adds a new component on the detectable signal. Moreover, generic low frequency mechanical vibrations of the structure on which the system is mounted have an influence on the final signal. The pure output

of the photodiode is therefore very noisy and a signal filtering is requested. At this purpose a lock-in amplifier is used, to filter only the part of the signal which is related to the vibration of the cantilever, that is to say the signal at the same frequency of the vibrating piezodriver. A lock-in amplifier works as a narrow band-pass filter, centred around an input main frequency (which in the case that corresponds to the driving frequency of the piezo actuator). The used lock-in (IG&G 7260 DSP) exploits the phase sensitive detection (PSD) technique.

The output of the lock-in is proportional to the amplitude of the cantilever signal and takes into account only the vibration component related to the driving frequency of the piezo vibration. The phase difference of the two PSDs is given as an output of the instrument as well. The application of the lock-in filtering is very useful to analyse such noisy and weak signal as the ones revealed by the photo-detector. The main limitation of our lock-in amplifier is its frequency range of operation, because it can work up to a maximum frequency of 250 kHz. The electronic chain, constituted by the lock-in amplifier and the function generator, is controlled by a Labview® code program. The program allows to set up the amplitude of the frequency scan, to control the main acquisition parameters (mainly the scanning velocity, regulating the delay time of the lock-in) and to store data on a pc.

2.4.4. Vacuum System

The cantilever with the piezo actuator was mounted into a vacuum chamber (see Figure 3.14 and Figure 3.16). The customized chamber is an aluminium hollow cylinder, with an internal diameter of 100 mm. At the centre of the chamber there is a cylindrical pivot (with a diameter of 30 mm), on which a peltier element and its relative thermal heatsink was mounted. The piezoelectric disc with the cantilever sensor chip was locked over the peltier. The chamber was closed on the upper side by a transparent plexiglass stopper. Passing across the transparent closing system, the laser light can hit the cantilever surface, from which it is reflected towards the PSD detector. A Viton® circular o-ring was positioned between the plexiglass and the chamber, to avoid leakages. At this purpose, no clamping system was necessary. In fact, the force related to the pressure difference between the chamber and the external ambient is sufficient to pull down the stopper and so to obtain a good vacuum value in the analysis chamber. The pumping system is constituted by a series of a membrane and a turbo molecular pump (MINI-Task System, Varian Inc. Vacuum Technologies). The membrane pump supplies the primary vacuum, down to a minimum pressure of about 1 mbar. The turbo molecular pump allows to reach the maximum vacuum value of at least 10-5 mbar. The two pumps were connected to an interlock, which gives the opportunity to use both of them or only the primary one. The pressure inside the chamber was measured with two capacitive sensors (MKS

Baraton 627 for the primary vacuum and MKS Baraton 127 for the molecular vacuum), connected to an electronic controller (MKS PR4000F). The pressure can be precisely controlled and regulated by a needle valve with a incorporated micropositioner. Starting from the vacuum conditions, a little amount of ambient air can be introduced into the chamber and stable intermediate pressure values can be reached between the maximum vacuum value and a pressure of 700 mbar. The pressure conditions obtained with this method were uniform inside the chamber and stable during time.

2.4.5. Temperature Controller

To properly mechanically lock the sensor to the piezo disc and to improve the heat transfer between peltier element (PF-127-14-15, 40x40x3.9 mm3, 58W, SuperCool) and sensor chip the different parts were locked through a thermal glued (Thermal Bonding System by Electrolube Derbyshire, UK). The peltier element and its heat-sink were block on the pivot of the vacuum chamber through a thermally conductive grease (T-grease 2500 Termagon inc.). The temperature was set by a temperature controller (MPT5000 by WAVELENGTH Electronics), the feedback necessary to regulate the temperature was obtained interfacing the proportional integral derivative (PID) controller to a thermistor placed in contact to the upper surface of the peltier element. The temperature measure on the upper sensor surface was stabilized in the range of 0.1C° (see Figure 2.8).

2.4.6. Liquids Pumping System

The handling of liquids into the chip was obtained by a syringe pump (Syringe Pump 11 Pico Plus, Harvard Apparatus). The pumping system (see Figure …) was interfaced to a PC and it was controlled by a program written with LabVIEW 8.

The parameters that can be set are:

– the diameter of the syringe

– the pumping rate

– the duration of the pumping step

the delay among the different syringes to start pumping.

To connect the singe to microfluidic connection present on the sensor chip flexible transparent LDPE tube (1mm inner diameter, 2mm outer diameter, Em-Technik Italy) were used. More details about realization and characterization of microfluidic connections are described and discussed in the last Chapter.

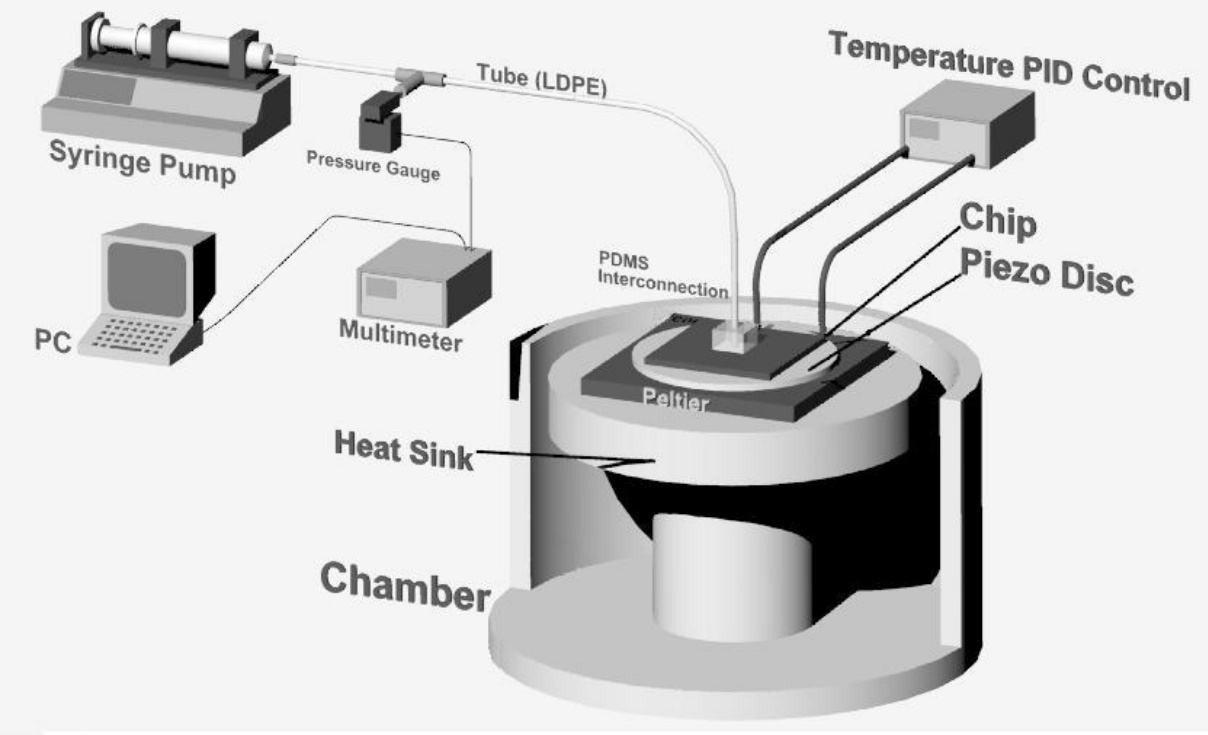

Figure 2.8 - Draft of the thermal control apparatus and the pumping system employed in the characterization set up for cantilever LOC.

For the excitation of the MCs, a small piezoelectric disk (PI Ceramic) was used. A function generator (HP 33120A) produced a sinusoidal signal that was amplified and sent to the piezoelectric actuator, to give us the possibility to control the frequency of the oscillation. The actuator was linked to a holding cell, the cantilevers were attached to the actuator with double sided tape, and the cell was evacuated to a minimum pressure of 5×10^{-4} mbar by a series of a membrane and turbomolecular pump (MINI-Task System, Varian Inc. Vacuum Technologies). Cantilever vibrational characteristics were measured with the optical lever technique.

The position of a focused laser beam reflected off the top side of the cantilever onto a position sensitive detector (PSD) was monitored.

The current output of the PSD was amplified and converted into a voltage output, sent to a lock-in amplifier (EG&G 7260) for signal extraction and filtering, and stored to a personal computer, together with the stimulus signal for the function generator.

The procedure was controlled in a LABVIEW® environment, while data were fitted with a Lorentzian curve and analyzed by software OriginTM.

Chapter 3

Biodesign for the Detection of Angiopoietin-1

3.1. Introduction

This chapter is composed by two main parts. The former regards the proof of concept used to investigate the possibility to applied microcantilever mass sensor for the quantification of protein involved in the regulatory process of angiogenesis. In this design "real" antibody antigen system has been substituted by a simulating structure based on a fusion protein. In the latter part the "real" antibody antigen system is used. Selective interaction between biological substances and the inorganic cantilever surface is possible only after a chemical functionalization and surface activation. For this purpose each section concerns a bio-design and includes a briefly description of the biological and functionalization background on which the experimental detection procedure is based. To this purpose, descriptions of different functionalization and activation procedures are reported and the obtained results are discussed.

Applicability of cantilever array as biosensors is demonstrated in order to evaluate the quantity of a protein involved in the cancer angiogenesis mechanism. This kind of measurements is innovative and can provide a lot of information for a better understanding of this complex phenomenon.

3.2. Biological background

Tumour angiogenesis, the formation of new blood vessels from the existing vasculature, is a complex dynamic process consisting of extra-cellular matrix re-modelling, endothelial cell proliferation and capillary differentiation, coordinated by several classes of growth factors acting through cognate tyrosine kinase receptors. It is established that angiogenesis is an essential process in the development and progression of malignancy [102].

A deep understanding of angiogenesis process opens new ways in the field of cancer care, with the possible design of new anti-angiogenic drugs acting during the first steps of tumour development. At this purpose, the goal is to be able to characterize all the vectors (commonly, different kind of proteins) involved in such phenomena.

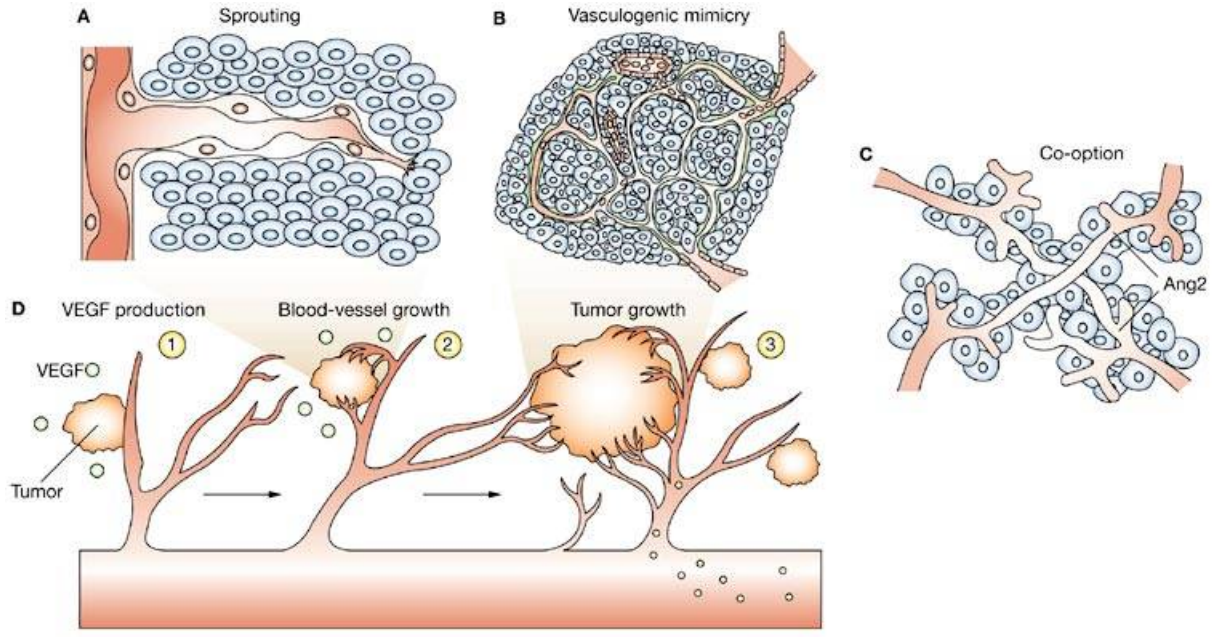

Figure 3.1 – Simple drawing of the cancer angiogenesis process

Thus angiogenesis is a complex multistep process regulated by extra-cellular matrix remodelling and by endothelial cells (ECs) proliferation, survival and motility. Angiogenic program is triggered

predominantly by several different Growth Factors (GFs) and their associated Tyrosine Kinase Receptors (TKRs) [103]. Foremost among GFs and TKRs is the Vascular Endothelial Growth Factor (VEGF) family and VEGFRs (VEGF receptors). Considerable progress has recently been made towards delineating the signal transduction pathways distal to activation of VEGFRs. In particular, VEGF-A_{165} was identified approximately 15 years ago and has been recognized as the major growth factor that is relatively specific for Ecs. Beside the vascular endothelial growth factor (VEGF) and its receptor Flt-1, the most widely studies concerns the angiopoietin family of molecules, angiopoietin-1 (Ang-1) and angiopoietin-2 (Ang-2), and their receptor Tie-2 [104]. Angiopoietin-1 and Ang-2 have both been identified as ligands for Tie-2, a receptor expressed on endothelial cells, and it has been shown previously that Ang- 1 and Ang-2 play critical roles in angiogenesis, in concert with VEGF [105]. Angiopoietin-1 binding to Tie-2 maintains and stabilizes mature vessels by promoting interaction(s) between endothelial cells and surrounding extra-cellular matrix. Angiopoietin-2, however, competitively binds to Tie-2, and antagonizes the stabilizing ability of Ang-1, resulting in an overall destabilization of vessels. These destabilized vessels may undergo regression in the absence of VEGF; however, when VEGF is present, these destabilized vessels may undergo angiogenic changes. Thus, angiogenesis is controlled by a dynamic balance between vessel regression and growth, mediated by VEGF, Ang-1 and Ang-2, which has been shown in numerous experimental studies [106].

Despite the accumulating histological data reporting differences in the expression of members of the Angiopoietin family on the surface of various normal and tumour cells [107], data of these growth factors in plasma from cancer patients are scarce. Indeed, one of the few recent papers reporting plasma Ang-1 levels was in rheumatoid arthritis [102]. Increased levels of VEGF, but not soluble (plasma) Flt-1 (i.e. sFlt-1), are present in the plasma of subjects with breast, hematological and renal cell neoplasia. The importance of sFlt-1 in plasma is unclear, but as it retains the ability to bind to VEGF, it may have some modulatory role, or alternatively may simply be an artefact of the effects of the disease on the endothelium.

So even if it is clear that the mechanism through which cells process extracellular signals from membrane receptors by consequent transduction of biological responses is mediated by a dynamic network, spatially oriented among biomolecules a major problem is to understand how a receptor generates a specific signal. For instance, in the same cell type the same receptor induces different responses. To explain this phenomenon one hypothesis is based on quantitative differences in protein recruited downstream the receptor, in the number of receptors activated, in the amount of ligand and in the time frame of the stimulus. The low concentration marker released during such kind of phenomena is not detectable with conventional biological analysis techniques. Thus to

achieve new and relevant insight in biomolecular sciences it is necessary to develop new tools for fine and precise quantitative measurements. At this purpose microcantilever biosensors have the potentiality to give a relevant improvement to that kind of measurements. A quantitative evaluation of molecules involved in the receptor-ligand binding interaction can provide important information for a deeper understanding of the problem, helping to obtain a most reliable model for those phenomena. Moreover one of the most important challenges in the fight against cancer is the ability to detect cancer cells early in the disease [108]. To achieve this overall goal, new and innovative technologies that will allow detection of early stages of cancer cells sensitively and accurately are needed. This goal is central to reducing most cancer-associated deaths as the available cancer drugs and treatment procedures can lengthen the lifespan of most cancer patients if the disease is detected early. A major shortcoming associated with the early detection and treatment of cancer is the lack of sensitive and robust technology to detect the signatures of cancer cells from minute quantities of available tissues or serum. The lack of technological platform has significantly slowed the identification of reliable biomarkers to accurately diagnose most types of cancers [109]. Defining the molecular mechanisms that give rise to the cancer phenotype is also believed to represent a critical step in developing an effective therapeutic regimen for cancer patients [108]. Thus, effective treatment will require specific genotyping of expressed genes or proteins in the cancerous tissue. Once the expression profile associated with the underlying pathogenesis of the cancer is determined, one can presumably select a treatment regimen that is best suited for a specific type of cancer. To get inside this problem it is interesting take a look at the numbers involved in cancer pathologies. Breast cancer is the leading cancer in women, accounting for 16% of female cancer deaths, translating to some 40,000 new cases and 12,000 deaths in the UK each year [108]. Characterized by inappropriate and abnormal cell growth and potential to metastasize, a principal factor in this tumour enlargement is the requirement of an increased blood supply to feed the growing mass of cells. This process, orchestrated by growth factors such as vascular endothelial growth factor (VEGF) and the angiopoietins (all measurable in the blood), involves new blood vessel development (angiogenesis). However, the clinical relevance of increased levels of angiogenic growth factors in the blood is unclear [107]. Increased levels of the cell receptors (e.g., Flt-1, Tie-2) for these growth factors are present in the blood but, once more, implications for cell biology and clinical outcome need development [110]. Whilst the literature on VEGF is considerable, there are relatively little clinical data on angiopoietin-1 and angiopoietin-2. For example, raised plasma VEGF in breast cancer is commonly reported and is higher in metastatic disease [105], and fall 5 days and 3 weeks after surgery. Furthermore, therapy aimed at VEGF is promising and provides a possible link with clinical outcome. The majority of published work on

the angiopoietins and its receptor (Tie-2) focuses on tissue culture and animal models, levels in tissues, or on RNA/DNA (e.g., [111]). More recently, changes in levels of cytokines such as interleukin-6 (IL-6) in breast cancer imply a degree of inflammation in these patients. Furthermore, IL-6 and angiogenic growth factors can also be found within platelets although the significance of this is unknown. Raised levels of the platelet marker soluble P-selectin in cancer may be related to this finding. The frontier of oncological therapies is the use of targeted drugs, which act on specific phases of neoplastic progression. However it is difficult to evaluate the efficacy of these therapies, because the classical parameters used in evaluation of chemo-therapic drugs (survival, cytoreduction, time free of disease) are not appropriate for these drugs, which act with more sophisticated mechanisms and act and earlier stages of the disease, when the recruitment of patients in phase I clinical trials is not allowed. Therefore it is mandatory to find out specific biomarkers and precise tools for their quantification to measure their variation during the therapy.

Angiogenesis is one of most promising target therapies in clinical oncology and recently a humanized monoclonal Antibody anti- vascular endothelial growth factor A (bevacizumab) has been successfully used in the treatment of some solid tumor [109]. However many other clinical trials have failed over the years. This has been related to the design of the phase I clinical trial done in end-stage patients and the lack of surrogate markers. Actually the preclinical models have clearly demonstrated that angiogensis inhibition reveals its optimal efficacy and the onset of tumor progression [111]. Right now the surrogate markers available to follows the following:

i) the count of microvessels in bioptic specimens. This technique however is too many invasive, requires the identification of specific area of tumor growth in which the vascularization really correlates with the tumor growth and therefore it is not suitable for timely monitoring;

ii) the count of endothelial cell precursor in the blood. This technique seems to be sensitive and parallel the effect of bevacizumab treatment in a phase I trial in colon cancer, but it may be performed exclusively in highly specialized centers,

iii) magnetic resonance imagining, but the current level of sensitivity to monitor the decrease of capillaries is not always sufficient ;

iv) the measurement of angiogenic inducers in bloodstream by immunological techniques. This is the simpler method, but the present sensitivity is not completely appropriate.

3.3. State of the art of standard Angiopoietin detection procedures

Most recently developed biosensors rely heavily on labelled reagents, as in enzymelinked immunosorption assay (ELISA), enhanced immunoassay in conjunction with multiphoton detection

method (IA-MPD), fiber-optics, and other optical measurements, such as surface plasmon resonance (SPR). Other techniques, including immuno-PCR (polymerase chain reaction), depend on complex amplification schemes to detect targets. Each of these methods has been used extensively in biosensing applications; however, each method has a specific set of limitations – they require sample preparation, are limited by low sensitivity (pg/ml to ng/ml), and/or exhibit poor specificity in complex matrices with a high degree of background noise.

Growth factors and receptors were measured by enzyme-linked immunosorbent assay (ELISA) as follows [598, 655-657]: mouse anti-human Ang-1, biotinylated goat anti-human Ang-1 and recombinant human Ang-for the Ang-1 assay, mouse anti-human Ang-2, biotinylated mouse anti-human Ang-2 and recombinant Ang-2 for the Ang-2 assay, goat anti-human tie-2, biotinylated goat anti-human tie-2 and recombinant human tie-2/Fc chimera for the tie-2 assay, and rabbit anti-human VEGF, biotinylated goat anti-human VEGF, biotinylated goat antihuman Flt-1 and recombinant human VEGF-165 for the VEGF assays (all obtained from R&D Systems, Abingdon, Oxfordshire, United Kingdom). The precise methods for VEGF, tie-2, and Ang-2 are available elsewhere [112].

Chapter 4

Results

MicroCantilever Funtionalization

The molecular recognition via cantilever-based sensing is deeply related with the activation processes of the surface of a MC, the ability of the Antibody (Ab) to recognize its specific target (Antigen - Ag) and the evaluation of the frequency shift due to the mass loaded on the MC.
Therefore, MC functionalization is a crucial step which determine the successfulness and the performances of the measurement. It consists firstly on a chemical functionalization which activate the silicon surface for the binding of bio-molecules. In fact, since the inorganic silicon surface does not allow any interaction and binding with biological substances, a chemical functionalization is necessary. At this purpose a sequence of six stages of chemical activation and protein binding have been performed on the cantilever surface.
Briefly, the surface functionalization steps are:

- ✓ a thermal oxidation of the cantilever, in order to obtain a silicon oxide flat surface. A dipping in piranha solution allows to obtain an active surface which exhibit hydroxyl (-OH) groups;

- ✓ a surface silanization of the surface. The chosen silanization agent is the 3-aminopropyltriethoxylsilane (APTES). A Self-Assembled Monolayer (SAM) is produced through a wet process. Active amino groups (-NH_2) are exposed on the surface after the treatment;
- ✓ a surface activation with glutaraldehyde, which allows to obtain the exposition of aldehyde (-CHO) groups.

After that, the following sequence of protein bindings on the activated surface has been exploited:

- ✓ Protein G binding;
- ✓ Antibody binding;
- ✓ Exposure to the target analyte (Antigen, Ang-1)

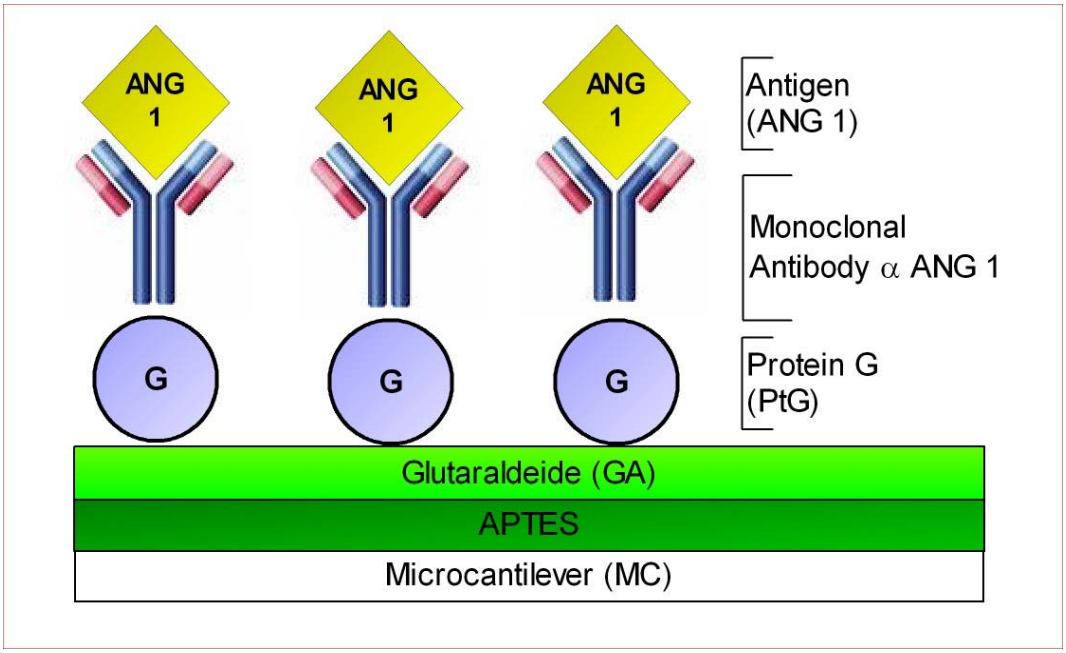

Figure 4.1 - Scheme of the functionalization procedure adopted for the development of MC biosensor.

The six steps will be described in sequence. After every functionalization and binding step, the vibration properties of the cantilevers have been measured to evaluate the frequency shift.

4.1. Surface Chemical Activation

The surface functionalization that lead to the formation of an active surface able to bind biomolecules consists in five steps, that will be described in details above.

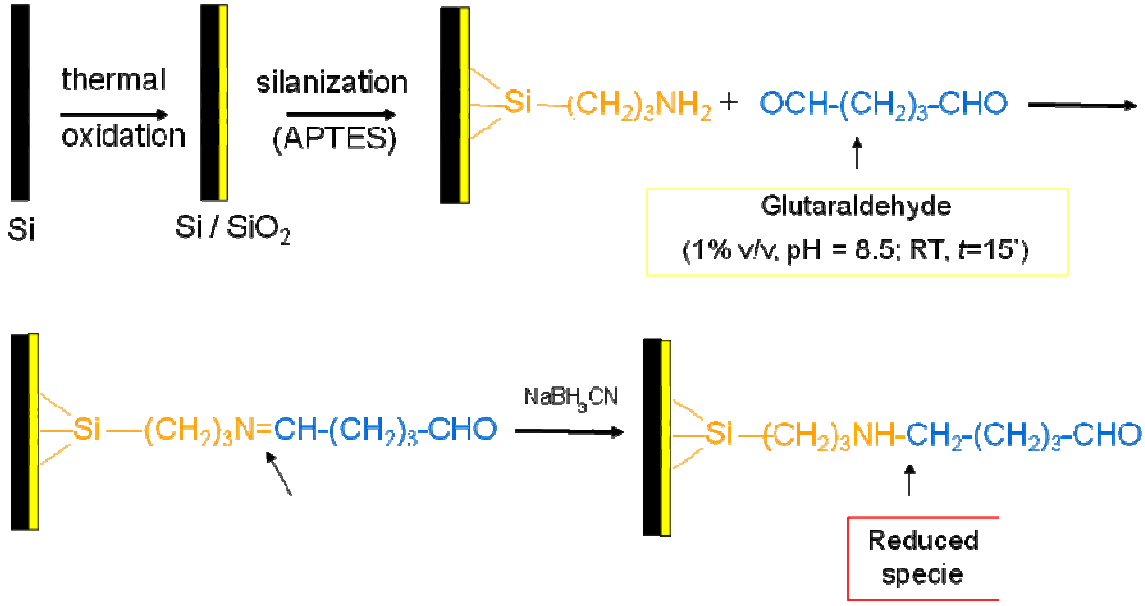

Figure 4.2 - The surface chemical activation steps: (1) thermal oxidation of the silicon surface; (2) silanization; (3) activation with glutaraldehyde.

4.2.1. Oxidation

The samples have been thermally oxidized on a tubular quartz furnace (Tempress), heated with a series of resistances. The procedure foresees a dry oxidation in air, at ambient pressure, without any carrier gas. The operation temperature is 1050°C, the oxidation time is about three hours. A 100 nm thick SiO_2 layer is produced. The thickness of the deposited layer has been measured with a profilometer (Tencor P-10) after a HF oxide etching on a selected area to draw a step. At this purpose a square 1x1 cm^2 silicon sample is putted in the furnace together with the cantilever samples. Since the beam is suspended, the oxidation occurs on all the cantilever surfaces.

After the oxidation the samples are cleaned in acid "piranha" solution (H_2SO_4 : H_2O_2, 4:1). This cleaning procedure allows the removal of all the organic residues on the surface. Since the acid mixture is a strong oxidizer, it removes most organic matter, and it also hydroxylates the oxide surface (adding -OH groups), making it extremely hydrophilic (water compatible).

4.1.2. Silanization

The first chemical step consists in a wet silanization process. The formation of organosilane monolayer on silicon oxide surface by a liquid phase reaction is a well known procedure to obtain amino-terminated surfaces. At this purpose the chosen silanization agent is the (3-Aminopropyl) triethoxysilane (APTES).

APTES: $H_2N(CH_2)3Si(OC_2H_5)3$

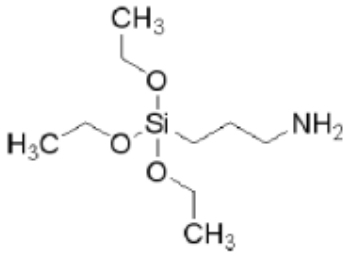

The APTES molecule binds to the silicon oxide surface (now exposing hydroxyl groups), creating a Self-Assembled Monolayer (SAM). The surface after the silanization procedure has been characterized with X-Ray Photoelectron Spectroscopy (XPS).

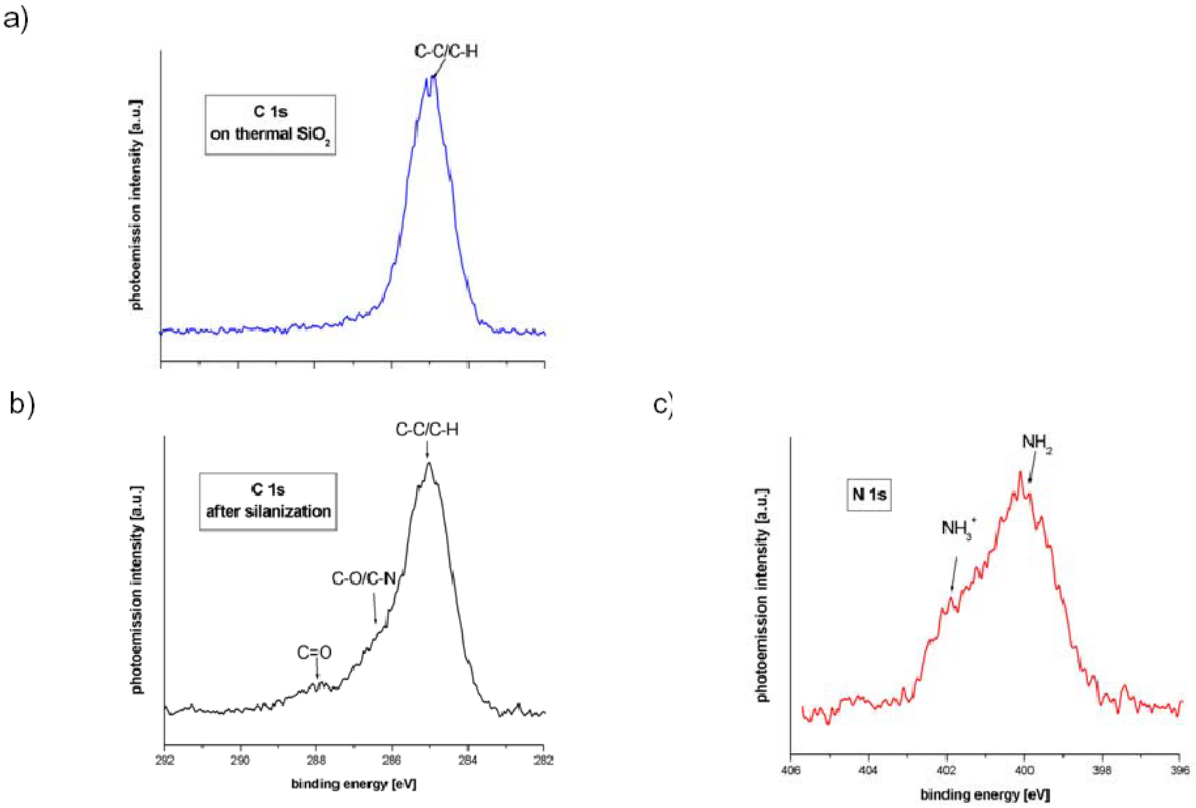

Figure 4.3. - XPS spectra analysis shows the formation of amine groups on the oxide surface and confirms the goodness of the silanization procedure. XPS analysis of the SiO2 surface, (a) before and [(b), (c)] after the silanization.

4.1.3. Functionalization with glutaraldehyde

The silanization process creates a surface which exposes active amine groups. For a good protein binding it is better to have a surface with aldehyde (CHO) groups. At this purpose a functionalization with glutaraldehyde has been carried out.

Glutaraldehyde: $OHC(CH_2)3CHO$

The activation of silicon MCs is based on chemical steps, that provide the linkers for biological molecules, and antibodies binding that enable the measurement of antigens mass with extraordinary sensitivity. Topographic analysis (FESEM, AFM) shows a very flat surface, compatible with a SAM formation, both after the silanization procedure and after the glutaraldehyde reaction.

	Contact Angle water [°]	Contact angle diiodomethane [°]	Surface energy [mN/m]	Dispersive component [mN/m]	Polar component [mN/m]
Thermal oxide	35.3	34.9	61.92	29.04	32.89
APTES	62.8	39.9	45.75	31.7	14.04
Glutaraldehyde	89.5	43.6	37.79	36.36	1.43

Table 4.1 Contact angle analysis of silicon surfaces before and after the funcionalization processes

4.2. Biological functionalization

The immobilization of antibodies is a critical component for the design of a successfully nano-mechanical biosensor. Monoclonal antibodies can be directly immobilized on the silicon surface of cantilevers, functionalized by aminosilan and glutaraldehyde. However, better results are achieved when protein G is applied as a crosslinker between the modified interface of the silicon cantilever surface and the IgG. In fact, attachment of antibodies directly to substrates frequently reduces their ability to bind antigen. Binding antibodies in controlled orientation or allowing them mobility on the end of a "tether" molecule can enhance the fraction of antibodies that remain fully functional, potentially improving the sensitivity of the biosensor. The use of protein G avoid random IgG variable domain orientation and, therefore, provide more binding sites for target antigens.

4.2.1. Antibody characterization: ELISA assay

As described previously, the specificity of a MC biosensor is directly related with the ability of the sensing element (Ab) to recognize and bind the specific target (Ag) without the interference of un-specific bindings. Thus, the choice and the characterization of the Ab is crucial for the development of a MC biosensor.

Firstly, we design and developed an Enzyme Linked ImmunoSorbent Assay (**ELISA**), to evaluate the performance of the Ab. The ELISA assay was based on a sandwich non-competitive ELISA (see Figure 4.4), consisting of an Human anti-Ang-1 Antibody (capture antibody) and a biotinylated goat antihuman Ang-1 (detection system). ExtrAvidin peroxidase was used to amplify the antibody-antigen reaction, and the color was developed using ortho-phenylenediamine dihydrochloride tablets. Mouse anti-human Ang-1 antibody was adsorbed onto 96-well microtitre immunoassay plates for a minimum of 15 h at 4°C (i.e., overnight) at concentrations ranging from 0.5 to 10 μg/ml. Biotinylated goat anti-human antibody at concentrations ranging from 250 to 500 ng/ml was combined to measure plasma Ang-1. Optimum titres were determined using checkerboard titration, seeking high optical density from standards and minimum optical density from blanks. Standard curves were generated using recombinant human Ang-1 (rHAng-1) protein at 0 to 1.000 ng/ml. The final protocol for Ang-1 ELISA is as follows (18): First, 96-well microtitre immunoassay plates were coated with 100 μl/well of 2 μg/ml mouse anti-human Ang-1 in 0.05 mol/l carbonate/bicarbonate buffer (pH 9.6) for a minimum of 15 h at 4°C. Plates were then washed three times in assay buffer (0.05% Tween 20 in 0.1 mol/l phosphate buffered saline, pH 7.2) and in

between each subsequent incubation period. After blocking for 2 h at room temperature with 5% dried powdered milk in phosphate buffered saline-Tween (200 µl/well), recombinant human Ang-1 standards (ranging from 0 to 100 ng/ml) and plasma samples were added in duplicate (100 µl/well) for 2 h at room temperature; 100 µl/well biotinylated detection antibody (500 ng/ml) was then added for a further 2 h at room temperature. ExtrAvidin peroxidase (1:1,000 dilution) was added for 45 min at room temperature (100 µl/well) before the development of color with 10 mg orthophenylenediamine dihydrochloride dissolved in 20 ml 0.05 mol/l citrate buffer (pH 5.0) and 10 µl 1 mol/l hydrogen peroxide. The reaction was stopped using 1 mol/l hydrochloric acid and the absorbance read at 492 nm. The intra-assay coefficient of variation was 3.87% at 20 ng/ml Ang-1 (n = 24), and 4.13% at 40 ng/ml. Inter-assay coefficient of variation was 9.45% at 20 ng/ml (n =8) and 9.78% at 40 ng/ml (n = 7). The lower limit of sensitivity for the assay was a concentration of 1 ng/ml Ang-1.

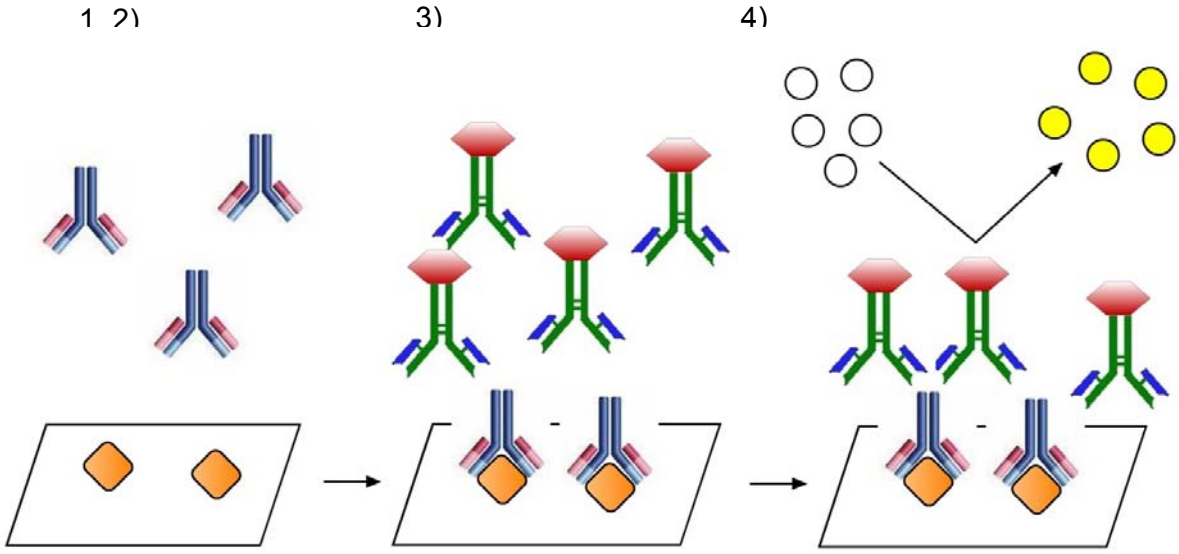

Figure 4.4. - Scheme of the ELISA procedure. The sequence is: (1) rHAng-1 (antigen); (2) Human anti-Ang-1 Antibody (capture antibody); (3) Goat antihuman Ang-1 –HRP (secondary Antibody); (4) detection (color change of the solution).

4.2.1. Antibody characterization: ImmunoPrecipitation assay

The specificity function of antibodies has been detected in detail to avoid the recognition of non-specific antigens. The ImmunoPrecipitation (**IP**) assay provided an useful tool to evaluate the physical interaction between an antibody and its target in solution and to estimate the presence of

non-specific recognitions. We identified a monoclonal Ab (A0604, Sigma Aldrich) able to recognize specifically our target analyte, ANG-1, and we tested the quantity (2.5 μg) necessary to detect the maximum concentration of ANG-1 in pathological conditions.

To visualize the interactions the IP assay is followed by Western Blot: the molecules transferred on membrane can be targeted with specific antibodies conjugated with enzymes which provide a chemi-luminescent signal.

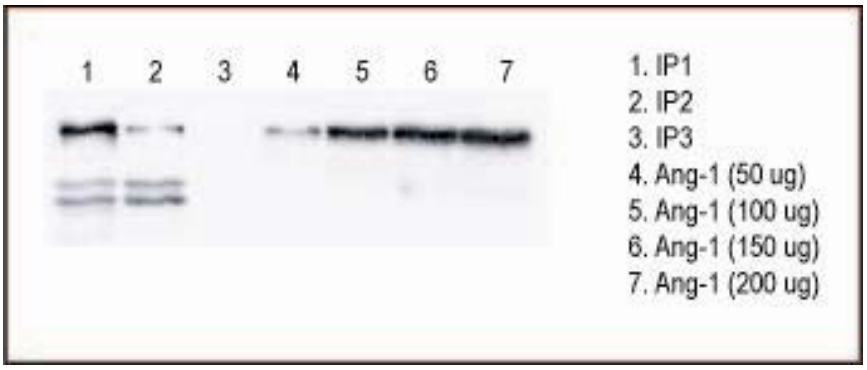

Figure 4.5 – Western Blot obtained to visualize the IP developed to capture Ang-1 and standard curve of Ang-1 to calibrate the quantification

4.3. Proof of Principle: in vacuum measurements

4.3.1. Preparatory measurements

First of all, we performed a critical run of measurements aimed at the evaluation of primary sources of uncertainty of the experimental set-up. The first and second flexural mode of vibration in vacuum were monitored, while changing one by one the following parameters: vacuum level (4×10^{-2} to 8×10^{-4} mbar), laser spot on MC (3 positions between middle and free end), PSD angle with respect to laser reflected spot (33–40°), piezo-actuator applied tension (0.05–9 V), cantilever dimensions (3 different size MCs), operator (3 different researchers did optimize the same measurement). First flexural modes of vibration (M_1) were found in the range 4–8 kHz, while second modes (M_2) in the range 30–50 kHz. In such a way, we wanted to understand how the measurement uncertainty could be affected by the optimization of the experimental set-up. In particular, we wanted to compare the two modes in terms of precision (i.e. the variability of a measurement around its average value) rather than sensitivity. As a matter of fact, more than one research group has recently demonstrated the significant advantages in mass sensitivity when monitoring higher modes of vibration respect to

the fundamental one [113]. However, such works usually focus just on the improved detector sensitivity (essentially given by the increasing of resonance curve Q-factor), while a careful analysis of repeatability and reproducibility of frequency measurement is needed, in our opinion, to corroborate such advantages.

To this purpose, 49 measurements of both M_1 and M_2 were collected in the above-mentioned conditions and 4 different histograms were created, using relative frequency shifts Δf/f instead of absolute frequencies in order to compare different MCs and different vibration modes (see Figure 4.6.).

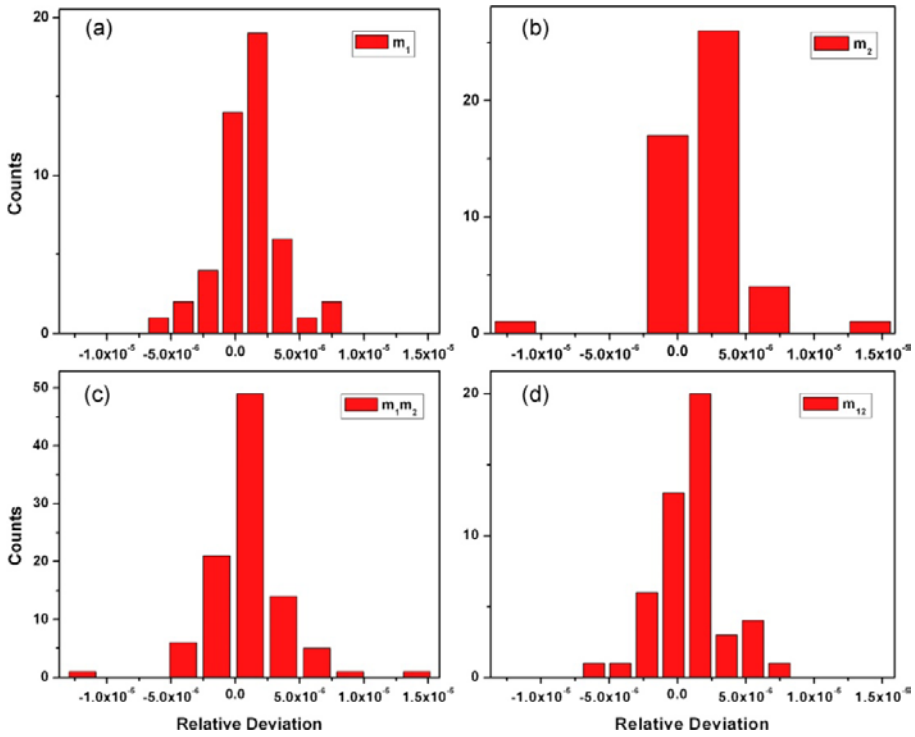

Figure 4.6. – Histograms with the plot of the relative frequency shifts Δf/f obtained for M_1, M_2, M_1M_2 and M_{12}

The standard deviation of the first mode resulted to be $\sigma_{M1} = 2.7 \times 10^{-6}$, while the standard deviation of the second mode resulted to be $\sigma_{M2} = 3.5 \times 10^{-6}$: therefore,$M_2$ uncertainty is evaluated to be roughly 30% greater than M_1 one. Furthermore, the range (i.e. the difference between the highest and lowest values) of the first set is half of the second: 1.3×10^{-5} versus 2.6×10^{-5}. Then, although both distributions are characterized by a significant and satisfying low uncertainty, we can deduce that, in our experimental set-up, measuring the second mode instead of the first one give a

less precise result. If we consider all the data as a single distribution with 49×2 = 98 data (M_1M_2), we have $\sigma_{M1M2} = 3.1 \times 10^{-6}$, that is still larger than σ_{M1}, and the range is clearly as large as M_2: 2.6×10^{-5}. On the contrary, if we calculate the arithmetic mean of the two modes as $M_{12} = (M_1 + M_2)/2$, the related distribution is characterized by the lowest standard deviation $\sigma_{M12}= 2.5 \times 10^{-6}$, and the range is roughly the same as M_1: 1.4×10^{-5}. Furthermore, the Chi-squared test shows that M_{12} distribution is the only one that follows a Gaussian distribution. We merged the external bins of the 4 histograms to have at least 5 counts for each bin and then we calculated the reduced , in order to easily compare distributions with different degrees of freedom [114].

The results are χ^{-2} $M_1 = 5.6$, χ^{-2} $M_2 = 8.4$, χ^{-2} $M_1M_2 = 8.1$, χ^{-2} M12 = 4.1. With a confidence level (P-value) of 5% we can state that just M_{12} has a non-significant discrepancy with a Gaussian distribution since $Pd(\chi^{-2} \geq \chi^{-2} M_{12}) \geq 5$, while it is significant for M_1 since $1 \leq Pd(\chi^{-2} \geq \chi^{-2} M_1) < 5$, and highly significant for M_2 and M_1M_2 since $Pd(\chi^{-2} \geq \chi^{-2} M_2, \chi^{-2} M_1M_2) < 1$ [114].

Preliminary results, not reported here, on $\tilde{\chi}_0^2$ third and fourth modes show a similar behaviour. We can then argue that higher modes can reduce the repeatability and reproducibility of the frequency measurement, while mediating them with the fundamental one represents a suitable tool to easily obtain precise and normally distributed measurements. The obtained standard deviation $\sigma_{M12}= 2.5 \times 10^{-6}$ can represent the uncertainty of the detector, which is remarkably lower with respect to the uncertainty of the whole bio-experiment. We performed negative control experiments, in which the protein immobilized MCs are dipped into PBS solution to evaluate the influence of non-specific adsorption/desorption on resonance curves. We found that typical relative frequency shifts after PBS dipping are of the order of $(\Delta f/f)PBS = 1\times10^{-4}$ although this value is 50 times larger than _M_{12}, it is still one order of magnitude lower than typical variations due to protein binding.

Since non-specific binding is often addressed as the major limit on ultimate cantilever-based sensitivity [113], we will use $(\Delta f/f)PBS$ as our experimental limit of detection: frequency variation below this limit was labelled as statistical fluctuation.

4.3.2. Ang-1 Quantification

Once that the chemical and biological functionalizations has been tested it has been possible to investigate the vibration characteristic directly on MCs. Since complex samples such as plasma, serum or cellular extract contain a high concentration of heterogeneous analyte, the protein binding steps for the proof of principle got to be run on a simplex media such as saline buffer (PBS) enriched with the target antigen.

The experiment consisted in characterizing the first and second flexural mode of different sized MCs in vacuum before and after protein immobilization. Using the equation described previously (see section 1.3.2) it is possible to link the shift of the eigen frequency value to the corresponding mass.

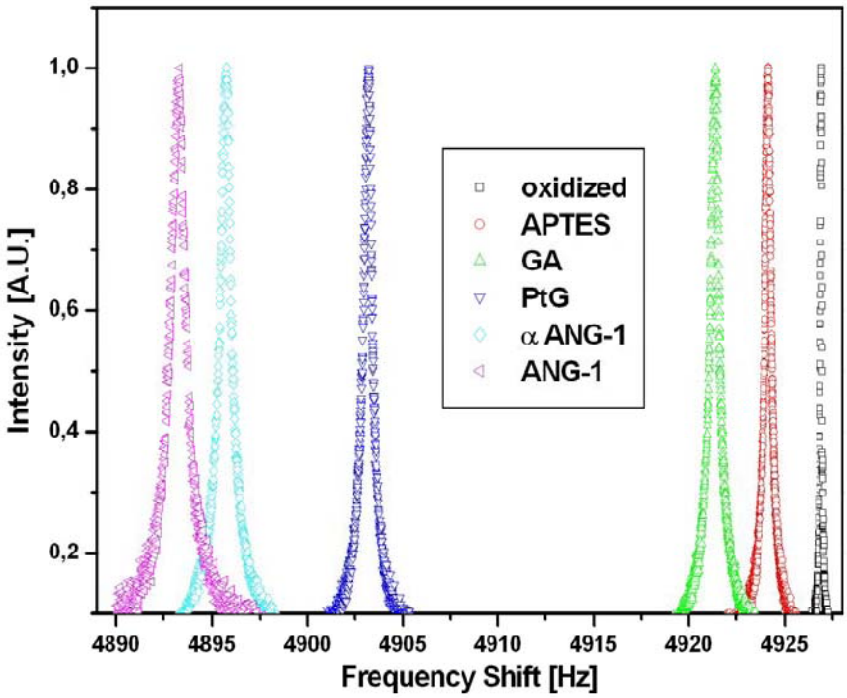

Figure 4.7 - Representation of Lorentian resonance curves after each experimental step. The increased mass is directly proportional to the negative shift of the resonance of the cantilever.

The direct relationship is applicable if the added mass is uniformly deposited on cantilever surface and if the beam spring constant k remains essentially constant after molecule binding. These requirements are commonly proofed in microcantilever-based biosensing, because the adsorbate properties such as thickness, stiffness and surface stress, have a neglecting influence on the vibrational characteristics of the Si resonator [115-117]. Measurements were performed in high vacuum conditions (with a pressure of about 10^{-5} mbar), to avoid the air damping effect.

Preliminary results on different samples have been used for the analysis and, according to the theory, shift of the resonance peaks towards the lower frequencies after every step indicates the mass increase of the structure.

Specific binding of the antibody anti-Ang-1 on different sized MC induced resonant frequency shifts corresponding to mass increments in the range of 0,2-0,5 nanograms, which in terms of

molecules per surface unit leads to an average value of $2x10^{12}$ molecules/cm^2. This attached protein density is really close with the theoretical maximum density estimated from the known size of an antibody, IgG molecules have an estimated planar dimension equal to 23.5 x 2.5 nm^2, which corresponds to $2x10^{12}$ molecules/cm^2. Hybridization with Ang-1 induced resonant frequency shifts corresponding to added mass in the range of 2-0,2 nanograms, which in terms of molecules per surface unit leads to an average value of $14x10^{12}$ molecules/cm^2 [118].

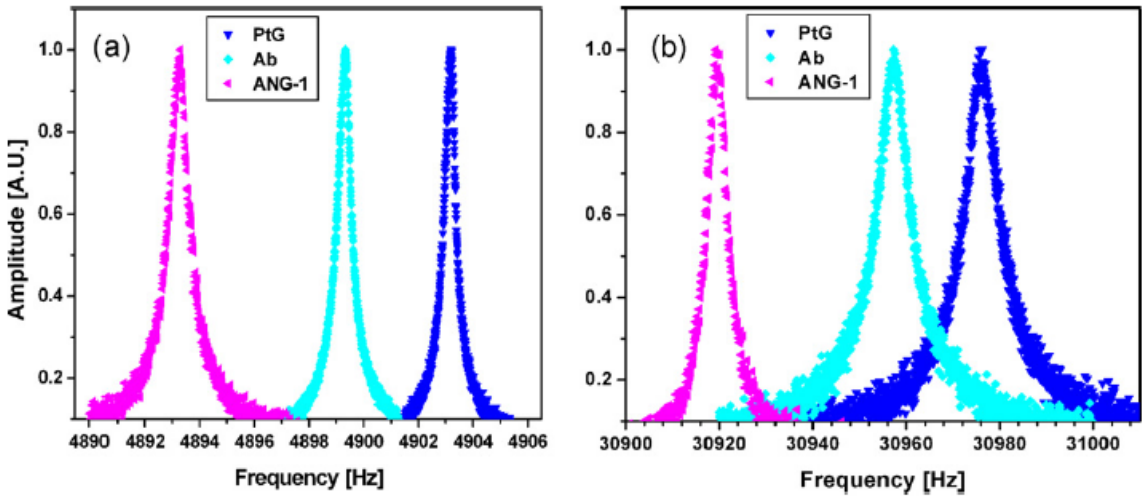

Fig. 4.8 - Resonant curve for the Antibody–Antigen experiment: (a) first flexural mode, (b) second flexural mode. PtG is used as abbreviation of Protein G

4.3.3. Specificity Test: Buffer Effect

The measurements specificity is an important feature that has to be investigated. To assure a correct mass evaluation of the analyte one has to verify that no non-specific binding of different substances during the reaction baths are present. An example of specificity measurement is reported in Fig. 6.11. On this example the cantilever, after the pA binding, has been dipped in the buffer solution used for the antibody binding, but without the receptor. On this experiment only non-specific binding can be present. Non-specific binding causes the frequency shift between the pA (blue) and the buffer (cyan) curve of Figure 4.9. It is possible to note that a very little frequency shift (lower than 1 Hz, which can be considered the frequency resolution limit) is revealed on this measurement.

Therefore, the non-specific signal on mass detection is lower than the experimental error estimation and mass measurements can be considered as reliable and they confirm the goodness of the binding protocol.

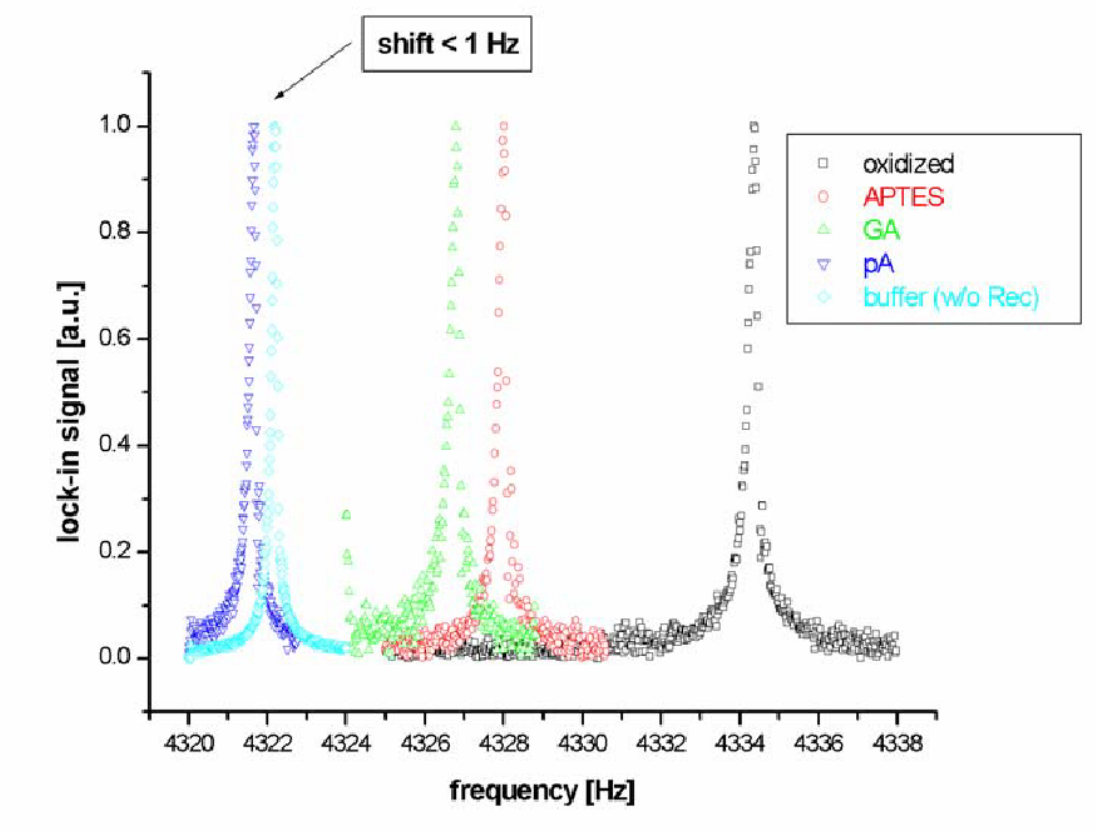

Figure 4.9 - Specificity measurements, to test the effect of non-specific binding on the cantilever frequency shift. The first mode vibration spectra are showed. The (nominal) beam dimensions are 800 x 100 x 2 μm^3

4.3.4. Selectivity Test

While the sensitivity of the method has been calculated in the Proof of Concept experiments, the selectivity of the developed system is here discussed.

Another growth factor, VEGF, is chosen as a false antigen to check the chemical and physical interaction of the cantilever-based platform with different antigens.

The figure below reports the graphical comparison between resonance curves of one cantilever dipped in Ang-1 solution versus one dipped in VEGF-A165 solution ("false" antigen). The same

relative scale on x-axis is used to better evidence the large difference in the frequency shift induced by protein adsorption. The average relative frequency shift resulted $\overline{(\Delta f / f)_{VEGF}} = (-1.1 \pm 0.8) \cdot 10^{-5}$, lower than our experimental limit of detection and nearly two orders of magnitude lower than typical shifts due to specific recognition.

These results underline the nearly perfect selectivity of the developed system. Besides, further measurements with both the antigens at different levels in blood should be investigated.

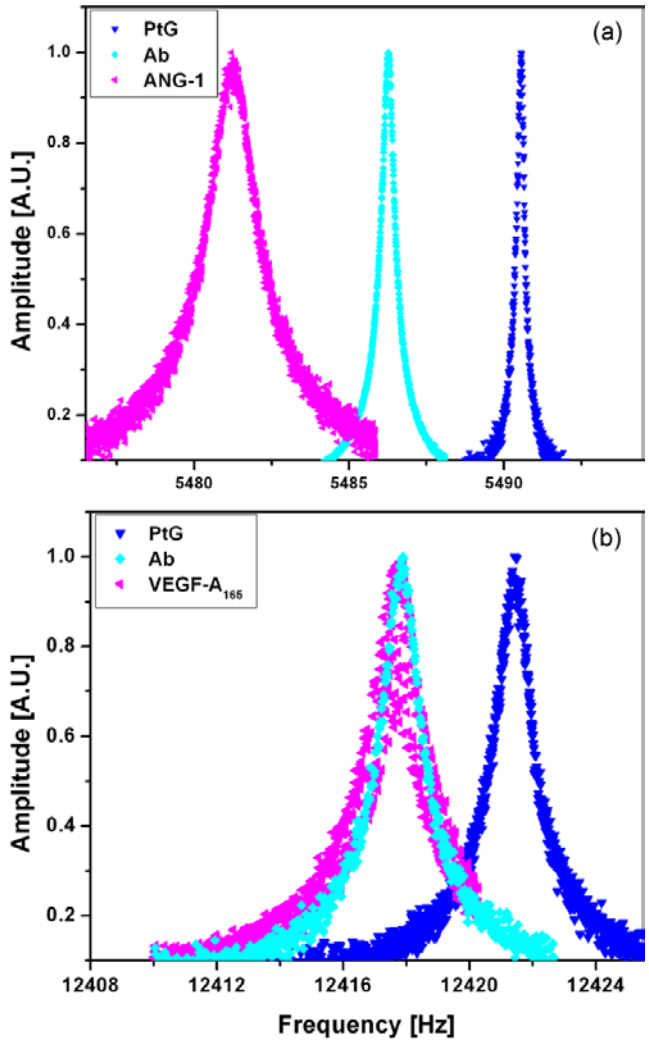

Figure4.10 - Specificity test: (a) true antigen, Ang-1, (b) false antigen, VEGF-A165. PtG is used as abbreviation of Protein G.

4.4. Measurements in Real Matrix

4.4.1. Sample Preparation: Plasma Depletion

Since complex samples such as plasma, serum or cellular extract contain a high concentration of heterogeneous analyte, the proof of principle got to be run on a simplex media such as saline buffer (PBS) enriched with the target antigen.

Once that all parameters (specificity and efficiency of IgG coated on a silicon surface) has been detected in a simplex media it is possible to translate the measurements into a more complex media, plasma, to mime the environment in which a diagnostic tool got to be used. Since the 80-90 % of plasma or serum is represented by Albumin or its precursor, it is fundamental to study a method to eliminate those molecules, being sure to preserve all the other components. The remaining fraction, representing the low abundant protein, is the main focus of many investigations into new plasma biomarkers, since it is proposed that subtle changes in the patho-physiological of various conditions may be reflected in this small pool of proteins. Therefore, the removal of highly abundant protein is essential to discover new biomarkers for disease such as cancer. A chemical-based extraction method, focus on salt fractionation, has been optimized to reach this purpose. The plasma was obtain form murine models, thanks to IRCC. The plasma clarification procedure has been validate by IP and Western Blot assays, confirming the effective and specific removal of Albumin (Figure 4.11).

Those are the requirements for the development of mass detector biosensor based on MC systems that would permit to shift from qualitative data to quantitative measurements of key molecules involved in physiological processes. Thus it will be possible to quantify the presence in plasma of small amounts of cancer markers, such as Angiopoietin-1 (Ang-1), and their modulation during the early stages of tumor development. Published results underline in fact that abnormal levels of Ang-1, Ang-2 and their receptor, Tie-2, are present in breast and prostate cancer, and their interrelationships may be important in the pathophysiology of these conditions.

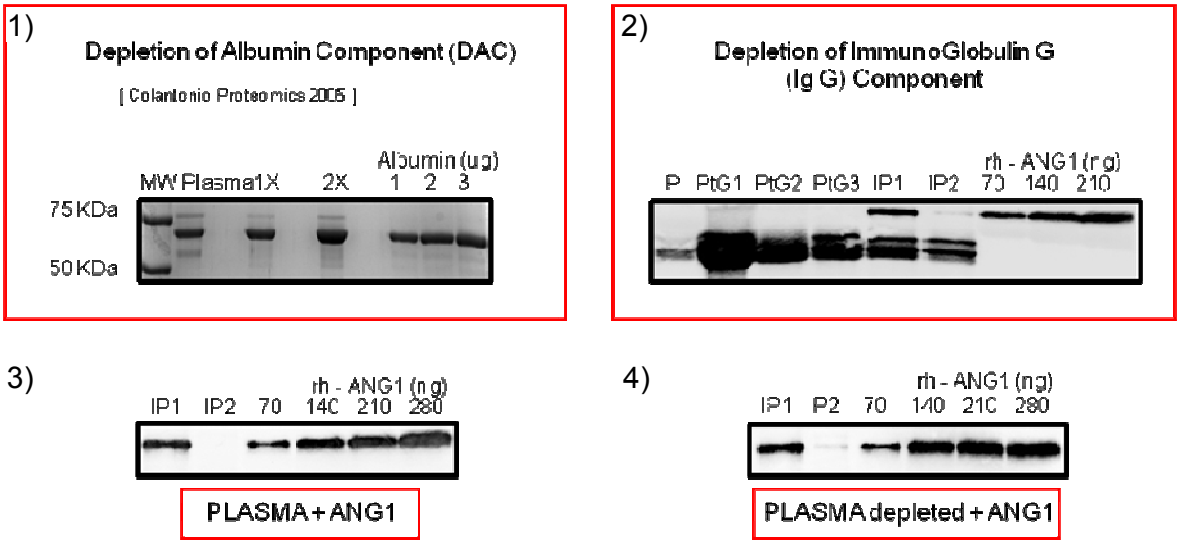

Figure 4.11 – Western Blots of the different steps of the plasma clarification processes. 1) Depletion of the Albumin component, of the IgG (2) and verification of the presence of the target analyte, Ang-1, after the depletions (3, 4).

4.4.1. Ang-1 Quantification in Plasma

The murine clarified plasma was enriched with a know amount of Ang-1 (20 µL, with a concentration of 25 ng/µL), and then used to incubate functionalized MC biosensors. As described previously, after each experimental step the resonance frequency was monitored to evaluate the mass loaded on the cantilever. The negative control consisted in the use of murine clarified plasma without Ang-1, to evaluate the effect of unspecific binding. The histogram of the Relative Frequency Shift obtained after the incubation of Ab functionalized MCs arrays with standard plasma and enriched with Ang-1 is shown in Figure 4.12. As imaginable, the Negative control presented a high value of relative shift not related with the specific binding of Ang-1, comparing with the results obtained with PBS solutions as negative control.

Nevertheless, it is clearly notable that the specific binding with the target analyte resulted in a relative frequency shift that is almost 70% higher than the negative control. The standard deviation underlined that the result is affected by an uncertainty (20%) that is probably related with the effect of the complexity of the buffer. Therefore, the development of more stringent washing steps is needed to optimize these measurements but once obtained these improvements it will possible to

directly quantify the concentration of endogenous amount of Ang-1 and the modulation during the early stages of development of cancer pathologies.

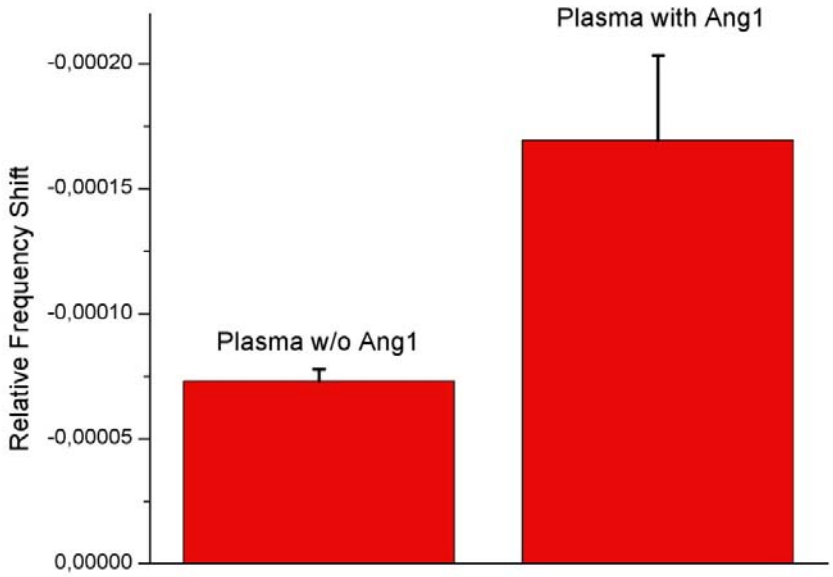

Figure 4.12. Histogram of the relative frequency shift after the incubation of MCs in plasma with or without the enrichment with Ang-1.

4.5. Micro-fluidic integration

Microcantilever based oscillators have shown the possibility of highly sensitive label-free detection by allowing the transduction of a target mass into a resonant frequency shift.

Our measurements were initially performed in vacuum environment, since immersion in liquid dramatically deteriorates the mechanical response of the sensor. Besides, once obtained those promising results, we focused on the integration of microcantilever detection in a microfluidic platform. In fact, microfluidic integration appears as a highly performing technological solution to exploit real time monitoring of biomolecular interactions, while limiting sample handling and promoting portability and automation of routine diagnostic tests (Point-Of-Care devices). Therefore, we focused on the realization and optimization of a microcantilever-based Lab-on-Chip, showing that microplates rather than microbeams exhibit largest mass sensitivity in liquid, while pirex rather

than polymers represents the best choice for microfluidic channels. Maximum Q factor achieved was 140 (for fifth resonance mode of Pirex prototype), as our knowledge the highest value reported in literature for cantilever biosensors resonating in liquid environment without electronic feedback. Then, we proved the successfully detection of Angiopoietin-1, showing that the related frequency shifts coming from non-specific interactions (negative controls) are roughly one order of magnitude lower than typical variations due to specific protein binding. Furthermore, we monitored the formation of antibody–antigen complex on MC surface in real-time. The proposed tool could be extremely useful for the comprehension of complex biological systems such as angiogenic machinery and cancer progression.

4.5.1. Theory

According to Euler–Bernoulli theory, the nth mode resonance frequency of a rectangular cantilever beam in vacuum fvn is given by:

$$f_n^v = \frac{\kappa_n^2}{2\pi}\sqrt{\frac{E}{12\rho}}\frac{t}{l^2} \tag{4.1}$$

where E and _ are respectively the elastic modulus and the density of the cantilever material, while t and l are the beam thickness and length. The constants *k*n are dimensionless parameters depending on boundary conditions. For rectangular cantilever beam, the numerical values are: $k_1 = 1.875$, $k_2 = 4.694$, $k_3 = 7.85$, . . ., $k_n = (n-0.5\ \pi)$ when $n > 5$ [119].

When such a structure oscillates in a viscous fluid, inertial and viscous forces act against its motion so that resonant frequency and quality factor Q are significantly affected. In the case of an unbounded fluid environment, an analytical model, holding for low mode numbers, is available for estimating the fluid induced Q factors and resonance frequencies, in the case in which the magnitude of the dissipative effects is small, i.e. Q >> 1 [29]. Defining f and w respectively the fluid density, the fluid viscosity and the beam width, the nth mode resonance frequency in fluid can be written as [29]:

$$f_n^f = \frac{f_n^v}{\sqrt{1+(\pi\rho_f/4\rho t)(c_1\delta + c_2 w)}} \tag{4.2}$$

being:

$$\delta = \sqrt{\frac{2\eta}{2\pi\rho_f f_n^f}} \tag{4.3}$$

The parameter ı represents the unsteady viscous layer thickness, i.e. thickness of the fluid layer, sticking to the cantilever surfaces, where viscous forces are significant. In the frequency range of 1–200 kHz, values of viscous layer in water environment are in the range of 1–10 μm.
For what concerns mode Q factors, one has:

$$Q_n = \frac{(4\rho wt/\pi\rho_f) + c_1\delta w + c_2 w^2}{c_3\delta^2 + c_4\delta w} \tag{4.4}$$

Values of coefficients c1–4 can be found in [120] as:

$$c_1 = 3.7997, \quad c_2 = 1.0553, \quad c_3 = 2.7374, \quad c_4 = 3.8018 \tag{4.5}$$

Since ı only slightly depends onw (as one can verify by simply iteratively solving Eqs. (4.2) and (4.3) for a given value of f v n), a nearly linear increase of Q with w is obtained from Eq. (4.4). Therefore, wider structures are expected to exhibit narrower curves (and thus enhanced mass detection limits) in fluid, a behaviour that commonly seems a little surprising and counterintuitive. In other words, this means that a reduction of microcantilever planar aspect ratio (AR) = l/w, while keeping constant l and t, is in favour of an increase of Q, a fact that also finds confirmation in experiments [121]. It is worth to point out anyway that the above treatment is strictly valid for beams, i.e. structures for which the condition l >> w >> t holds (typical values are l ≈ 10w ≈ 100t). Therefore, in case of low AR structures such as cantilever microplates.

4.5.2. Design optimization

First objective of the task is the optimization of device geometry, in particular MC aspect ratio (AR). According to above guidelines, we designed and realized rather wide microstructures to achieve relative high Q resonators. While thickness and length were respectively fixed to 6 μm and

900 µm, three values of MC width were tested: 300 µm (i.e. AR = 3), 450 µm (i.e. AR = 2), 600 µm (i.e. AR = 1.5). Experimentally, first five flexural resonance modes of such structures when vibrating in water are in the following ranges: m_1 = 1–2 kHz, m_2 = 8–12 kHz, m_3 = 24–35 kHz, m_4 = 50–75 kHz, m_5 = 90–150 kHz (differences in resonance frequencies are due to unavoidable fabrication tolerances and SOI substrates thickness uncertainties). Figure 4.13 shows the experimental quality factors of the first three normal modes (m_1, m_2 and m_3) in water environment as a function of the three different aspect ratios. It arises that Q factor can be easily tuned both employing higher modes and reducing the cantilever aspect ratio, from a minimum of 5 to a maximum of 24, a value comparable with most of similar literature works.

Therefore, although being quite counterintuitive, minimum detectable mass of microplates (structures with l ~ w) increments with oscillator width, as theoretically demonstrated for beams (structures with l >> w) previously. On the other hand, the increment of Q with higher modes is simply due to the reduction of viscous layer (Eq. (4.3)), and thus dumping effects, with frequency increment.

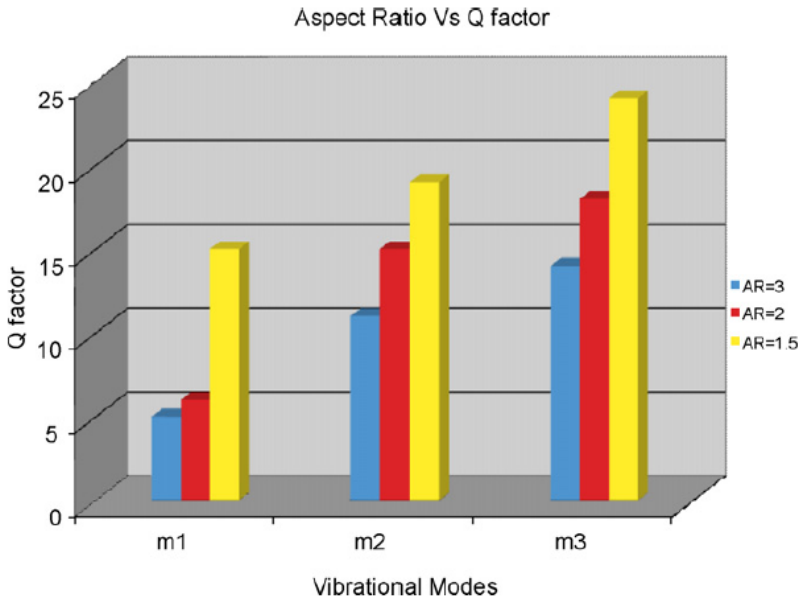

Fig. 4.13 - Histogram of Q factor of the first three normal modes of MCs with different aspect ratios (3-2-1.5) resonating in water.

4.5.3. Fabrication

The second objective of the task mainly concerns with finding the best material to be employed for the microfluidic platform. Such material should generally be compatible with biological protocols and LOC technology, but, in particular, it should also exhibit suitable mechanical and vibrational

characteristics. Due to our peculiar design, the microfluidic platform is also responsible for the propagation of mechanical vibration from the piezo actuator to MC (Figure 4.14).

Therefore, we fabricated three different prototypes in order to investigate the influence on the sensor performance of the following materials: Pirex, SU-8, PDMS (for details concerning device fabrication, please refer to Supplementary text and figures). The Si MCs have nominally the same dimensions (900 μm ×600 μm ×6 μm), except for unavoidable fabrication tolerances and SOI substrates thickness uncertainties. Fig. 3 shows the experimental quality factors (extrapolated from fit introduced in Eq. (1)) of the first five normal modes (m_1, m_2, m_3, m_4 and m_5) in water environment for the three prototypes. It can be clearly seen that the presence of a soft polymeric layer (SU-8 or PDMS) between the piezo actuator and the cantilever seriously affects the oscillator response. While at low frequency (first three modes, $f \leq 35$ kHz) Q factors are similar, at high frequencies (fourth and fifth mode, $f \geq 75$ kHz) the damping effects of the polymeric platform are so relevant that the resonance peaks completely flatten for PDMS chips, drastically weaken for SU-8 chips (which has a larger stiffness respect to PDMS). Raw data and fittings related to Fig. 3 are reported in Supplementary Material.

Maximum Q factor achieved was 140 (for m_5 of Pirex prototype), as our knowledge the highest value reported in literature for MC biosensors resonating in liquid environment without electronic feedback.

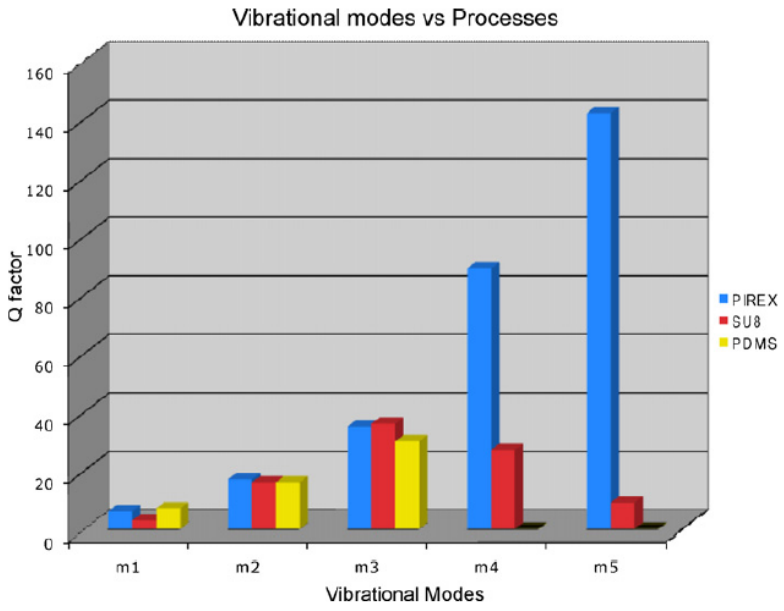

Fig. 4.14 - Histogram of Q factor of the first five normal modes of microcantilevers (AR = 1.5) with different microfluidic channel materials: Pirex, SU-8, PDMS.

4.5.4. Measurements in liquid environment

The high quality factor in a viscous liquid environment obtained thanks to the integration of new cantilever design with microfluidic technology and the use of proper materials entail to perform in situ real time monitoring of bio-molecular interactions by characterizing resonance frequency shift induced by the specific binding occurred on the Ab-immobilized cantilever surface. Since highest Q values were obtained with the pirex-silicon chip, the third device design has been chosen for biosensing experiments of Ang-1 detection.

MC dimensions were increased to 1200 µm × 800 µm ×7 µm, while keeping AR = 1.5, to further enhance resonator quality factor.

As reported previously, the biodesign is composed by 2 functionalization steps (APTES and GA), and 3 biomolecule binding steps (Protein G, anti-Ang-1 Ab, Ang-1); previous experiments in vacuum environment have shown that such biodesign exhibits optimal specificity and fine precision, with a ratio of Ang-1/Ab surface density of 2.06±0.05.

We fabricated and functionalized five chips (FC1-5) that present two independent cantilevers and wells on the same LOC platform (Fig. 4.15): the first resonator is used for the Ang-1 specific recognition, while the second is used as a negative control.

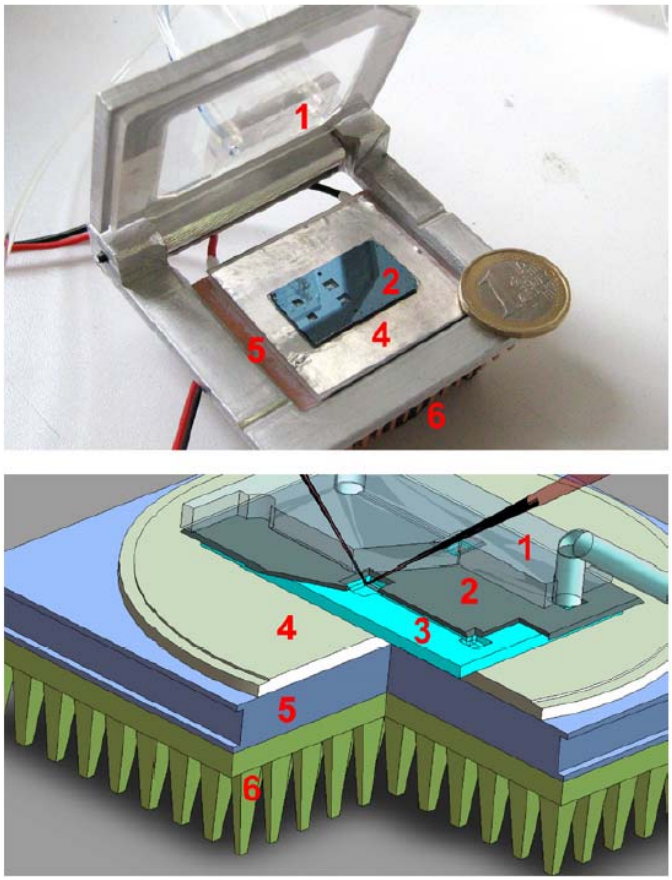

Fig. 4.15 - Microcantilever-based LOC: (a) picture and (b) 3D sketch. Most important parts of the device are labeled as: (1) PDMS interconnections; (2) cantilever chip; (3) micro.uidic platform (Pirex, SU-8 or PDMS); (4) piezo disk; (5) Peltier cell; (6) heat sink.

We considered two type of negative control (also referred as "blank"): (1) PBS solution without the target analyte .owing on Ab-coated MC, and (2) Ang-1 solution in PBS (25 μg/mL) .owing on Ab-uncoated MC (coated with Protein G). Such negative controls are fundamental to determine the influence of non-specific adsorption/desorption on resonance curves, therefore setting up the experimental limit of detection of the system.

All the solutions were delivered at a flow rate of 0.5 μL/min at controlled temperature 23±0.2 °C. Since we used MC with slightly different geometrical dimensions (due to inherent tolerances in the fabrication process) and three resonance modes are usually detected, bioexperiments are compared in terms of relative frequency deviation Δf/f rather than absolute frequency shift. For each MC, we calculate the arithmetic mean of relative frequency deviation Δf/f over the modes and the uncertainty as half-deviation of the modes. Finally, the "weighted average" method is applied to have the best estimation of the true value Δf /f of all the MCs [112]. Fig. 4.16 shows the histograms of average relative frequency deviation for Ang-1 specific binding, negative control 1 (PBS on Ab-coated MC) and negative control 2 (Ang-1 on Ab-uncoated MC), while data for each MC are reported in Table 4.1. The calculated values are, respectively: $(\Delta f / f)$ Ang-1 = $(-1.59 \pm 0.52) \times 10^{-2}$, $(\Delta f / f)$ $blank_1$ = $(-0.17 \pm 0.20) \times 10^{-2}$, $(\Delta f / f)$ $blank_2$ = $(-0.36 \pm 0.470) \times 10^{-2}$.

Chip	Bioexperiment	Relative frequency change, $\Delta f/f$ ($\times 10^{-2}$)
FC1	Ang-1 25 μg/mL	-1.12 ± 0.72
	Negative control 1	0.17 ± 0.20
FC2	Ang-1 25 μg/mL	-1.52 ± 0.94
	Negative control 2	-0.10 ± 1.05
FC3	Ang-1 25 μg/mL	-2.80 ± 1.54
	Negative control 2	0.47 ± 0.53
FC4	Ang-1 25 μg/mL	-6.10 ± 3.77
	N/A	N/A

Table 4.1

As can be noticed, the average relative frequency shift of negative control experiments resulted roughly one order of magnitude lower than successfully Ang-1 detection. As could be expected the non specific protein–protein interaction between Ang-1 and protein G coated MC (negative control 2, Ang-1 on Ab-uncoated MC) is a larger interferon respect to standard blank experiments (negative control 1, PBS on Ab-coated MC). Calculating the ratio of Ang-1/Ab surface density, we obtain 5.2±1.4, a value characterized by a considerably larger relative uncertainty, as expected for measurements in liquid respect to previously reported results in vacuum [112].

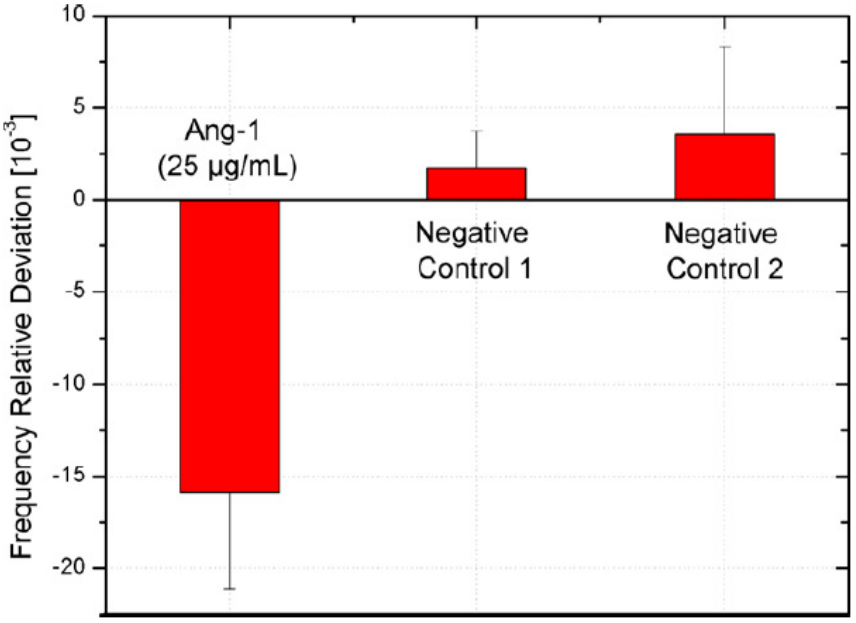

Figure 4.16 - Histogram of average relative frequency deviation for Ang-1 specific binding, negative control 1 (PBS on Ab-coated MC) and negative control 2 (Ang-1 on Ab uncoated MC).

Last fabricated and functionalized chip (FC5) was used for the real-time monitoring of antibody–antigen biomolecular interactions, as reported in Figure 4.17. After few minutes, probably needed for the antigen to reach a minimal detectable concentration on MC surface, the (normalized) resonant frequency of the Ab-coated MC clearly decreases and quickly reaches saturation. On the contrary, the signal coming from negative control (PBS on Ab-coated MC) just exhibits negligible fluctuations. Similar measurements at different concentrations are planned to deeply investigate the Ab/Ang-1 binding model and kinetics, as well as to better compare the stoichiometry of such interaction in liquid environment with previously reported results in vacuum .

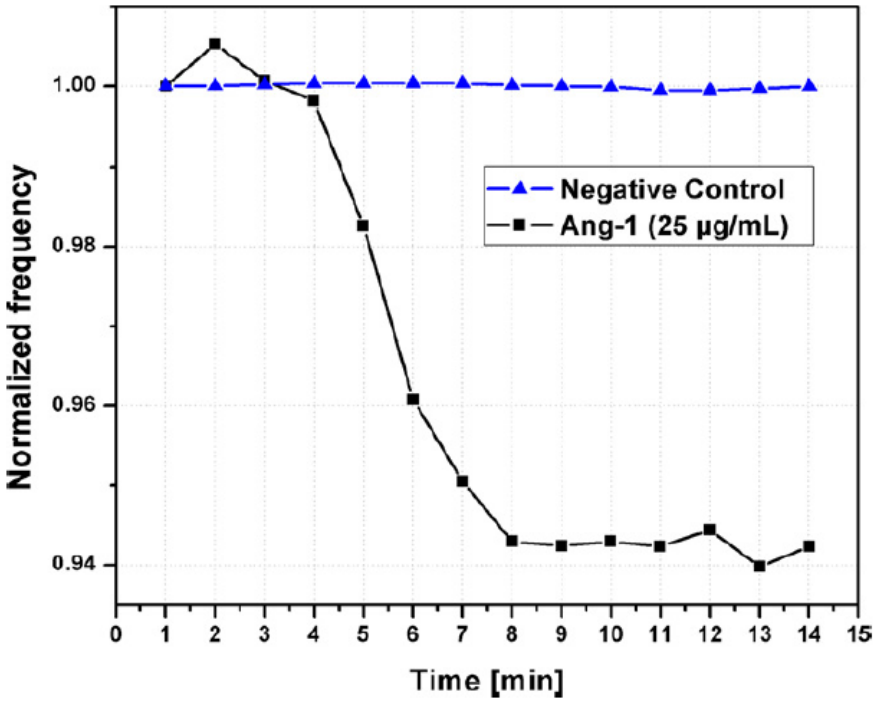

Fig. 4.17 - Real-time monitoring of antigen–antibody hybridization compared to negative control experiment (PBS on Ab-coated MC).

Chapter 5

Discussion and Conclusion

The goal of this project was the development of a microcantilever based biosensor able to detect and directly quantify small amounts of a potential cancer marker, Ang-1, thanks to a simple formula (Eq. 1.5) that correlates the resonance frequency of the cantilever with the mass of the sensor.

Our approached focused on the use of monoclonal Antibody for the functionalization of the cantilever, combining the high sensitivity of microcantilevers with the ability of antibodies to specifically recognize the target analyte.

Within this scientific work, we developed and optimized a procedure for the fabrication of silicon microcantilevers, thanks to a technological process based on bulk micromachining and Reactive Ion Etching technique.

Moreover, a custom made system for the characterization of dynamic properties of microcantilever in several environment conditions has been set up.

We particularly focused on the precision and accuracy of our cantilever-based analysis, proposing the combination of results coming from both the first and second mode of vibration. A careful analysis of repeatability and reproducibility was performed as preparatory measurements.

The Antibody – Antigen bio-design gave promising results in terms of highest surface density and lowest uncertainty: Ang-1 masses of the order of few hundreds of picograms were detected with less than 0.5% of relative uncertainty.

Furthermore, we evaluated the protein surface density (number of molecules per cm^2), opening new perspectives for the study of complex systems and revealing interesting features concerning the multimeric state of the targeted protein. We also performed negative controls (dipping the sample in PBS without proteins) and specificity tests (dipping the sample in PBS with a "false" antigen). The related frequency shifts (coming from non-specific interactions) were found to be at least one order of magnitude lower than typical variations due to specific protein binding.

These promising results encouraged us to shift from a proof of concept approach developed with standard solutions to the detection of the target analyte in a real matrix. Thus, we developed and optimized a protocol to deplete the albumin and immunoglobulin components of plasma and successfully performed measurements of such clarified plasma enriched with Ang-1.

Moreover, we report on the development, realization and optimization of a microcantilever-based LOC, showing that microplates rather than microbeams exhibit largest mass sensitivity in liquid, while pirex rather than polymers represents the best choice for microfluidic channels. Maximum Q factor achieved was 140 (for fifth resonance mode of Pirex prototype), as our knowledge the highest value reported in literature for cantilever biosensors resonating in liquid environment without electronic feedback. Then, we proved the successfully detection of Ang-1, showing that the related frequency shifts coming from non-specific interactions (negative controls) are roughly one order of magnitude lower than typical variations due to specific protein binding. Furthermore, we monitored the formation of antibody–antigen complex on MC surface in real-time.

In the end, thanks to its fine precision and optimal specificity, our microcantilever-based system can be successfully applied as a quantitative tool for systems biology studies such as the comprehension of angiogenic machinery and cancer progression.

REFERENCES

1. Mohanty, S.P. and E. Kougianos, *Biosensors: a tutorial review.* Potentials, IEEE, 2006. **25**(2): p. 35-40.
2. Nicu, L. and T. Leichle, *Biosensors and tools for surface functionalization from the macro- to the nanoscale: The way forward.* Journal of Applied Physics, 2008. **104**(11): p. 111101-111101-16.
3. Drukier, A.K., et al., *High-Sensitivity Blood-Based Detection of Breast Cancer by Multi Photon Detection Diagnostic Proteomics.* Journal of Proteome Research, 2006. **5**(8): p. 1906-1915.
4. Huang, C.-S., et al., *Application of Photonic Crystal Enhanced Fluorescence to Cancer Biomarker Microarrays.* Analytical Chemistry. **83**(4): p. 1425-1430.
5. Wolfbeis, O.S., *Fiber-Optic Chemical Sensors and Biosensors.* Analytical Chemistry, 2008. **80**(12): p. 4269-4283.
6. Rickert, J., A. Brecht, and W. Gopel, *QCM Operation in Liquids: Constant Sensitivity during Formation of Extended Protein Multilayers by Affinity.* Anal. Chem., 1997. **69**(7): p. 1441-1448.
7. Janz, S., et al., *SURFACE PLASMON RESONANCE (SPR) BIOSENSORS AND THEIR APPLICATIONS IN FOOD SAFETY AND SECURITY*, in *Frontiers in Planar Lightwave Circuit Technology*. 2006, Springer Netherlands. p. 101-118.
8. Rosi, N.L. and C.A. Mirkin, *Nanostructures in Biodiagnostics.* Chemical Reviews, 2005. **105**(4): p. 1547-1562.
9. Fu, Z., S. Rogelj, and T.L. Kieft, *Rapid detection of Escherichia coli O157:H7 by immunomagnetic separation and real-time PCR.* International Journal of Food Microbiology, 2005. **99**(1): p. 47-57.
10. Ziegler, C., *Cantilever-based biosensors.* Analytical and Bioanalytical Chemistry, 2004. **379**(7): p. 946-959.
11. Gupta, A., D. Akin, and R. Bashir, *Single virus particle mass detection using microresonators with nanoscale thickness.* Applied Physics Letters, 2004. **84**(11): p. 1976-1978.
12. Ilic, B., *Attogram detection using nanoelectromechanical oscillators.* J. Appl. Phys., 2004. **95**: p. 3694-3703.
13. Ilic, B., *Enumeration of DNA molecules bound to a nanomechanical oscillator.* Nano Lett., 2005. **5**: p. 925-929.
14. Ilic, B., et al. *Single cell detection with micromechanical oscillators*. in *The 45th international conference on electron, ion, and photon beam technology and nanofabrication*. 2001. Washington, DC (USA): AVS.
15. David, R.B., U.L. Gil, and J.C. Richard. *Biosensor based on force microscope technology*. 1996: AVS.
16. Zang, J. and F. Liu, *Theory of bending of Si nanocantilevers induced by molecular adsorption: a modified Stoney formula for the calibration of nanomechanochemical sensors.* Nanotechnology, 2007. **18**(40): p. 405501.
17. Watari, M., et al., *Investigating the Molecular Mechanisms of In-Plane Mechanochemistry on Cantilever Arrays.* J. Am. Chem. Soc., 2007. **129**(3): p. 601-609.
18. Lavrik, N.V., M.J. Sepaniak, and P.G. Datskos, *Cantilever transducers as a platform for chemical and biological sensors.* Rev. Sci. Instrum., 2004. **75**: p. 2229-2253.
19. Lee, J.H., et al., *Immunoassay of prostate-specific antigen (PSA) using resonant frequency shift of piezoelectric nanomechanical microcantilever.* Biosensors and Bioelectronics, 2005. **20**(10): p. 2157-2162.

20. Campbell, G.A. and R. Mutharasan, *Detection and quantification of proteins using self-excited PZT-glass millimeter-sized cantilever.* Biosensors and Bioelectronics, 2005. **21**(4): p. 597-607.
21. Campbell, G.A. and R. Mutharasan, *Detection of pathogen Escherichia coli O157:H7 using self-excited PZT-glass microcantilevers.* Biosensors and Bioelectronics, 2005. **21**(3): p. 462-473.
22. Lee, J.H., et al., *Label free novel electrical detection using micromachined PZT monolithic thin film cantilever for the detection of C-reactive protein.* Biosensors and Bioelectronics, 2004. **20**(2): p. 269-275.
23. Gfeller, K.Y., N. Nugaeva, and M. Hegner, *Micromechanical oscillators as rapid biosensor for the detection of active growth of Escherichia coli.* Biosensors and Bioelectronics, 2005. **21**(3): p. 528-533.
24. Yan, X., et al., *Surface Stress Changes Induced by the Conformational Change of Proteins.* Langmuir, 2006. **22**(26): p. 11241-11244.
25. Hosaka, S., et al., *Possibility of a femtogram mass biosensor using a self-sensing cantilever.* Current Applied Physics, 2006. **6**(3): p. 384-388.
26. Maraldo, D., et al., *Method for Label-Free Detection of Femtogram Quantities of Biologics in Flowing Liquid Samples.* Anal. Chem., 2007. **79**(7): p. 2762-2770.
27. Thundat, T., et al., *Detection of mercury vapor using resonating microcantilevers.* Appl. Phys. Lett., 1995. **66**: p. 1695-1697.
28. Bonnell, D., *Scanning Probe Microscopy and Spectroscopy: Theory, Techniques, and Applications,* . 2nd Edition ed. 2001: Wiley.
29. Sader, J.E., *Frequency response of cantilever beams immersed in viscous fluids with applications to the atomic force microscope.* Journal of Applied Physics, 1998. **84**(1): p. 64-76.
30. Braun, T., et al., *Micromechanical mass sensors for biomolecular detection in a physiological environment.* Physical Review E (Statistical, Nonlinear, and Soft Matter Physics), 2005. **72**(3): p. 031907.
31. Michel, G. and et al., *Cantilever-based sensing: the origin of surface stress and optimization strategies.* Nanotechnology. **21**(7): p. 075501.
32. Weaver, W., J.S.P. Timoshenko, and D.H. Young, *Vibration Problems in Engineering,* . ed, ed. 5th. 1990: Wiley.
33. Hu, Z., T. Thundat, and R.J. Warmack, *Investigation of adsorption and absorption-induced stresses using microcantilever sensors.* Journal of Applied Physics, 2001. **90**(1): p. 427-431.
34. Frink, L.J.D. and F. van Swol, *A common theoretical basis for surface forces apparatus, osmotic stress, and beam bending measurements of surface forces.* Colloids and Surfaces A: Physicochemical and Engineering Aspects, 2000. **162**: p. 25-36.
35. Couthon, F., et al., *The role of surface stress in reconstruction, epitaxial growth and stabilization of mesoscopic structures.* Surface Science Reports, 1997. **29**: p. 195-263.
36. Kohale, S., et al., *Monitoring the formation of self-assembled monolayers of alkanedithiols using a micromechanical cantilever sensor.* Langmuir, 2007. **23**(3): p. 1258-1263.
37. Schell-Sorokin, A.J. and R.M. Tromp, *Measurement of surface stress during epitaxial growth of Ge on arsenic terminated Si(001).* Surface Science, 1994. **319**(1-2): p. 110-118.
38. Burg, T.P., et al., *Weighing of biomolecules, single cells and single nanoparticles in fluid.* Nature, 2007. **446**(7139): p. 1066-1069.
39. Sader, J.E., *Surface stress induced deflections of cantilever plates with applications to the atomic force microscope: Rectangular plates* journal of applied physics 2001. **89**(2911).
40. Lavrik, N.V., et al., *Gold Nano-Structures for Transduction of Biomolecular Interactions into Micrometer Scale Movement.* Biomedical Microdevices, 2001. **3**: p. 35-41.
41. Raiteri, R., et al., *Micromechanical cantilever-based biosensors.* Sensors and Actuators B: Chemical, 2001. **79**(2-3): p. 115-126.

42. Wu, G., et al., *Origin of nanomechanical cantilever motion generated from biomolecular interactions.* Proceedings of the National Academy of Sciences, 2001. **98**(4): p. 1560-1564.
43. Hölscher, H. and U.D. Schwarz, *Theory of amplitude modulation atomic force microscopy with and without Q-Control.* International Journal of Non-Linear Mechanics, 2007. **42**(4): p. 608-625.
44. Tamayo, J., M. Alvarez, and L.M. Lechuga, *Digital tuning of the quality factor of micromechanical resonant biological detectors.* Sensors and Actuators B: Chemical, 2003. **89**: p. 33-39.
45. Carrascosa, L.G., et al., *Nanomechanical biosensors: a new sensing tool.* TrAC Trends in Analytical Chemistry, 2006. **25**(3): p. 196-206.
46. Wee, K.W., et al., *Novel electrical detection of label-free disease marker proteins using piezoresistive self-sensing micro-cantilevers.* Biosensors and Bioelectronics, 2005. **20**(10): p. 1932-1938.
47. Kang, G.Y., et al., *Label-free protein assay with site-directly immobilized antibody using self-actuating PZT cantilever.* Sensors and Actuators B: Chemical, 2006. **117**(2): p. 332-338.
48. Shekhawat, G., S.-H. Tark, and V.P. Dravid, *MOSFET-Embedded Microcantilevers for Measuring Deflection in Biomolecular Sensors.* Science, 2006: p. 1122588.
49. Backmann, N., et al., *A label-free immunosensor array using single-chain antibody fragments.* Proceedings of the National Academy of Sciences, 2005. **102**(41): p. 14587-14592.
50. Arntz, Y., et al., *Label-free protein assay based on a nanomechanical cantilever array.* Nanotechnology, 2003(1): p. 86.
51. Shu, W., E.D. Laue, and A.A. Seshia, *Investigation of biotin-streptavidin binding interactions using microcantilever sensors.* Biosensors and Bioelectronics, 2007. **22**(9-10): p. 2003-2009.
52. Campbell, G.A., et al., Biosens. Bioelectron., 2007. **22**: p. 1296.
53. Kooser, A., et al., *Investigation of the antigen antibody reaction between anti-bovine serum albumin (a-BSA) and bovine serum albumin (BSA) using piezoresistive microcantilever based sensors.* Biosensors and Bioelectronics, 2003. **19**(5): p. 503-508.
54. Capobianco, J.A., et al., *Label free detection of white spot syndrome virus using lead magnesium niobate-lead titanate piezoelectric microcantilever sensors.* Biosensors and Bioelectronics. **26**(3): p. 964-969.
55. Ilic, B., et al., *Mechanical resonant immunospecific biological detector.* Applied Physics Letters, 2000. **77**(3): p. 450-452.
56. Gupta, A.K., et al., *Anomalous resonance in a nanomechanical biosensor.* Proceedings of the National Academy of Sciences of the United States of America, 2006. **103**(36): p. 13362-13367.
57. Campbell, G.A. and R. Mutharasan, Biosens. Bioelectron., 2006. **22**: p. 78.
58. Davila, A.P., et al., *Microresonator mass sensors for detection of Bacillus anthracis Sterne spores in air and water.* Biosensors and Bioelectronics, 2007. **22**(12): p. 3028-3035.
59. McKendry, R., et al., *Multiple label-free biodetection and quantitative DNA-binding assays on a nanomechanical cantilever array.* Proceedings of the National Academy of Sciences, 2002. **99**(15): p. 9783-9788.
60. Hansen, K.M., et al., *Cantilever-Based Optical Deflection Assay for Discrimination of DNA Single-Nucleotide Mismatches.* Anal. Chem., 2001. **73**(7): p. 1567-1571.
61. Hansen, K.M. and T. Thundat, *Microcantilever biosensors.* Methods, 2005. **37**(1): p. 57-64.
62. Calleja, M., et al., *Highly sensitive polymer-based cantilever-sensors for DNA detection.* Ultramicroscopy, 2005. **105**(1-4): p. 215-222.

63. Marie, R., et al., *Adsorption kinetics and mechanical properties of thiol-modified DNA-oligos on gold investigated by microcantilever sensors.* Ultramicroscopy, 2002. **91**(1-4): p. 29-36.
64. Valsesia, A., et al., *Protein Nanopatterns for Improved Immunodetection Sensitivity.* Analytical Chemistry, 2008. **80**(19): p. 7336-7340.
65. Campbell, G.A. and R. Mutharasan, *Piezoelectric-excited millimeter-sized cantilever (PEMC) sensors detect Bacillus anthracis at 300 spores/mL.* Biosensors and Bioelectronics, 2006. **21**(9): p. 1684-1692.
66. Campbell, G.A. and R. Mutharasan, Langmuir, 2005. **21**: p. 11568.
67. Berger, R., et al., *Surface Stress in the Self-Assembly of Alkanethiols on Gold.* Science, 1997. **276**(5321): p. 2021-2024.
68. Yan, X.D., H.F. Ji, and T. Thundat, *Microcantilever (mcl) biosensing.* Curr. Anal. Chem., 2006. **2**: p. 297-307.
69. Peiro, C., et al., *High glucose induces cell death of cultured human aortic smooth muscle cells through the formation of hydrogen peroxide.* British journal of pharmacology, 2001. **133**(7): p. 967-74.
70. Detzel, A.J., G.A. Campbell, and R. Mutharasan, *Rapid assessment of Escherichia coli by growth rate on piezoelectric-excited millimeter-sized cantilever (PEMC) sensors.* Sensors and Actuators B: Chemical, 2006. **117**(1): p. 58-64.
71. Nugaeva, N., et al., *An Antibody-Sensitized Microfabricated Cantilever for the Growth Detection of Aspergillus niger Spores.* Microscopy and Microanalysis, 2007. **13** p. 13-17.
72. Maluf, N., *An introduction to microelectromechanical systems engineering.* Boston Artech House., 2000.
73. Wada, Y., *NEMS/MEMS tools for nanoelectronics development.* Current Applied Physics, 2002. **2**(4): p. 331-334.
74. Baltes, et al., *CMOS MEMS: Present and future*. 2002. XLIII, 736 p.
75. Trimmer, W.S.N., *Microrobots and micromechanical systems.* Sensors and Actuators, 1989. **19**(3): p. 267-287.
76. Bustillo, J.M., R.T. Howe, and R.S. Muller, *Surface micromachining for microelectromechanical systems.* Proceedings of the IEEE, 1998. **86**(8): p. 1552-1574.
77. Bühler, J. and et al., *Silicon dioxide sacrificial layer etching in surface micromachining.* Journal of Micromechanics and Microengineering, 1997. **7**(1): p. R1.
78. Teng, J. and P.D. Prewett, *Focused ion beam fabrication of thermally actuated bimorph cantilevers.* Sensors and Actuators A: Physical, 2005. **123-124**: p. 608-613.
79. Girgis, E., J. Liu, and M.L. Benkhedar, *Fabrication of metallic air bridges using multiple-dose electron beam lithography.* Applied Physics Letters, 2006. **88**(20): p. 202103.
80. Forsén, E. and et al., *Fabrication of cantilever based mass sensors integrated with CMOS using direct write laser lithography on resist.* Nanotechnology, 2004. **15**(10): p. S628.
81. Hierlemann, A., et al., *Microfabrication techniques for chemical/biosensors.* Proceedings of the IEEE, 2003. **91**(6): p. 839-863.
82. Stowe, T.D., et al., *Attonewton force detection using ultrathin silicon cantilevers.* Applied Physics Letters, 1997. **71**(2): p. 288-290.
83. Villarroya, M., et al., *System on chip mass sensor based on polysilicon cantilevers arrays for multiple detection.* Sensors and Actuators A: Physical, 2006. **132**(1): p. 154-164.
84. Chen, Q., et al., *Micromachined SiO2 microcantilever for high sensitive moisture sensor.* Microsystem Technologies, 2008. **14**(6): p. 739-746.
85. Hata, S., et al., *Behavior of joining interface between thin film metallic glass and silicon nitride at heating.* Materials Science and Engineering: B, 2008. **148**(1-3): p. 149-153.
86. Hascík, S., et al., *The fabrication of thin GaAs cantilever beams for power sensor microsystem using RIE.* Vacuum, 1996. **47**(10): p. 1215-1217.

87. Sheeja, D., et al., *Fabrication of amorphous carbon cantilever structures by isotropic and anisotropic wet etching methods.* Diamond and Related Materials, 2003. **12**(9): p. 1495-1499.
88. Anirban, C. and L. Cheng, *Fabrication and application of metallic nano-cantilevers.* Microelectron. J., 2006. **37**(11): p. 1306-1312.
89. Uetsuka, H., T. Yamada, and S. Shikata, *ICP etching of polycrystalline diamonds: Fabrication of diamond nano-tips for AFM cantilevers.* Diamond and Related Materials. **17**(4-5): p. 728-731.
90. Zhu, X., D.M. Aslam, and J.P. Sullivan, *The application of polycrystalline diamond in a thin film packaging process for MEMS resonators.* Diamond and Related Materials. **15**(11-12): p. 2068-2072.
91. Yang, Z., et al., *Optomechanical uncooled infrared imaging system: design, microfabrication, and performance.* Microelectromechanical Systems, Journal of, 2002. **11**(2): p. 136-146.
92. Fujitsuka, N. and J. Sakata, *A new processing technique to prevent stiction using silicon selective etching for SOI-MEMS.* Sensors and Actuators A: Physical, 2002. **97-98**: p. 716-719.
93. Kirstein, K.U. *Cantilever-Based Biosensors in CMOS Technology*. 2005.
94. Voldman, J., M.L. Gray, and M.A. Schmidt, *Microfabrication in Biology and Medicine.* Annual Review of Biomedical Engineering, 1999. **1**(1): p. 401-425.
95. Fonseca, M.A., et al., *Wireless micromachined ceramic pressure sensor for high-temperature applications.* Microelectromechanical Systems, Journal of, 2002. **11**(4): p. 337-343.
96. Maria, N.m. and et al., *A novel fabrication technique for free-hanging homogeneous polymeric cantilever waveguides.* Journal of Micromechanics and Microengineering, 2008. **18**(1): p. 015017.
97. Genolet, G., et al., *All-photoplastic, soft cantilever cassette probe for scanning force microscopy.* Journal of Vacuum Science & Technology B: Microelectronics and Nanometer Structures, 2000. **18**(2): p. 617-620.
98. Wang, J., et al., Langmuir, 2003. **19**: p. 989.
99. Gammelgaard, L., et al., *Microfabricated photoplastic cantilever with integrated photoplastic/carbon based piezoresistive strain sensor.* Applied Physics Letters, 2006. **88**(11): p. 113508-3.
100. Thaysen, J., et al. *SU-8 based piezoresistive mechanical sensor*. in *Micro Electro Mechanical Systems, 2002. The Fifteenth IEEE International Conference on*. 2002.
101. Lee, L.P., et al., *High aspect ratio polymer microstructures and cantilevers for bioMEMS using low energy ion beam and photolithography.* Sensors and Actuators A: Physical, 1998. **71**(1-2): p. 144-149.
102. Carmeliet, P., *Mechanisms of angiogenesis and arteriogenesis.* Nat Med, 2000. **6**(4): p. 389-395.
103. Cébe-Suarez, S., A. Zehnder-Fjällman, and K. Ballmer-Hofer, *The role of VEGF receptors in angiogenesis; complex partnerships.* Cellular and Molecular Life Sciences, 2006. **63**(5): p. 601-615.
104. Davis, S., et al., *Isolation of Angiopoietin-1, a Ligand for the TIE2 Receptor, by Secretion-Trap Expression Cloning.* Cell, 1996. **87**(7): p. 1161-1169.
105. Hayes, A.J., et al., *Expression and function of angiopoietin-1 in breast cancer.* Br J Cancer, 2000. **83**(9): p. 1154-1160.
106. Brindle, N.P.J., P. Saharinen, and K. Alitalo, *Signaling and Functions of Angiopoietin-1 in Vascular Protection.* Circ Res, 2006. **98**(8): p. 1014-1023.
107. Metheny-Barlow, L.J. and L.Y. Li, *The enigmatic role of angiopoietin-1 in tumor angiogenesis.* Cell Res, 2003. **13**(5): p. 309-317.

108. Smith, R.A., et al., *American Cancer Society guidelines for the early detection of cancer.* CA Cancer J Clin, 2000. **50**(1): p. 34-49.
109. Kelly, K.A., et al., *Detection of Early Prostate Cancer Using a Hepsin-Targeted Imaging Agent.* Cancer Research, 2008. **68**(7): p. 2286-2291.
110. Yu, Q., *The dynamic roles of angiopoietins in tumor angiogenesis.* Future Oncology, 2005. **1**(4): p. 475-484.
111. Steeg, P.S., *Tumor metastasis: mechanistic insights and clinical challenges.* Nat Med, 2006. **12**(8): p. 895-904.
112. Ricciardi, C., et al., *Integration of microfluidic and cantilever technology for biosensing application in liquid environment.* Biosensors and Bioelectronics, 2010.
113. Waggoner, P.S. and H.G. Craighead, *Micro- and nanomechanical sensors for environmental, chemical, and biological detection.* Lab on a Chip, 2007. **7**(10): p. 1238-1255.
114. Taylor, J.R., *An Introduction to Error Analysis: The Study of Uncertainties in Physical Measurements.* second ed. University Science Books, 1997.
115. Lu, P., et al., *Surface stress effects on the resonance properties of cantilever sensors.* Physical Review B, 2005. **72**(8): p. 085405.
116. Oliviero, G., et al., *A biofunctional polymeric coating for microcantilever molecular recognition.* Analytica Chimica Acta, 2008. **630**(2): p. 161-167.
117. Tamayo, J., et al., *Effect of the adsorbate stiffness on the resonance response of microcantilever sensors.* Applied Physics Letters, 2006. **89**(22).
118. Ricciardi, C., et al., *Development of microcantilever-based biosensor array to detect Angiopoietin-1, a marker of tumor angiogenesis.* Biosensors and Bioelectronics, 2010. **25**(5): p. 1193-1198.
119. Lochon, F., I. Dufour, and D. Rebiere, *An alternative solution to improve sensitivity of resonant microcantilever chemical sensors: comparison between using high-order modes and reducing dimensions.* Sensors and Actuators B: Chemical, 2005. **108**(1-2): p. 979-985.
120. Maali, A., et al., *Hydrodynamics of oscillating atomic force microscopy cantilevers in viscous fluids.* Journal of Applied Physics, 2005. **97**(074907).
121. Vancura, C., et al., *Analysis of resonating microcantilevers operating in a viscous liquid environment.* Sensors and Actuators A: Physical, 2008. **141**(1): p. 43-51.